

Neutrophils promote CXCR3-dependent itch in the development of atopic dermatitis

Authors and Affiliations: Carolyn M. Walsh^{1‡}, Rose Z. Hill^{1‡}, Jamie Schwendinger-Schreck¹, Jacques Deguine¹, Emily C. Brock¹, Natalie Kucirek¹, Ziad Rifi¹, Jessica Wei², Karsten Gronert², Rachel B. Brem^{3,4}, Gregory M. Barton¹, Diana M. Bautista^{1,5}

1. Department of Molecular and Cell Biology, University of California, Berkeley, CA 94720, USA.
2. Vision Science Program, School of Optometry, University of California, Berkeley, CA 94720, USA.
3. Department of Plant and Microbial Biology, University of California, Berkeley, CA 94720, USA.
4. Buck Institute for Research on Aging, Novato, CA 94945, USA.
5. Helen Wills Neuroscience Institute, University of California, Berkeley, CA 94720, USA.

‡ These authors contributed equally and order determined by coin toss.

1 **Abstract**

2 Chronic itch remains a highly prevalent disorder with limited treatment options. Most chronic itch
3 diseases are thought to be driven by both the nervous and immune systems, but the
4 fundamental molecular and cellular interactions that trigger the development of itch and the
5 acute-to-chronic itch transition remain unknown. Here, we show that skin-infiltrating neutrophils
6 are key initiators of itch in atopic dermatitis, the most prevalent chronic itch disorder. Neutrophil
7 depletion significantly attenuated itch-evoked scratching in a mouse model of atopic dermatitis.
8 Neutrophils were also required for several key hallmarks of chronic itch, including skin
9 hyperinnervation, enhanced expression of itch signaling molecules, and upregulation of
10 inflammatory cytokines, activity-induced genes, and markers of neuropathic itch. Finally, we
11 demonstrate that neutrophils are required for induction of CXCL10, a ligand of the CXCR3
12 receptor that promotes itch via activation of sensory neurons, and we find that that CXCR3
13 antagonism attenuates chronic itch.

14 **Introduction**

15 Chronic itch is a debilitating disorder that affects millions of people worldwide.¹⁻³ It is a symptom
16 of a number of skin diseases and systemic disorders, as well as a side effect of a growing list of
17 medications. Like chronic pain, chronic itch can be a disease in and of itself.⁴⁻⁶ Unlike acute itch,
18 which can facilitate removal of crawling insects, parasites, or irritants, persistent scratching in
19 chronic itch disorders has no discernable benefit; scratching damages skin, leading to
20 secondary infection, disfiguring lesions, and exacerbation of disease severity.^{2,7,8} The most
21 common chronic itch disorder is atopic dermatitis (AD; commonly known as eczema), which
22 affects fifteen million people in the United States alone.⁹ Severe AD can trigger the atopic
23 march, where chronic itch and inflammation progress to food allergy, allergic rhinitis, and
24 asthma.^{9,10}

25
26
27 Little is known about the underlying mechanisms that drive chronic itch pathogenesis. As such,
28 studies of human chronic itch disorders have sought to identify candidate mechanisms of
29 disease progression. A number of studies have identified biomarkers and disease genes in itchy
30 human AD lesions.¹¹⁻¹⁵ Indeed, a recent study compared the transcriptomes of healthy skin to
31 itchy and non-itchy skin from psoriasis and AD patients, revealing dramatic changes in
32 expression of genes associated with cytokines, immune cells, epithelial cells, and sensory
33 neurons.¹⁶ However, due to the difficulty in staging lesion development and obtaining staged
34 samples from patients, there is currently no temporal map of when individual molecules and cell
35 types contribute to chronic itch pathogenesis. Furthermore, the use of human patient data does
36 not allow for rigorous mechanistic study of how disease genes contribute to chronic itch. To this
37 end, we used a well-characterized inducible animal model of itch to define where, when, and
38 how these genes identified from patient data contribute to chronic itch pathogenesis.

39
40 We employed the MC903 mouse model of AD and the atopic march¹⁷⁻²¹ to provide a framework
41 within which to identify the molecules and cells that initiate the development of atopic itch. The
42 MC903 model is ideal for our approach because of its highly reproducible phenotypes that
43 closely resemble human AD and the ability to induce the development of lesions and
44 scratching.^{18-20,22-24} By contrast, it is difficult to synchronously time the development of lesions in
45 commonly used genetic models of AD, such as filaggrin mutant mice or Nc/Nga mice. Another
46 advantage of the MC903 model is that it displays collectively more hallmarks of human AD than
47 any one particular genetic mouse model. For example, the commonly used IL-31¹⁹
48 overexpressor model^{25,26} lacks strong Th2 induction,²⁷ and itch behaviors have not yet been
49 rigorously characterized in the keratinocyte-TSLP overexpressor model. As MC903 is widely
50 used to study the chronic phase of AD, we hypothesized that MC903 could also be used to

51 define the early mechanisms underlying the development of chronic itch, beginning with healthy
 52 skin. We performed RNA-seq of skin at key time points in the model. We complemented this
 53 approach with measurements of itch behavior and immune cell infiltration. The primary goal of
 54 our study was to identify the inciting molecules and cell types driving development of chronic
 55 itch. To that end, we show that infiltration of neutrophils into skin is required for development of
 56 chronic itch. Additionally, we demonstrate that neutrophils direct early hyperinnervation of skin,
 57 and the upregulation of itch signaling molecules and activity-induced genes in sensory neurons.
 58 Finally, we identify CXCL10/CXCR3 signaling as a key link between infiltrating neutrophils and
 59 sensory neurons that drives itch behaviors.

60
 61 **MC903 triggers rapid changes in expression of skin barrier, epithelial cell-derived**
 62 **cytokine, and axon guidance genes**

63 Although a variety of AD- and chronic itch-associated genes have been identified, when and
 64 how they contribute to disease pathogenesis is unclear. Using RNA-seq of MC903-treated skin,
 65 we observed distinct temporal patterns by which these classes of genes are differentially
 66 expressed across the first eight days of the model (Figure 1A-B, Figure 1-Figure Supplement
 67 1A). Overall, we found that 62% of genes from a recent study of human chronic itch lesions¹⁶
 68 (Figure 1-Figure Supplement 1A) and 67% of AD-related genes (Figure 1B) were significantly
 69 changed for at least one of the time points examined, suggesting that the MC903 mouse model
 70 recapitulates many key transcriptional changes occurring in human chronic itch and AD. MC903
 71 dramatically alters the transcriptional profile of keratinocytes by derepressing genomic loci
 72 under the control of the Vitamin D Receptor. In line with rapid changes in transcription,
 73 proteases (*Klk6*, *Klk13*, among others) and skin barrier genes (*Cdhr1*) changed as early as six
 74 hours after the first treatment, before mice begin scratching (Figure 1B). Increased protease
 75 activity in AD skin is thought to promote breakdown of the epidermal barrier and release of
 76 inflammatory cytokines from keratinocytes.^{28,29} One such cytokine, thymic stromal lymphopoietin
 77 (TSLP) is a key inducer of the Type 2 immune response, which is characteristic of human AD
 78 and the MC903 model, via signaling in CD4⁺ T cells, basophils, and other immune cells.^{19,20,30-33}
 79 Beginning at day two, before any significant itch-evoked scratching (Figure 1C), immune cell
 80 infiltration (Figure 1E-G, Figure 1-Figure Supplements 3A, 4A, 5A-C), or skin lesions (data not
 81 shown)²³ were observed, we saw increases in *Tslp*, as well as several other epithelial-derived
 82 cytokines, including the neutrophil chemoattractant genes *Cxcl1*, *Cxcl2*, *Cxcl3*, and *Cxcl5*
 83 (Figure 1D). To ask whether upregulation of these chemokine genes was dependent on
 84 protease activity, we treated human keratinocytes with the Protease Activated Receptor 2
 85 agonist SLIGRL. SLIGRL treatment triggered increased expression of several of these
 86 chemokine genes, including *IL8*, the human ortholog of mouse *Cxcl1/Cxcl2*, and *CXCL2* (Figure
 87 1-Figure Supplement 6A). These increases occurred after a few hours of exposure to SLIGRL,
 88 suggesting that increased protease activity can rapidly trigger increases in neutrophil
 89 chemoattractants in skin, similar to what we observe in MC903-treated mouse skin.

90
 91 Unexpectedly, in the skin we observed early changes in a number of transcripts encoding
 92 neuronal outgrowth factors (*Ngf*, *Artn*) and axon pathfinding molecules (*Slit1*, *Sema3d*,
 93 *Sema3a*), some of which are directly implicated in chronic itch³⁴⁻³⁸; Figure 1-Figure Supplement
 94 7A), prior to when mice began scratching. We thus used immunohistochemistry (IHC) of whole-
 95 mount skin to examine innervation at this time point. We saw increased innervation of lesions at
 96 day two but not day one of the model (Figure 1H-I, Figure 1-Figure Supplement 8A). Our RNA-
 97 seq data showed elevation in skin CGRP transcript *Calca*, along with other markers of
 98 peptidergic nerve endings, specifically at day 2. Indeed, we saw an increase in CGRP⁺
 99 innervation of skin at day 2 (Figure 1J, Figure 1-Figure Supplement 9A), which suggests that
 100 elevation of neuronal transcripts in skin is due to hyperinnervation of peptidergic itch and/or pain
 101 fibers. The increased innervation was surprising because such changes had previously only

102 been reported in mature lesions from human chronic itch patients.^{16,39–44} Our findings suggest
 103 that early hyperinnervation is promoted by local signaling in the skin and is independent of the
 104 itch-scratch cycle.

105

106 **Neutrophils are the first immune cells to infiltrate AD skin**

107 By day five, mice exhibited robust itch behaviors (Figure 1C) and stark changes in a number of
 108 AD disease genes (Figure 1A-B). For example, loss-of-function mutations in filaggrin (*FLG*) are
 109 a major risk factor for human eczema.^{45,46} Interestingly, *Flg2* levels sharply decreased at day
 110 five. In parallel, we saw continued and significant elevation in neutrophil and basophil
 111 chemoattractant genes (*Cxcl1,2,3,5*, and *Tsfp*, Figure 1D). Using flow cytometry, we observed a
 112 number of infiltrating immune cells in the skin at day 5. Of these, we neutrophils were the most
 113 abundant immune cell subtype (Figure 1E, Figure 1-Figure Supplement 3A). It was not until day
 114 eight that we observed the classical AD-associated immune signature in the skin,⁴⁷ with
 115 upregulation of *Il4*, *Il33* and other Th2-associated genes (Figure 1B, Figure 1D). We also
 116 observed increases in the T cell chemoattractant genes *Cxcl9*, *Cxcl10*, and *Cxcl11* (Figure 1D),
 117 which are thought to be hallmarks of chronic AD lesions in humans.^{48,49} Neutrophils and a
 118 number of other immune cells that started to infiltrate on day five were robustly elevated in skin
 119 by day eight, including basophils (Figure 1F), CD4⁺ T cells (Figure 1G, Figure 1-Figure
 120 Supplement 4A), eosinophils (Figure 1-Figure Supplement 5C), and mast cells (Figure 1-Figure
 121 Supplement 5B), but not inflammatory monocytes (Figure 1-Figure Supplement 5A).

122

123 CD4⁺ T cells are ubiquitous in mature human AD lesions⁵⁰ and promote chronic AD itch and
 124 inflammation. More specifically, they play a key role in IL4R α -dependent sensitization of
 125 pruriceptors in the second week of the MC903 model.²² Thus, we were quite surprised to find
 126 that itch behaviors preceded significant CD4⁺ T cell infiltration. Therefore, neutrophils drew our
 127 attention as potential early mediators of MC903 itch. While neutrophil infiltration is a hallmark of
 128 acute inflammation, it remains unclear whether neutrophils contribute to the pathogenesis of
 129 chronic itch. Moreover, neutrophils release known pruritogens, including proteases, reactive
 130 oxygen species, and/or histamine, inflammatory lipids, and cytokines that sensitize and/or
 131 activate pruriceptors.^{51,52} Increased levels of the prostaglandin PGE₂ and the neutrophil-specific
 132 leukotriene LTB₄ have also been reported in skin of AD patients.⁵³ Indeed, by mass
 133 spectrometry, we observed increases in several of these inflammatory lipids, PGD₂ and PGE₂,
 134 as well as LTB₄ and its precursor 5-HETE (Figure 1-Figure Supplement 10A) in MC903-treated
 135 skin, implicating neutrophils in driving AD itch and inflammation. Thus, we next tested the
 136 requirement of neutrophils to itch in the MC903 model.

137

138 **Neutrophils are required for early itch behaviors in the MC903 model of AD**

139 We first asked whether neutrophils, the most abundant population of infiltrating immune cells in
 140 this chronic itch model, were required for MC903-evoked itch. Systemic depletion of neutrophils
 141 using daily injections of an anti-Gr1 (aGr1) antibody^{54,55} dramatically attenuated itch-evoked
 142 scratching through the first eight days of the model (Figure 2A). Consistent with a key role for
 143 neutrophils in driving chronic itch, our depletion strategy significantly and selectively reduced
 144 circulating and skin infiltrating neutrophils on days five and eight, days on which control, but not
 145 depleted mice, scratched robustly (Figure 2B; Figure 2-Figure Supplement 1A-C). In contrast,
 146 basophils and CD4⁺ T cells continued to infiltrate the skin following aGr1 treatment (Figure 2C-
 147 D), suggesting that these cells are not required for early MC903 itch.

148

149 We next used the cheek model of acute itch⁵⁶ to ask whether neutrophil recruitment is sufficient
 150 to trigger scratching behaviors. As expected, we observed significant and selective recruitment
 151 of neutrophils to cheek skin within 15 minutes after CXCL1 injection (Figure 2-Figure
 152 Supplement 2A-B). CXCL1 injection also triggered robust scratching behaviors (Figure 2E) on a

153 similar time course to neutrophil infiltration (Figure 2-Figure Supplement 2B). Thus, we next
154 acutely depleted neutrophils with aGr1 to determine whether neutrophils were required for
155 CXCL1-evoked acute itch. Indeed, aGr1-treatment rapidly reduced circulating neutrophils
156 (Figure 2-Figure Supplement 2C) and resulted in a dramatic loss of CXCL1-evoked itch
157 behaviors (Figure 2C). This effect was specific to neutrophil-induced itch, as injection of
158 chloroquine, a pruritogen that directly activates pruriceptors to trigger itch, still triggered robust
159 scratching in aGr1-treated animals (Figure 2-Figure Supplement 3A). Given that CXCL1 has
160 been shown to directly excite and/or sensitize sensory neurons,^{57,58} it is possible that the
161 mechanism by which CXCL1 elicits itch may also involve neuronal pathways. However, our
162 results show that CXCL1-mediated neutrophil infiltration is sufficient to drive acute itch
163 behaviors, and that neutrophils are necessary for itch in the MC903 model.

164
165 We also examined MC903-evoked itch behaviors in mice deficient in *Cr1f2*, the gene encoding
166 the TSLP Receptor (TSLPR KO mice⁵⁹). TSLPR is expressed by both immune cells and
167 sensory neurons and is a key mediator of AD in humans and in mouse models.^{18–20,31,60}
168 Surprisingly, MC903-treated TSLPR KO mice displayed robust scratching behaviors through the
169 first eight days of the model (Figure 2F). In contrast to our results in aGr1-injected mice, TSLPR
170 KO mice displayed robust neutrophil infiltration (Figure 2G), but completely lacked basophil and
171 CD4⁺ T cell infiltration into the skin (Figure 2H-I, Figure 2-Figure Supplement 4A), and
172 additionally displayed a reduction in mast cells (Figure 2-Figure Supplement 4A). These results
173 suggest that basophils and CD4⁺ T cells are not required for early itch and further support an
174 inciting role for neutrophils. Previous studies have shown that TSLP drives the expression of
175 Type 2 cytokines and related immune cells that promote itch and inflammation in mature AD
176 skin lesions.^{18–20,31,60} Consistent with a later role for TSLP signaling in AD, we did observe a
177 significant reduction in itch-evoked scratching in TSLPR KO mice in the second week of the
178 model (Figure 2F). Thus, our data support a model in which neutrophils are necessary for
179 initiation of AD and itch behaviors early in the development of AD, whereas TSLPR signaling
180 mediates the recruitment of basophils and CD4⁺ T cells to promote later stage itch and chronic
181 inflammation.

182
183 The incomplete loss of itch behaviors on day 12 in the TSLPR KO animals (Figure 2F) raised
184 the question of whether neutrophils might also contribute to itch during the second week of the
185 MC903 model. To directly answer this question, we measured neutrophil infiltration and itch-
186 evoked scratching on day 12 in mice that received either aGr1 or PBS on days 8-11 of the
187 model to selectively deplete neutrophils solely during the second week. Neutrophil depletion in
188 the second week with aGr1 robustly decreased skin-infiltrating neutrophils (Figure 2J), and
189 substantially reduced scratching behaviors at day 12 (Figure 2K), supporting a role for
190 neutrophils in chronic itch. Interestingly, we observed a 79% mean reduction in time spent
191 scratching after neutrophil depletion at day 12, whereas loss of TSLPR effected a 44%
192 reduction in time spent scratching. We speculate that neutrophils and TSLP signaling comprise
193 independent mechanisms that together account for the majority of AD itch. In order to ascertain
194 whether neutrophils could be salient players in other models of AD, and not just MC903, we
195 measured neutrophil infiltration into ear skin in the 1-fluoro-2,4-dinitrobenzene (DNFB) model of
196 atopic dermatitis, which relies on hapten-induced sensitization to drive increased IgE, mixed
197 Th1/Th2 cytokine response, skin thickening, inflammation, and robust scratching behaviors in
198 mice.^{61–63} Indeed, neutrophils also infiltrated DNFB- but not vehicle-treated skin (Figure 2-Figure
199 Supplement 5A). Taken together, these observations are complementary to published datasets
200 showing evidence for neutrophil chemokines and transcripts in human AD lesions.^{11,12,13–15}
201 Overall, our data support a key role for neutrophils in promoting AD itch and inflammation.

202
203 **MC903 drives rapid and robust changes in the peripheral and central nervous systems**

204 But how do neutrophils drive AD itch? Itchy stimuli are detected and transduced by specialized
 205 subsets of peripheral somatosensory neurons. Thus, to answer this question we first profiled the
 206 transcriptional changes in somatosensory neurons in the MC903 model, which were previously
 207 unstudied. In general, little is known regarding neuronal changes in chronic itch. Our initial
 208 examination of early hyperinnervation and changes in axon guidance molecules in skin
 209 suggested that neurons are indeed affected early on in the MC903 model, before the onset of
 210 itch-evoked scratching behaviors. In contrast to the skin, where we saw many early
 211 transcriptional changes, we did not see any significant transcriptional changes in the trigeminal
 212 ganglia (TG) until five days after the first treatment, and in total only 84 genes were differentially
 213 expressed through the eighth day (Figure 3A-B). These hits included genes related to
 214 excitability of itch sensory neurons,^{51,64} neuroinflammatory genes,⁶⁵ and activity-induced or
 215 immediate early genes (Figure 3A). Interestingly, we observed enrichment of neuronal markers
 216 expressed by one specific subset of somatosensory neurons that are dedicated to itch (*Il31ra*,
 217 *Osmr*, *Trpa1*, *Cysltr2*, and *Nppb*), termed “NP3” neurons.^{51,64,66,67} Similar to what has been
 218 reported in mouse models of chronic pain, we observed changes in neuroinflammatory (*Bdnf*,
 219 *Nptx1*, *Nptx2*, *Nptxr*) and immune genes (*Itk*, *Cd19*, *Rag*, *Tmem173*). However, these
 220 transcriptional changes occurred just a few days after itch onset, in contrast to the slow changes
 221 in nerve injury and pain models that occur over weeks, indicating that neuropathic changes may
 222 occur sooner than previously thought in chronic itch. These changes occurred in tandem with
 223 the onset of scratching behaviors (Figure 1C), suggesting that the early molecular and cellular
 224 changes we observed by this time point may be important for development or maintenance of
 225 itch-evoked scratching.

226
 227 The changes we observed in immune-related genes in the TG were suggestive of infiltration or
 228 expansion of immune cell populations, which has been reported in models of nerve injury and
 229 chronic pain, but has never been reported in chronic itch. To validate our observations, we used
 230 IHC to ask whether CD45⁺ immune cells increase in the TG. We observed a significant increase
 231 in TG immune cell counts at day eight but not day five (Figure 3C-F, Figure 3-Figure
 232 Supplement 1A-D). Because we observed such dramatic expression changes in the TG on day
 233 eight of the model, we postulated that the CNS may also be affected by this time point. Thus,
 234 we performed RNA-seq on spinal cord segments that innervate the MC903-treated rostral back
 235 skin of mice. To date, only one study has examined changes in the spinal cord during chronic
 236 itch.⁶⁸ The authors showed that upregulation of the STAT3-dependent gene *Lcn2* occurred three
 237 weeks after induction of chronic itch and was essential for sustained scratching behaviors.
 238 Surprisingly, we saw upregulation of *Lcn2* on day eight of the MC903 model and, additionally,
 239 we observed robust induction of immediate early genes (*Fos*, *Junb*, Figure 3G), suggesting that
 240 MC903 itch drives activity-dependent changes in the spinal cord as early as one week after
 241 beginning treatment. Together, our findings show that sustained itch and inflammation can drive
 242 changes in the PNS and CNS much sooner than previously thought, within days rather than
 243 weeks after the onset of scratching. We next set out to explore how loss of neutrophils impacts
 244 the molecular changes observed in skin and sensory neurons in the MC903 model, and which
 245 of these changes might contribute to neutrophil-dependent itch.

246
 247 **Neutrophils are required for upregulation of select itch- and atopic-related genes,**
 248 **including the itch-inducing chemokine CXCL10**

249 To ask how neutrophils promote itch in the MC903 model, we examined the transcriptional
 250 changes in skin and sensory ganglia isolated from non-itchy neutrophil-depleted animals and
 251 from the TSLPR KO mice, which scratched robustly. A number of AD-associated cytokines that
 252 were upregulated in control MC903 skin were not upregulated in TSLPR KO and neutrophil-
 253 depleted skin. For example, *Il33* upregulation is both neutrophil- and TSLPR-dependent (Figure
 254 4A, Figure 4-Figure Supplement 1A). By contrast, upregulation of epithelial-derived cytokines

255 and chemokines *Tslp*, *Cxcl1*, *Cxcl2*, *Cxcl3*, and *Cxcl5* was unaffected by either loss of TSLPR
256 or neutrophil depletion (Figure 4B), suggesting these molecules are produced by skin cells even
257 when the MC903-evoked immune response is compromised. Consistent with previous studies,
258 *Ilf4* upregulation was completely dependent on TSLPR but not neutrophils, establishing a role for
259 TSLP signaling in the Type 2 immune response. Among the hundreds of MC903-dependent
260 genes we examined, only a handful of genes were uniquely affected by neutrophil depletion.
261 One such gene was *Cxcl10*, a chemokine known to be released by skin epithelial cells,
262 neutrophils, and other myeloid cells.^{52,69-74} *Cxcl10* expression was increased in TSLPR KO but
263 not neutrophil-depleted skin (Figure 4B, Figure 4-Figure Supplement 1A). CXCL10 has been
264 previously shown to drive acute itch in a model of allergic contact dermatitis via CXCR3
265 signaling in sensory neurons,⁷⁵ and is elevated in skin of AD patients.⁴⁹ Expression of *Cxcl9* and
266 *Cxcl11*, two other CXCR3 ligands that are elevated in AD but have an unknown role in itch, was
267 also decreased in AD skin of neutrophil-depleted mice (Figure 4B).

268

269 CXCR3 signaling is necessary for MC903-evoked chronic itch

270 We hypothesized that neutrophil-dependent upregulation of CXCL10 activates sensory neurons
271 to drive itch behaviors. Consistent with this model, neutrophil depletion attenuated the
272 expression of activity-induced immediate early genes (*Vgf*, *Junb*) in the TG, suggestive of
273 neutrophil-dependent sensory neuronal activity (Figure 4C, Figure 4-Figure Supplement 1B).
274 We found that neutrophils also contributed to other sensory neuronal phenotypes in the model.
275 For example, we observed that expression of *Lcn2*, a marker of neuropathic itch, and activity-
276 induced genes *Fos* and *Junb* were not increased in spinal cord isolated from neutrophil-
277 depleted animals, indicating that neutrophil-dependent scratching behaviors may indeed drive
278 changes in the CNS (Figure 4D). We also observed that neutrophil-depleted animals displayed
279 no skin hyperinnervation at day two (Figure 4E). This result was surprising because we did not
280 observe significant neutrophil infiltration at this early time point, but these data suggest that low
281 numbers of skin neutrophils are sufficient to mediate these early effects.

282

283 To test our model wherein CXCL10 activates CXCR3 to drive neutrophil-dependent itch, we first
284 asked whether this CXCR3 ligand is in fact released in MC903-treated skin. We performed
285 ELISA on cheek skin homogenate and found that CXCL10 protein was increased in MC903-
286 treated skin from uninjected wild-type and TSLPR KO animals, but not in skin from neutrophil-
287 depleted mice (Figure 4F). To test whether CXCR3 signaling directly contributes to AD itch, we
288 asked whether acute blockade of CXCR3 using the antagonist AMG 487⁷⁵ affected scratching
289 behaviors in the MC903 model. We found that the CXCR3 antagonist strongly attenuated
290 scratching behaviors on days five, eight, and twelve (Figure 4G), with the greatest effect at day
291 eight. In contrast, CXCR3 blockade did not attenuate scratching behaviors in naive mice
292 injected with the pruritogen chloroquine (Figure 4G), demonstrating that CXCR3 signaling
293 contributes to chronic itch but is not required for scratching in response to an acute pruritogen.
294 Thus, we propose that neutrophils promote chronic itch in atopic dermatitis via upregulation of
295 CXCL10 and subsequent activation of CXCR3-dependent itch pathways (Figure 5).

296

297 Discussion

298 There is great interest in unraveling the neuroimmune interactions that promote acute and
299 chronic itch. Here, we show that neutrophils are essential for the early development of MC903-
300 evoked itch. We further show that the recruitment of neutrophils to the skin is sufficient to drive
301 itch behaviors within minutes of infiltration. While neutrophils are known to release a variety of
302 pruritogens, their roles in itch and AD were not studied.⁵² Only a few studies have even reported
303 the presence of neutrophils in human AD lesions.^{12,76-78} Neutrophils have been implicated in
304 psoriatic inflammation and inflammatory pain,⁷⁹⁻⁸⁶ where they are thought to rapidly respond to
305 tissue injury and inflammation,⁸⁷ but they have not been directly linked to itch.

306
307 There is a strong precedence for immune cell-neuronal interactions that drive modality-specific
308 outcomes, such as itch versus pain, under distinct inflammatory conditions. In allergy, mast cells
309 infiltrate the upper dermis and epidermis and release pruritogens to cause itch,^{67,88} whereas in
310 tissue injury, mast cell activation can trigger pain hypersensitivity.⁸⁹ Likewise, neutrophils are
311 also implicated in both pain and itch. For example, pyoderma gangrenosum, which causes
312 painful skin ulcerations recruits neutrophils to the deep dermal layers to promote tissue damage
313 and pain.⁵² In AD, neutrophils are recruited to the upper dermis and epidermis,^{12,78} and we now
314 show that neutrophils trigger itch in AD. Adding to the complex and diverse roles of neutrophils,
315 neutrophils recruited to subcutaneous sites during invasive streptococcal infection alleviate pain
316 by clearing the tissue of bacteria.⁹⁰ Several potential mechanisms may explain these diverse
317 effects of neutrophils. First, the location of the inflammatory insult could promote preferential
318 engagement of pain versus itch nerve fibers.⁵² This is supported by observations that neutrophil-
319 derived reactive oxygen species and leukotrienes can promote either itch or pain under different
320 inflammatory conditions.⁹¹⁻⁹⁴ Second, it has been proposed that there are distinct functional
321 subsets of neutrophils that release modality-specific inflammatory mediators.⁹⁵ Third, the
322 disease-specific inflammatory milieu may induce neutrophils to specifically secrete mediators of
323 either itch or pain. Indeed, all three of these mechanisms have been proposed to underlie the
324 diverse functions of microglia and macrophages in homeostasis, tissue repair, injury, and
325 neurodegenerative disease.⁹⁶ It will be of great interest to the field to decipher the distinct
326 mechanisms by which neutrophils and other immune cells interact with the nervous system to
327 drive pain and itch.

328
329 In addition to neutrophils, TSLP signaling and the Type 2 immune response plays an important
330 role in the development of itch in the second week of the MC903 model. Dendritic cells, mast
331 cells, basophils, and CD4⁺ T cells are all major effectors of the TSLP inflammatory pathway in
332 the skin. We propose that neutrophils play an early role in triggering itch and also contribute to
333 chronic itch in parallel with the TSLP-Type 2 response. While we have ruled out an early role for
334 TSLP signaling and basophils and CD4⁺ T cells in early itch,^{67,88} other cell types such as mast cells,
335 which have recently been linked directly to chronic itch,^{67,88} and dendritic cells may be playing
336 an important role in setting the stage for itch and inflammation prior to infiltration of neutrophils.

337
338 Given the large magnitude of the itch deficit in the neutrophil-depleted mice, we were surprised
339 to find fewer expression differences in MC903-dependent, AD-associated genes between
340 neutrophil depleted and non-depleted mice than were observed between WT and TSLPR KO
341 mice. One of the few exceptions were the Th1-associated genes *Cxcl9/10/11*.^{11,97} We found that
342 induction of these genes and of CXCL10 protein was completely dependent on neutrophils.
343 While our results do not identify the particular cell type(s) responsible for neutrophil-dependent
344 CXCL10 production, a number of cell types present in skin have been shown to produce
345 CXCL10, including epithelial keratinocytes, myeloid cells, and sensory neurons.^{52,69-74} In support
346 of a role for neutrophils in promoting chronic itch, we observed striking differences in neutrophil-
347 dependent gene expression in the spinal cord, where expression of activity-induced genes and
348 the chronic itch gene *Lcn2* were markedly attenuated by loss of neutrophils. Moreover, we also
349 demonstrate that depletion of neutrophils in the second week of the MC903 model can
350 attenuate chronic itch-evoked scratching. In examining previous characterizations of both
351 human and mouse models of AD and related chronic itch disorders, several studies report that
352 neutrophils and/or neutrophil chemokines are indeed present in chronic lesions.^{11-16,98-102} Our
353 observations newly implicate neutrophils in setting the stage for the acute-to-chronic itch
354 transition by triggering molecular changes necessary to develop a chronic, itchy lesion and also
355 contributing to persistent itch.

356

357 Additionally, we demonstrate a novel role of CXCR3 signaling in MC903-induced itch. The
358 CXCR3 ligand CXCL10 contributes to mouse models of acute and allergic itch;^{75,103,104} however,
359 its role in chronic itch was previously unknown. We speculate that the residual itch behaviors
360 after administration of the CXCR3 antagonist could be due to TSLPR-dependent IL-4 signaling,
361 as TSLPR-deficient mice display reduced itch behaviors by the second week of the model, or
362 due to some other aspect of neutrophil signaling, such as release of proteases, leukotrienes,
363 prostaglandins, or reactive oxygen species, all of which can directly trigger itch via activation of
364 somatosensory neurons.⁵² Our observations are in alignment with a recent study showing that
365 dupilumab, a new AD drug that blocks IL4R α , a major downstream effector of the TSLP
366 signaling pathway, does not significantly reduce CXCL10 protein levels in human AD lesions.¹⁰⁵
367 Taken together, these findings suggest that the TSLP/IL-4 and neutrophil/CXCL10 pathways are
368 not highly interdependent, and supports our findings that *Il4* transcript is robustly upregulated in
369 the absence of neutrophils. Additionally, targeting IL4R α signaling has been successful in
370 treating itch and inflammation in some, but not all, AD patients.¹⁰⁶ We propose that biologics or
371 compounds targeting neutrophils and/or the CXCR3 pathway may be useful for AD that is
372 incompletely cleared by dupilumab monotherapy. Drugs targeting neutrophils are currently in
373 clinical trials for the treatment of psoriasis, asthma, and other inflammatory disorders. For
374 example, MDX-1100, a biologic that targets CXCL10, has already shown efficacy for treatment
375 of rheumatoid arthritis in phase II clinical trials.¹⁰⁷ While rheumatoid arthritis and AD have
376 distinct etiologies,¹⁰⁸ our body of work indicates that CXCL10 or CXCR3 may be promising
377 targets for treating chronic itch. Our findings may also be applicable to other itch disorders
378 where neutrophil chemoattractants and/or CXCL10 are also elevated, such as psoriasis and
379 allergic contact dermatitis. Overall, our data suggest that neutrophils incite itch and inflammation
380 in early AD through several mechanisms, including: 1) directly triggering itch upon infiltration
381 into the skin, as shown by acute injection of CXCL10, and, 2) indirectly triggering itch by altering
382 expression of endogenous pruritogens (e.g. induction of *Cxcl10* expression^{52,69-74}). Together,
383 these direct and indirect mechanisms for neutrophil-dependent itch may explain why neutrophils
384 have a dramatic effect on scratching behaviors on not only days eight and twelve but also day
385 five of the model, when neutrophils are recruited in large numbers, but CXCR3 ligands are not
386 as robustly induced.

387
388 More generally, our study provides a framework for understanding how and when human
389 chronic itch disease genes contribute to the distinct stages of AD pathogenesis. Our analysis of
390 MC903-evoked transcriptional changes suggests we may be able to extend findings in the
391 model not only to atopic dermatitis, but also to related disorders, including specific genetic forms
392 of atopy. For example, we provide evidence that MC903 treatment may also model the filaggrin
393 loss-of-function mutations, which are a key inciting factor in human heritable atopic disease.^{45,46}
394 There are many rich datasets looking at mature patient lesions and datasets for mature lesions
395 in other mouse models of chronic itch.^{11-13,15,16,22,101,109} Our study adds a temporal frame of
396 reference to these existing datasets and sets the stage for probing the function of AD disease
397 genes in greater detail. Furthermore, we have mapped the time course of gene expression
398 changes in primary sensory ganglia and spinal cord during chronic itch development. We show
399 that the MC903 model recapitulates several hallmarks of neuropathic disease on a time course
400 much shorter than has been reported for chronic itch, or chronic pain. Nervous system tissues
401 are extremely difficult to obtain from human AD patients, and thus little is known regarding the
402 neuronal changes in chronic itch disorders in both mouse models and human patients. Our
403 findings can now be compared to existing and future datasets examining neuronal changes in
404 chronic pain, diabetic neuropathy, shingles, neuropathic itch, psoriasis, and other inflammatory
405 disorders where neuronal changes are poorly understood but may contribute to disease
406 progression. The early changes we see in skin innervation, sensory ganglia, and spinal cord
407 dovetail with recent studies examining neuroimmune interactions in other inflammatory

408 conditions,^{90,110–112} which all implicate early involvement of sensory neurons in the pathogenesis
 409 of inflammatory diseases.

410
 411 **Figure 1. The MC903 model parallels the progression of human atopic disease and**
 412 **suggests a temporal sequence of AD pathogenesis. A.** Exact permutation test (10,000
 413 iterations, see Methods) for significance of mean absolute log₂ fold change in gene expression
 414 at Day 8 (MC903 vs. ethanol) of custom-defined groups of genes for indicated categories (see
 415 **Figure 1-source data 1**). **B.** Log₂ fold change in gene expression (MC903 vs. ethanol) in
 416 mouse skin at indicated time points for key immune and mouse/human AD genes that were
 417 significantly differentially expressed for at least one time point in the MC903 model. Only genes
 418 from our initial list (see Methods) differentially expressed at corrected $p < 0.05$ and changing $>$
 419 2-fold between treatments for at least one condition are shown. Green bars = increased
 420 expression in MC903 relative to ethanol; magenta = decreased expression. Exact values and
 421 corrected p -values are reported in **Figure 1-source data 2** and **Supplemental Data**,
 422 respectively. D1 = 6 hours post-treatment; D2 = Day 2; D5 = Day 5; D8 = Day 8. **C.** Scratching
 423 behavior of mice treated with MC903 or ethanol for indicated length of time (two-way ANOVA:
 424 **** $p_{\text{interaction}} < 0.0001$, $F(2,409) = 13.25$; Sidak's multiple comparisons: $p_{\text{day } 3} = 0.1309$, $n=62,51$
 425 mice; * $p_{\text{day } 5} = 0.0171$, $n=69,56$ mice; **** $p_{\text{day } 8} < 0.0001$, $n=92,85$ mice). Exact values displayed
 426 in **Figure 1-source data 3**. **D.** Log₂ fold change in gene expression of neutrophil
 427 chemoattractants (upper), Th2 cytokines (middle) and T cell chemoattractants (lower, from
 428 RNA-seq data). **E.** Neutrophil counts in MC903- and ethanol-treated skin at indicated time
 429 points (two-way ANOVA: ** $p_{\text{treatment}} = 0.0023$, $F(1,102) = 9.82$; Sidak's multiple comparisons: $p_{\text{day } 2}$
 430 > 0.999 , $n=4,4$ mice; $p_{\text{day } 3} = 0.9801$, $n=5,5$ mice; *** $p_{\text{day } 5} = 0.0003$, $n=6,8$ mice; *** $p_{\text{day } 8}$
 431 $= 0.0001$, $n=40,38$ mice). **F.** Basophil counts in MC903- and ethanol-treated skin at indicated time
 432 points (two-way ANOVA: ** $p_{\text{treatment}} = 0.0051$, $F(1,102) = 8.17$; Sidak's multiple comparisons: $p_{\text{day } 2}$
 433 > 0.999 , $n=4,4$ mice; $p_{\text{day } 3} = 0.8850$, $n=5,5$ mice; $p_{\text{day } 5} = 0.0606$, $n=6,8$ mice; **** $p_{\text{day } 8} <$
 434 0.0001 , $n=40,38$ mice). **G.** CD4⁺ T cell counts in MC903- and ethanol-treated skin at indicated
 435 time points (two-way ANOVA: ** $p_{\text{time}} = 0.0042$, $F(1,44) = 9.10$; $p_{\text{day } 3} = 0.9998$, $n=8,6$ mice; $p_{\text{day } 5}$
 436 $= 0.2223$, $n=9,8$ mice; ** $p_{\text{day } 8} = 0.0021$, $n=11,8$ mice). Day 8 immune cell infiltrate represented
 437 as % of CD45⁺ cells in **Figure 1-Figure Supplement 2A-B** (see **Supplementary File 3** for all
 438 experimental conditions). Exact values displayed in **Figure 1-source data 4** and representative
 439 FACS plots for myeloid and T cell gating shown in **Figure 1-Figure Supplement 3A** and **Figure**
 440 **1-Figure Supplement 4A**. For Figure 4E-G, data from mice receiving i.p. injection of PBS (see
 441 Figure 4) in addition to MC903 or EtOH are also included. **H.** (Upper and Lower) Representative
 442 maximum intensity Z-projections from immunohistochemistry (IHC) of whole-mount mouse skin
 443 on Day 2 of the MC903 model. Skin was stained with neuronal marker beta-tubulin III (BTIII;
 444 green). Hair follicle autofluorescence is visible in the magenta channel. Images were acquired
 445 on a confocal using a 20x water objective. **I.** Quantification of innervation (see Methods) of
 446 mouse skin as determined from BTIII staining (* $p = 0.012$; two-tailed t-test ($t = 3.114$; $df = 9$); $n =$
 447 $7,4$ images each from 2 mice per treatment). Day 1 IHC results as follows: 31.78 ± 18.39 %
 448 (MC903) and 31.51 ± 16.43 % (EtOH); $p = 0.988$; two-tailed unpaired t-test; $n = 6$ images each
 449 from 2 mice per treatment. Exact values are reported in **Figure 1-source data 5**. **J.**
 450 Quantification of CGRP⁺ nerve fibers (see Methods) in skin (** $p = 0.0083$; two-tailed t-test (t
 451 $= 2.868$; $df = 25$); $n = 15$, 12 images from 3 mice per treatment). Exact values are reported in
 452 **Figure 1-source data 5**. Representative images in **Figure 1-Figure Supplement 9A**.

453
 454 **Figure 1-Figure Supplement 1. Expression of mouse and human itch genes. A.** Log₂ fold
 455 change in gene expression (MC903 vs. ethanol) in mouse skin at indicated time points for
 456 genes implicated in mouse or human acute or chronic itch that were significantly differentially
 457 expressed for at least one time point in the MC903 model. Green bars = increased expression

458 in MC903 relative to ethanol; magenta = decreased expression. Exact values and corrected p -
 459 values are reported in **Figure 1-source data 6** and **Supplemental Data**, respectively.

460
 461 **Figure 1-Figure Supplement 2. Immune cells represented as % of CD45⁺ cells. A.** Number
 462 of CD45⁺ cells in MC903-treated skin on days 2-8 of the model. **B.** Skin-infiltrating immune cell
 463 subtypes on days 2-8 of the MC903 model shown in **Figure 1**, represented as % of CD45⁺ cells.
 464 CD4⁺ T cell measurements were acquired using a separate staining panel from different animals
 465 than the myeloid cell measurements (see Methods) and were not included. See
 466 **Supplementary File 3** for % of CD45⁺ cell measurements for all flow cytometry experiments.
 467 Error bars represent mean \pm SEM.

468
 469 **Figure 1-Figure Supplement 3. Myeloid and granulocyte gating strategy. A-C.**
 470 Representative FACS plots of cells isolated from MC903-treated cheek skin showing gating
 471 strategy for neutrophils (A), inflammatory monocytes (A), mast cells (B), basophils (B), and
 472 eosinophils (C) as shown in **Figure 1E-F** and **Figure 1-Figure Supplement 5**.

473
 474 **Figure 1-Figure Supplement 4. T cell gating strategy. A.** Representative FACS plots of cells
 475 isolated from MC903-treated cheek skin showing gating strategy for CD4⁺ T cells as shown in
 476 **Figure 1G**.

477
 478 **Figure 1-Figure Supplement 5. Immune cell counts in MC903-treated skin. A.** Inflammatory
 479 monocyte counts in MC903- and ethanol-treated skin at indicated time points (two-way ANOVA:
 480 $p_{\text{treatment}} = 0.0662$, $F(1,102) = 3.44$; $n=4,4,5,5,6,8,40,38$ mice). **B.** Mast cell counts in MC903- and
 481 ethanol-treated skin at indicated time points (two-way ANOVA: $**p_{\text{treatment}} = 0.0024$, $F(1,102) =$
 482 9.69 ; Sidak's multiple comparisons: $p_{\text{day } 2} > 0.999$, $n=4,4$ mice; $p_{\text{day } 3} = 0.3019$, $n=5,5$ mice; $p_{\text{day } 5}$
 483 $= 0.0586$, $n=6,8$ mice; $****p_{\text{day } 8} < 0.0001$, $n=40,38$ mice). **C.** Eosinophil counts in MC903- and
 484 ethanol-treated skin at indicated time points (two-way ANOVA: $p_{\text{time}} = 0.0471$, $F(3,102) = 2.74$;
 485 Sidak's multiple comparisons: $p_{\text{day } 2} > 0.999$, $n=4,4$ mice; $p_{\text{day } 3} = 0.3596$, $n=5,5$ mice; $p_{\text{day } 5} =$
 486 0.9998 , $n=6,8$ mice; $**p_{\text{day } 8} = 0.0020$, $n=40,38$ mice). Data from mice receiving i.p. injection of
 487 PBS (see Figure 4) in addition to MC903 or EtOH are also included. Exact values displayed in
 488 **Figure 1-source data 4**.

489
 490 **Figure 1-Figure Supplement 6. Protease receptor activation triggers rapid upregulation of**
 491 **neutrophil chemoattractant genes in human keratinocytes. A.** Heat map showing \log_2 fold
 492 change in gene expression in cultured human keratinocytes 3 hours after SLIGRL treatment
 493 (100 μM ; bottom; see **Figure 1-source data 7**) compared to vehicle controls, as measured by
 494 RNA-seq. Genes are sorted by descending corrected p -value; only significantly differentially
 495 expressed ($p < 0.05$) are displayed. Exact values and corrected p -values are reported in **Figure**
 496 **1-source data 7** and **Supplemental Data**, respectively.

497
 498 **Figure 1-Figure Supplement 7. Expression of neuronal genes and axon guidance**
 499 **molecules in skin. A.** \log_2 fold change in gene expression (MC903 vs. EtOH) in mouse skin at
 500 indicated time points for markers of locally translated sensory neuronal transcripts or genes
 501 implicated in neurite remodeling and/or axon guidance that were significantly differentially
 502 expressed for at least one time point in the MC903 model. Green bars = increased expression
 503 in MC903 relative to ethanol; magenta = decreased expression. Exact values and corrected p -
 504 values are reported in **Figure 1-source data 8** and **Supplemental Data**, respectively.

505
 506 **Figure 1-Figure Supplement 8. Method of image quantification for whole mount skin. A.**
 507 Representative maximum intensity z-projection of beta tubulin III staining in cheek skin. **B.**

508 Binary image after edge-detection. **C.** % Area innervated was calculated from the percentage of
509 the image area which was occupied by the regions of interest (ROIs) outlined in red.

510
511 **Figure 1-Figure Supplement 9. Peptidergic fibers display hyperinnervation in MC903-**
512 **treated skin. A.** Representative maximum intensity Z-projections from immunohistochemistry
513 (IHC) of whole-mount mouse skin on day 2 of the MC903 model. Skin was stained with
514 peptidergic neuronal marker Calcitonin related-gene peptide (CGRP; white). Images were
515 acquired on a confocal microscope using a 20x water objective.

516
517 **Figure 1-Figure Supplement 10. Inflammatory lipids in MC903-treated skin. A.**
518 Quantification of indicated lipids from 6 mm biopsy punches of cheek skin of MC903- and EtOH-
519 treated mice (at day 8) by LC-MS/MS (**p = 0.006 ($t=4.148, df=6$), *p = 0.024 ($t=3.003, df=6$),
520 ***p = 0.0007 ($t=6.392, df=6$), *p = 0.022 ($t=3.058, df=6$); two-tailed unpaired t-tests; n = 4 mice
521 per group, see **Figure 1-source data 8**).

522
523 **Figure 1-source data 1.** Values displayed in the bar plot shown in Figure 1A.
524 **Figure 1-source data 2.** Values displayed in the heat map shown in Figure 1B.
525 **Figure 1-source data 3.** Values displayed in the bar plot shown in Figure 1C.
526 **Figure 1-source data 4.** Values displayed in the bar plots shown in Figure 1E-G and Figure 1-
527 Figure Supplement 5A-C.
528 **Figure 1-source data 5.** Values displayed in the bar plots shown in Figure 1I and Figure 1J.
529 **Figure 1-source data 6.** Values displayed in the heat map shown in Figure1-Figure
530 Supplement 1A.
531 **Figure 1-source data 7.** Values displayed in the heat map shown in Figure1-Figure
532 Supplement 6A.
533 **Figure 1-source data 8.** Values displayed in the heat map shown in Figure1-Figure
534 Supplement 7A.
535 **Figure 1-source data 9.** Values displayed in the bar plot shown in Figure1-Figure Supplement
536 10A.

537
538 **Supplementary File 1.** Number of mapped reads and sample information for all RNA-seq
539 samples represented in the manuscript.

540
541 **Supplementary File 2.** Outputs of statistical tests performed on behavioral and flow cytometry
542 data to determine whether select data sets could be combined.

543
544 **Supplementary File 3.** All flow cytometry data from Figures 1-2 represented as % of CD45⁺
545 cells.

546
547 **Supplemental Data.** DESeq differential expression output tables for all RNA-seq experiments
548 in the manuscript.

549

550 **Figure 2. Neutrophils are necessary and sufficient for itch behaviors. A.** Scratching
 551 behavior of uninjected and PBS-injected mice (combined) and aGr1-injected mice treated with
 552 MC903 or ethanol for indicated length of time (two-way ANOVA: **** $p_{\text{interaction}} < 0.0001$, $F(4,447)$
 553 $= 7.16$; Tukey's multiple comparisons: $p_{\text{day 3 MC903 vs. EtOH}} = 0.1111$ $n=62,51,17$ mice; * $p_{\text{day 5 MC903 vs. EtOH}} = 0.0154$,
 554 $p_{\text{day 5 MC903 vs. aGr1}} = 0.9854$, $p_{\text{day 5 aGr1 vs. EtOH}} = 0.2267$, $n=69,56,17$ mice; **** $p_{\text{day 8 MC903 vs. EtOH}} < 0.0001$,
 555 **** $p_{\text{day 8 MC903 vs. aGr1}} = 0.0007$, $p_{\text{day 8 aGr1 vs. EtOH}} = 0.1543$, $n=92,85,17$ mice). **B.** Neutrophil count from cheek skin of uninjected/PBS-injected MC903- and ethanol-treated,
 556 and aGr1-injected MC903-treated mice on day 8 (one-way ANOVA: **** $p < 0.0001$, $F(2,92) = 10.59$; Tukey's multiple comparisons: **** $p_{\text{MC903 vs. EtOH}} < 0.00001$, $n=40,38$ mice; * $p_{\text{MC903 vs. aGr1 MC903}} = 0.0109$, $n=40,17$ mice; $p_{\text{aGr1 vs. EtOH}} = 0.8859$, $n=38,17$ mice). **C.** Basophil count from
 560 cheek skin of uninjected/PBS-injected MC903- and ethanol-treated, and aGr1-injected MC903-
 561 treated mice on day 8 (one-way ANOVA: **** $p = 0.0001$, $F(2,92) = 14.61$; Tukey's multiple
 562 comparisons: $p_{\text{MC903 vs. aGr1 MC903}} = 0.3217$, $n=40,17$ mice, **** $p_{\text{MC903 vs. EtOH}} < 0.0001$, $n=40,38$
 563 mice, * $p_{\text{aGr1 MC903 vs. EtOH}} = 0.0204$, $n=17,38$ mice). **D.** CD4⁺ T cell count from cheek skin of PBS-
 564 injected MC903- and ethanol-treated, and aGr1-injected MC903-treated mice on day 8 (two-way
 565 ANOVA: ** $p_{\text{treatment}} = 0.0035$, $F(1,35) = 9.82$; Holm-Sidak multiple comparisons for PBS versus
 566 aGr1: $p_{\text{MC903}} = 0.8878$, $n=9,11$ mice; $p_{\text{EtOH}} = 0.5201$, $n=8,9$ mice). Control MC903 and EtOH data
 567 from **Figure 2B-C** are also displayed in **Figure 1**. Exact values displayed for **Figure 2A-D** in
 568 **Figure 2-source data 1**. **E.** Scratching behavior of mice immediately after injection of 1 μg
 569 CXCL1 or PBS (s.c. cheek). For neutrophil-depletion experiments, mice received 250 μg anti-
 570 Gr1 (aGr1) 20 hours prior to cheek injection of CXCL1 or PBS (one-way ANOVA: **** $p < 0.0001$, $F(4,88) = 75.53$; Tukey's multiple comparisons: * $p_{\text{CXCL1 vs. PBS}} = 0.0126$, $n=36,31$ mice;
 571 $p_{\text{aGr1-CXCL1 vs. aGr1-PBS}} > 0.9999$, $n=10,10$ mice; $p_{\text{aGr1-CXCL1 vs. PBS}} = 0.9986$, $n=10,31$ mice). Exact
 572 values displayed in **Figure 2-source data 2**. **F.** Scratching behavior of WT and TSLPR KO
 573 (TSLPR KO) mice treated with MC903 or ethanol for indicated length of time (two-way ANOVA:
 574 **** $p_{\text{interaction}} < 0.0001$, $F(9,657) = 4.93$; Tukey's multiple comparisons: **** $p_{\text{day 8 WT MC903 vs. EtOH}} < 0.0001$,
 575 * $p_{\text{day 8 WT MC903 vs. KO MC903}} = 0.0194$, ** $p_{\text{day 8 KO MC903 vs. KO EtOH}} = 0.0039$, $n=92,85,36,26$ mice;
 576 **** $p_{\text{day 12 WT MC903 vs. EtOH}} < 0.0001$, ** $p_{\text{day 12 WT MC903 vs. KO MC903}} = 0.0028$, $p_{\text{day 12 KO MC903 vs. KO EtOH}} = 0.7061$, $n=26,26,27,23$ mice). **G.** Neutrophil count from cheek skin of wild-type MC903- and
 577 ethanol-treated, and TSLPR KO MC903-treated mice on day 5 (two-way ANOVA: ** $p_{\text{genotype}} = 0.0025$, $F(2,125) = 6.28$; Tukey's multiple comparisons: **** $p_{\text{day 5 WT MC903 vs. WT EtOH}} < 0.0001$,
 578 $n=6,8$ mice; $p_{\text{day 5 WT MC903 vs. KO MC903}} = 0.2198$, $n=6,6$ mice; * $p_{\text{day 5 WT EtOH vs. KO MC903}} = 0.0212$, $n=8,6$
 579 mice). **H.** Basophil count from cheek skin of wild-type MC903- and ethanol-treated, and TSLPR
 580 KO MC903-treated mice on day 8 (two-way ANOVA: ** $p_{\text{genotype}} = 0.0003$, $F(2,117) = 8.87$;
 581 Tukey's multiple comparisons: **** $p_{\text{day 8 WT MC903 vs. WT EtOH}} < 0.0001$, $n=40,38$ mice; **** $p_{\text{day 8 WT MC903 vs. KO MC903}} < 0.0001$, $n=40,15$ mice; $p_{\text{day 8 WT EtOH vs. KO MC903}} = 0.9519$, $n=38,15$ mice). See also
 582 **Figure 2-Figure Supplement 5A**. For **Figures 2G-H**, data from days 3, 5, and 8 are presented
 583 in **Figure 2-source data 3**. **I.** CD4⁺ T cell count from cheek skin of wild-type MC903- and
 584 ethanol-treated, and TSLPR KO MC903-treated mice on day 8 (one-way ANOVA: ** $p = 0.0053$,
 585 $F(2,24) = 6.564$; Tukey's multiple comparisons: * $p_{\text{WT MC903 vs. WT EtOH}} = 0.0163$, $n=11,8$ mice; * $p_{\text{MC903 vs. KO MC903}} = 0.0130$, $n=11,8$ mice; $p_{\text{WT EtOH vs. KO MC903}} = 0.9953$, $n=8,8$ mice). Wild-type
 586 MC903 and EtOH data from **2F-H** are also displayed in **Figure 1**. Exact values for **Figure 2F-I**
 587 displayed in **Figure 2-source data 3**. **J.** Neutrophil count from cheek skin of wild-type MC903-
 588 and ethanol-treated mice on day 12 of the MC903 model. MC903-treated animals received daily
 589 i.p. injections of 250 μg aGr1 antibody or PBS (250 μL) on days 8-11 of the model (one-way
 590 ANOVA: * $p = 0.01$, $F(2,13) = 6.69$; Tukey's multiple comparisons: * $p_{\text{MC903-PBS vs. EtOH}} = 0.0141$,
 591 $n=6,5$ mice; * $p_{\text{MC903-PBS vs. MC903-aGr1}} = 0.10330$, $n=6,5$ mice; $p_{\text{MC903-aGr1 vs. EtOH}} = 0.9005$, $n=5,5$
 592 mice). **K.** Time spent scratching over a thirty minute interval for wild-type MC903- and ethanol-
 593 treated mice on day 12 of the MC903 model. MC903-treated animals received daily i.p.
 594 injections of 250 μg aGr1 antibody or PBS (250 μL) on days 8-11 of the model (one-way
 595 ANOVA: **** $p < 0.0001$, $F(2,26) = 53.1$; Tukey's multiple comparisons: **** $p_{\text{MC903-PBS vs. EtOH}} < 0.0001$,
 596 $n=6,5$ mice; * $p_{\text{MC903-PBS vs. EtOH}} = 0.0141$, $n=6,5$ mice; * $p_{\text{MC903-PBS vs. EtOH}} = 0.0141$,
 597 $n=6,5$ mice). **K.** Time spent scratching over a thirty minute interval for wild-type MC903- and ethanol-
 598 treated mice on day 12 of the MC903 model. MC903-treated animals received daily i.p.
 599 injections of 250 μg aGr1 antibody or PBS (250 μL) on days 8-11 of the model (one-way
 600 ANOVA: **** $p < 0.0001$, $F(2,26) = 53.1$; Tukey's multiple comparisons: **** $p_{\text{MC903-PBS vs. EtOH}} < 0.0001$,

601 0.0001, n=12,5 mice; **** $p_{MC903-PBS \text{ vs. } MC903-aGr1} < 0.0001$, n=12,12 mice; $p_{MC903-aGr1 \text{ vs. } EtOH} =$
 602 0.3734, n=12,5 mice). Values from bar plots are reported in **Figure 2-source data 5**.

603
 604 **Figure 2-Figure Supplement 1. aGr1 treatment preferentially depletes neutrophils. A.**
 605 Representative flow cytometry plots of cells collected from blood of mice injected with PBS or
 606 aGr1 (250 μ g, i.p.) once-daily for five days concurrent with daily MC903 topical treatment.
 607 Shown are CD45.2⁺CD11b⁺ cells, plotted by Ly6G and Ly6C signal, with neutrophil (Neuts.) and
 608 inflammatory monocyte (IMs) populations indicated. Neutrophils were defined as
 609 Cd11b⁺Ly6G⁺Ly6C^{mid/high} and IMs were defined as Cd11b⁺Ly6G⁻Ly6C^{high} (see Methods). **B.**
 610 Representative flow cytometry plot as in **A**, depicting neutrophil and IM populations from blood
 611 collected on day 8. **C. (Left)** Neutrophil counts in blood shown as % of Cd11b⁺ cells from
 612 aGr1/MC903 (black triangles) and PBS/MC903 (gray circles)-treated animals on days 3, 5, and
 613 8 of the model (two-way repeated measures ANOVA: **** $p_{\text{treatment}} < 0.0001$, $F(1,31) = 299.5$;
 614 Sidak's multiple comparisons: **** $p_{\text{day } 3} < 0.0001$; **** $p_{\text{day } 5} < 0.0001$; **** $p_{\text{day } 8} < 0.0001$, n= 16,17
 615 mice). **(Right)** Inflammatory monocyte counts in blood shown as % of Cd11b⁺ cells from
 616 aGr1/MC903 and PBS/MC903-treated animals on days 3, 5, and 8 of the model (two-way
 617 repeated measures ANOVA: * $p_{\text{treatment}} = 0.0468$, $F(1,31) = 4.287$; Sidak's multiple comparisons:
 618 ** $p_{\text{day } 3} = 0.0015$; $p_{\text{day } 5} = 0.1918$; $p_{\text{day } 8} = 0.2013$, n= 16,17 mice). Exact values displayed in
 619 **Figure 2-source data 4**.

620
 621 **Figure 2-Figure Supplement 2. CXCL1 rapidly and selectively recruits neutrophils to skin.**
 622 **A.** Representative flow cytometry plots of cells from cheek skin of mice injected with PBS or
 623 CXCL1 (1 μ g in 20 μ L, s.c.). Shown are CD45.2⁺CD11b⁺ cells, plotted by Ly6G and Ly6C signal,
 624 with neutrophil and inflammatory monocyte (IMs) populations indicated. **B.** Neutrophil count
 625 from cheek skin of mice 5, 15, and 30 minutes after injection of CXCL1 or PBS (two-way
 626 ANOVA: * $p_{\text{interaction}} = 0.0239$, $F(2,21) = 4.48$; Sidak's multiple comparisons: $p_{5 \text{ min}} > 0.9999$, n=4,5
 627 mice; * $p_{\text{day } 15 \text{ min}} = 0.0141$, n=4,4 mice; ** $p_{\text{day } 30 \text{ min}} = 0.0031$, n=3,7 mice). Exact values displayed
 628 in **Figure 2-source data 2**. **C.** Blood neutrophils as % of Cd11b⁺ cells approximately 20 hours
 629 after injection of 250 μ g aGr1 (n=15 mice). Mice assayed for CXCL1-evoked itch behavior
 630 immediately preceding blood isolation (see **Figure 2E**). Exact values displayed in **Figure 2-**
 631 **source data 2**. See **Figure 2-Figure Supplement 1C** for representative blood neutrophil
 632 measurements from PBS-injected animals.

633
 634 **Figure 2-Figure Supplement 3. Neutrophil depletion does not affect chloroquine-evoked**
 635 **itch. A.** Scratching behavior of mice immediately after injection of chloroquine (CQ) or PBS (s.c.
 636 cheek). For neutrophil-depletion experiments, mice received 250 μ g anti-Gr1 (aGr1) 20 hours
 637 prior to cheek injection of CQ or PBS (two-tailed t-test: **** $p < 0.0001$ ($t=10.58$, $df=14$); n=6,10
 638 mice). Exact values displayed in **Figure 2-source data 2**.

639
 640 **Figure 2-Figure Supplement 4. Loss of TSLPR reduces skin basophil and mast cell**
 641 **numbers in the first week of AD development. A.** Basophil count from cheek skin of wild-type
 642 MC903- and ethanol-treated, and TSLPR KO MC903-treated mice after 3 or 5 days of treatment
 643 (two-way ANOVA: *** $p_{\text{time}} = 0.0003$, $F(2,117) = 8.87$; Tukey's multiple comparisons: $p_{\text{day } 3 \text{ WT MC903}}$
 644 $\text{vs. KO MC903} = 0.6540$, n=3,5 mice; * $p_{\text{day } 5 \text{ WT MC903 vs. KO MC903}} = 0.1023$, n=6,6 mice; $p_{\text{day } 5 \text{ WT EtOH vs. KO}}$
 645 $\text{MC903} = 0.9077$, n=8,6 mice; $p_{\text{day } 5 \text{ WT MC903 vs. WT EtOH}} = 0.0264$, n=6,8 mice). **B.** Mast cell count from
 646 cheek skin of wild-type MC903- and ethanol-treated, and TSLPR KO MC903-treated mice after
 647 3, 5, or 8 days of treatment (two-way ANOVA: * $p_{\text{genotype}} = 0.0384$, $F(2,117) = 3.35$; Tukey's
 648 multiple comparisons: $p_{\text{day } 3 \text{ WT MC903 vs. KO MC903}} = 0.4133$, n=3,5 mice; $p_{\text{day } 5 \text{ WT MC903 vs. KO MC903}} =$
 649 0.9882 , n=6,6 mice; * $p_{\text{day } 5 \text{ WT MC903 vs. WT EtOH}} = 0.0440$, n=6,5 mice; * $p_{\text{day } 5 \text{ KO MC903 vs. WT EtOH}} =$
 650 0.0294 , n=6,5 mice; * $p_{\text{day } 8 \text{ WT MC903 vs. KO MC903}} = 0.0188$, n=40,15 mice; **** $p_{\text{day } 8 \text{ WT MC903 vs. WT EtOH}} <$

651 0.0001, n=40,38 mice; $p_{\text{day 8 WT EtOH vs. KO MC903}} = 0.7810$, n=38,15 mice). Data from days 3, 5, and
652 8 are presented in **Figure 2-source data 3**.

653
654 **Figure 2-Figure Supplement 5. Neutrophils robustly infiltrate the skin in the DNFB mouse**
655 **model of atopic dermatitis. A.** Neutrophil count from ear skin of wild-type DNFB- and vehicle-
656 treated mice 24 hours after challenge with DNFB or vehicle performed five days after initial
657 DNFB sensitization on shaved rostral back skin (** $p = 0.0004$; two-tailed t-test ($t=4.290$; df
658 $=18$); n=10 mice per group). Values from bar plot is reported in **Figure 2-source data 6**.

659
660 **Figure 2-source data 1.** Values displayed in bar plots shown in Figure 2A-D.

661 **Figure 2-source data 2.** Values displayed in the bar plots shown in Figure 2E and Figs. 2-
662 Figure Supplement 2-3.

663 **Figure 2-source data 3.** Values displayed in the bar plots shown in Figure 2F-I and Figure 2-
664 Figure Supplement 4A-B.

665 **Figure 2-source data 4.** Values used to generate the line plots shown in Figure 2-Figure
666 Supplement 1C.

667 **Figure 2-source data 5.** Values displayed in the bar plots shown in Figure 2J-K.

668 **Figure 2-source data 6.** Values displayed in the bar plots in Figure 2-Figure Supplement 5A.

669 **Figure 3. The MC903 model induces rapid and robust changes in neuronal tissue. A.**
 670 Exact permutation test (10,000 iterations, see Methods) for significance of mean absolute log₂
 671 fold change in gene expression at Day 8 (MC903 vs. ethanol) of custom-defined groups of
 672 genes for indicated categories (see **Figure 3-source data 1**). **B.** Log₂ fold change in gene
 673 expression (MC903 vs. ethanol) in mouse trigeminal ganglia (TG) at indicated time points for all
 674 genes which were significantly differentially expressed for at least one time point in the MC903
 675 model. Green bars = increased expression in MC903 relative to ethanol; magenta = decreased
 676 expression. Exact values and corrected *p*-values are reported in **Figure 3-source data 2** and
 677 **Supplemental Data**, respectively. **C.** Representative composite images showing immune cells
 678 (CD45, green), and sensory neurons (Prph, magenta) with DAPI (blue) in sectioned trigeminal
 679 ganglia from mice treated with Vehicle or MC903 for five days on the cheek. **D.** Quantification of
 680 images examining average number of CD45⁺ cells per section and average ratio of
 681 CD45:Peripherin cells per section after five days of treatment (*p* = 0.562 (*t*=0.6318, *df*=4), 0.542
 682 (*t*=0.6660, *df*=4); two-tailed unpaired t-tests, *n*=33-159 fields of view (images) each of both
 683 trigeminal ganglia from 3 mice per condition treated bilaterally). **E.** Representative composite
 684 images showing immune cells (CD45, green), and sensory neurons (Peripherin (Prph),
 685 magenta) with DAPI (blue) in sectioned trigeminal ganglia from mice treated with Vehicle or
 686 MC903 for eight days on the cheek. **F.** Quantification of images examining average number of
 687 CD45⁺ cells per section and average ratio of CD45:Peripherin cells per section after eight days
 688 of treatment (***p* = 0.0019 (*t*=5.977, *df*=5), ***p* = 0.0093 (*t*=4.107, *df*=4); two-tailed unpaired t-
 689 tests; *n*=42-172 fields of view (images) each of both trigeminal ganglia from 3 EtOH or 4 MC903
 690 animals treated bilaterally). Scale bar = 100 μm. Images were acquired on a fluorescence
 691 microscope using a 10x air objective. Values from bar plots and all TG IHC data are available in
 692 **Figure 3-source data 3**. **G.** Log₂ fold change in gene expression (MC903 vs. ethanol) in mouse
 693 spinal cord on day 8 showing selected differentially expressed genes (*p*_{adjusted} < 0.05). Exact
 694 values and corrected *p*-values are reported in **Supplemental Data**.

695
 696 **Figure 3-Figure Supplement 1. Method of image quantification for sectioned trigeminal**
 697 **ganglia. A.** Representative composite image showing CD45 (green), Peripherin (magenta), and
 698 DAPI (blue). **B.** Single-channel CD45 image with automated min/max intensity thresholding. **C.**
 699 Resultant binary image generated from **B**. **D.** Cells were counted as the number of regions of
 700 interest (ROIs) outlined in blue.

701
 702 **Figure 3-source data 1.** Values displayed in the bar plot shown in Figure 3A.
 703 **Figure 3-source data 2.** Values displayed in the heat map shown in Figure 3B.
 704 **Figure 3-source data 3.** Quantification of all IHC samples from trigeminal ganglia, and Values
 705 displayed in the bar plots shown in Figure 3D,F.

706 **Figure 4. Neutrophils are required for induction of the itch-inducing chemokine CXCL10.**
 707 **A.** Log₂ fold change (Day 8 MC903 vs. EtOH) of Th2 genes in skin from uninjected wild-type,
 708 aGr1-treated, and TSLPR KO animals. **B.** Log₂ fold change (Day 8 MC903 vs. EtOH) of
 709 chemokine genes in skin from uninjected wild-type, aGr1-treated, and TSLPR KO animals. **C.**
 710 Log₂ fold change (Day 8 MC903 vs. EtOH) of activity-induced genes in trigeminal ganglia from
 711 uninjected wild-type, aGr1-treated, and TSLPR KO animals. **D.** Log₂ fold change (Day 8 MC903
 712 vs. EtOH) of *Lcn2* and activity-induced genes in spinal cord from uninjected and aGr1-treated
 713 wild-type mice on day 8. For **Figure 4A-D**, exact values and corrected *p*-values are reported in
 714 **Supplemental Data**. **E.** Quantification of innervation (see Methods) of MC903 and EtOH-
 715 treated mouse skin as determined from BTIII staining (*p* = 0.8985; two-tailed t-test (*t* = 0.1294; *df*
 716 = 18); *n* = 9,11 images each from 2 mice per treatment. Exact values are reported in **Figure 4-**
 717 **source data 1**. **F.** CXCL10 levels in skin homogenate as measured by ELISA on day 8 of the
 718 MC903 model for uninjected animals (left; **p* = 0.029 (*t* = 2.715, *df* = 7); two-tailed t-test; *n* = 4,5
 719 animals), animals which received aGr1 for 8 days (middle; *p* = 0.43 (*t* = 0.815, *df* = 11); two-tailed
 720 t-test; *n* = 6,6 animals), and TSLPR KO animals (right; **p* = 0.0357 (*t* = 2.696, *df* = 6); two-tailed t-
 721 test; *n* = 4,4 animals. Skin homogenates were isolated on separate days and so uninjected, WT
 722 samples were not compared to aGr1-treated samples or to TSLPR KO samples. **G.** (Left) Time
 723 spent scratching over a thirty minute interval on days 5, 8, and 12 of the MC903 model, one
 724 hour after mice were injected with either 3.31 mM of the CXCR3 antagonist AMG 487 or vehicle
 725 (20% HPCD in PBS; 50 μL s.c. in rostral back); (two-way ANOVA: *****p*_{treatment} < 0.0001, *F*(1,67)
 726 = 50.64; Tukey's multiple comparisons: **p*_{day 5} = 0.0216, *n* = 8,10 mice; ****p*_{day 8} = 0.0007, *n* = 18,21
 727 mice; *****p*_{day 12} < 0.0001, *n* = 8,8 mice). (Right) Time spent scratching over a thirty minute interval
 728 one hour after mice were injected with either 3.31 mM of the CXCR3 antagonist AMG 487 or
 729 vehicle (20% HPCD in PBS; 50 μL s.c. in rostral back), and immediately after mice were
 730 injected with 50 mM chloroquine (20 μL i.d., cheek). *p* = 0.92 (*t* = 0.0964, *df* = 8); two-tailed t-test;
 731 *n* = 5,5 mice. Values from bar plots in **Figures 4F-G** are displayed in **Figure 4-source data 2**.

732
 733 **Figure 4-Figure Supplement 1. MC903-dependent gene expression changes in aGr1-**
 734 **treated and TSLPR KO animals.** **A.** Heat map showing log₂ fold change in gene expression
 735 (Day 8 MC903 vs. EtOH) for itch-associated genes in wild-type, aGr1-treated, and TSLPR KO
 736 skin. Green bars = increased expression in MC903 relative to ethanol; magenta = decreased
 737 expression. Exact values and corrected *p*-values are reported in **Figure 4-source data 3** and
 738 **Supplemental Data**, respectively. **B.** Heat map showing log₂ fold change in gene expression
 739 (Day 8 MC903 vs. EtOH) for wild-type, aGr1-treated, and TSLPR KO mouse trigeminal ganglia
 740 (TG) at indicated time points for all genes which were significantly differentially expressed for at
 741 least one time point in the MC903 model (See **Figure 2D**). Green bars = increased expression
 742 in MC903 relative to ethanol; magenta = decreased expression. Exact values and corrected *p*-
 743 values are reported in **Figure 4-source data 4** and **Supplemental Data**, respectively.

744
 745
 746 **Figure 4-source data 1.** Values displayed in the bar plot shown in Figure 4E.

747 **Figure 4-source data 2.** Values displayed in the bar plots shown in Figure 4F-G.

748 **Figure 4-source data 3.** Values displayed in the heat map shown in Figure 4-Figure
 749 Supplement 1A.

750 **Figure 4-source data 4.** Values displayed in the heat map shown in Figure 4-Figure
 751 Supplement 1B.

752

753 **Figure 5. Model of early AD pathogenesis. A.** AD induction first results in increased protease
754 expression and barrier dysfunction, which drives production of the cytokines TSLP and CXCL1
755 via PAR2 activation within keratinocytes. CXCL1 can recruit neutrophils via its receptor CXCR2.
756 Neutrophils may evoke itch by multiple pathways, including degranulation and release of
757 proteases and histamine, production of sensitizing lipids such as PGE₂ and LTB₄,⁵² and
758 induction of CXCL10 expression, which can activate sensory neurons via CXCR3. TSLP
759 activates a number of immune cells to elicit IL-4 production, including basophils, which results in
760 increased IL-4, recruitment of CD4⁺ T cells,²² and sensitization of neurons to promote itch later
761 in the model.

762

763 **Supplementary Data** - The outputs of all differential expression analyses used to determine
764 adjusted *p* value and log₂ fold change for RNA-seq experiments.

765

766 **Methods**

Key Resources Table				
Reagent type (species) or resource	Designation	Source or reference	Identifiers	Additional information
strain, strain background(Mus musculus)	C57BL/6; WT; wild-type	The Jackson Laboratory	Jackson Stock #: 000664; RRID:IMSR_JAX:000664	
strain, strain background(Mus musculus)	C57BL/6; WT; wild-type	Charles River Laboratories	RRID:IMSR_CRL:27; Charles River strain code #: 027;	
strain, strain background(Mus musculus)	Cr1f2m1Jni; TSLPR KO	PMID:14993294	RRID:MGI:3039553; MGI Cat# 3039553	Obtained from the laboratory of Steven F. Ziegler (Ben Aroya Research Institute)
antibody()	Purified anti-mouse Ly-6G/Gr-1 antibody. Low endotoxin, no azide, in PBS; anti-GR1 (RB6-8C5); aGr1	UCSF Core	UCSF Core Cat# AM051	Obtained from the laboratory of Daniel Portnoy (UC Berkeley)
antibody()	LEAF Purified anti-mouse Ly-6G/Ly-6C (Gr-1); antibody; RB6-8C5; aGr1	Biolegend	RRID:AB_313379; BioLegend Cat# 108414	
antibody()	Anti- β -tubulin III (Rabbit polyclonal; 1:1000)	Abcam	RRID:AB_444319; Cat # ab18207	
antibody()	Anti-CGRP (Rabbit polyclonal; 1:1000)	Immunostar	RRID:AB_572217; Cat # 24112	
antibody()	Anti-Peripherin (Chicken polyclonal; 1:1000)	Abcam	RRID:AB_777207; Cat # ab39374	
antibody()	Goat Anti-Mouse IgG H&L Alexa Fluor 488 (Goat polyclonal; 1:1000)	Abcam	RRID:AB_2688012; Cat # ab150117	
antibody()	Goat anti-Chicken IgY (H+L) Secondary Antibody, Alexa Fluor 488 (Goat polyclonal; 1:1000)	ThermoFisher Scientific	RRID:AB_2534096; Cat # A-11039	
antibody()	Goat Anti-Chicken IgG (H+L) Secondary Antibody, Alexa Fluor 594 (Goat polyclonal; 1:1000)	ThermoFisher Scientific	RRID:AB_2534099; Cat # A11042	
antibody()	Goat anti-Rabbit IgG (H+L) Secondary Antibody, Alexa Fluor 594 (Goat polyclonal; 1:1000)	Invitrogen	RRID:AB_2556545; Cat # R37117	
commercial assay or kit()	Promocell Keratinocyte Growth Medium 2	Promocell	Cat # C-20011	
cell line(human)	Normal Human Epidermal Keratinocytes (NHEK), single juvenile donor, cryopreserved	Promocell	Cat # C-12001	
other()	Liberase TM Research Grade; Liberase	Roche	Cat # 5401119001	
other()	Dnase I from bovine pancreas	Sigma	Cat # 11284932001	

other()	Ambion [®] DNase I (RNase-free); DNase	Ambion	Cat # AM2222	
peptide, recombinant protein()	SLIGRL-NH ₂ ; SLIGRL	Tocris	Cas 171436-38-7 ; Cat #1468	
commercial assay or kit()	Qiagen RNeasy mini kit	Qiagen	Cat # 74104	
commercial assay or kit()	RNAzol RT	Sigma-Aldrich	Cat # R4533-50ML	
chemical compound, drug()	(2-Hydroxypropyl)- β -cyclodextrin ;HPCD	Sigma-Aldrich	Cas 128446-35-5; Cat # H107	
chemical compound, drug()	Methyl alcohol; Methanol; MeOH	Sigma-Aldrich	Cas 67-56-1; Cat # 34860	
chemical compound, drug()	Ethanol, Absolute (200 Proof), Molecular Biology Grade, Fisher BioReagents™; Absolute Ethanol, Molecular-Biology grade; Ethanol; EtOH	Fischer Scientific	Cas 64-17-5; Cat # BP2818100	
chemical compound, drug()	MC903; Calcipotriol	Tocris	Cas 112965-21-6; Cat # 2700	
chemical compound, drug()	(\pm)-AMG 487; AMG	Tocris	Cas 947536-03-0; Cat # 4487	
chemical compound, drug()	Chloroquine diphosphate; Chloroquine	Sigma-Aldrich	CAS 50-63-5; Cat # C6628	
chemical compound, drug()	Dimethyl sulfoxide; DMSO	Sigma-Aldrich	Cat # 8418-100mL	
chemical compound, drug()	Formaldehyde, 16%, methanol free, Ultra Pure ; Paraformaldehyde; PFA	Polysciences, Inc.	Cat # 18814-10	
chemical compound, drug()	Tissue Tek Optimal cutting temperature compound (OCT)	Sakura Finetek USA	Cat # 4583	
chemical compound, drug()	Triton X-100 solution ; Triton X-100	BioUltra	CAS 9002-93-1; Cat # 93443	
chemical compound, drug()	Phosphate-buffered saline (PBS), pH 7.4; PBS	Gibco	Cat # 10010023	
chemical compound, drug()	Benzyl benzoate	Sigma-Aldrich	CAS 120-51-4; Cat # B6630	
chemical compound, drug()	Benzyl alcohol	Sigma-Aldrich	CAS 100-51-6; Cat # 305197	

chemical compound, drug()	Sucrose	Sigma-Aldrich	CAS 57-50-1; Cat # S0389	
chemical compound, drug()	LIVE/DEAD Fixable Aqua Dead Cell Stain Kit, for 405 nm excitation ; Aqua	ThermoFisher Scientific	Cat # L34957	
chemical compound, drug()	Isoflurane	Piramal	CAS 26675-46-7	
chemical compound, drug()	4',6-Diamidino-2-Phenylindole, Dihydrochloride; DAPI	ThermoFisher Scientific	CAS 28718-90-3; Cat # 1306	
chemical compound, drug()	4',6-Diamidino-2-Phenylindole, Dihydrochloride; DAPI LIVE/DEAD	Invitrogen	Cat # L34961	
chemical compound, drug()	Fluoromount-G	ThermoFisher Scientific	Cat # 00-4958-02	
antibody()	Goat Anti-Mouse IgG - H&L - Fab Fragment Polyclonal Antibody, Unconjugated, Abcam; F(ab) anti-mouse IgG (Goat polyclonal; 1:200)	Abcam	RRID:AB_955960; Cat # ab6668	
antibody()	Anti-Mouse CD45.2 Purified 100 ug antibody, Thermo Fisher Scientific; Mouse anti-CD45.2 (Mouse monoclonal; 1:1000)	eBioscience	RRID:AB_467261; Cat # 14-0454-82	
antibody()	Purified anti-mouse CD16/32 antibody. Low endotoxin, no azide, in PBS; Rat anti-Mouse CD16/32 (2.4G2) (Rat monoclonal; 1:1000)	UCSF Core	UCSF Core Cat# AM004	
commercial assay or kit()	DuoSet ELISA Ancillary Reagent Kit 2	R&D Systems	Cat # DY008	
commercial assay or kit()	Mouse CXCI10 DuoSet ELISA	R&D Systems	Cat # DY466	
commercial assay or kit()	Pierce™ BCA Protein Assay Kit - Reducing Agent Compatible	ThermoFisher Scientific	Cat # 23250	
chemical compound, drug()	2-Amino-2-(hydroxymethyl)-1,3-propanediol; Trizma base, TRIS, TRIS base	Sigma-Aldrich	Cas 77-86-1 ; Cat # T4661	
chemical compound, drug()	Ethylene glycol-bis(2-aminoethylether)-N,N,N',N'-tetraacetic acid; EGTA	Sigma-Aldrich	Cas 67-42-5 ; Cat # E3889	
chemical compound, drug()	Ethylenedinitrilo)tetraacetic acid; EDTA	Sigma-Aldrich	Cas 60-00-4 ; Cat # E9884	
commercial assay or kit()	PhosSTOP inhibitor	Roche	Cat # 4906845001	

chemical compound, drug()	Sodium deoxycholate, ≥97% (titration); Sodium deoxycholate	Sigma-Aldrich	Cas 302-95-4; Cat # D6750	
chemical compound, drug()	Phenylmethylsulfonyl fluoride; PMSF	Sigma-Aldrich	Cas 329-98-6; Cat # 10837091001	
chemical compound, drug()	1-Fluoro-2,4,-dinitrobenzene; DNFB	Sigma	Cas 70-34-8; Cat # D1529	
commercial assay or kit()	cOMplete protease inhibitor cocktail	Roche	Cat # 11697498001	
other()	Advanced RPMI Medium 1640; RPMI	Gibco	Cat # 12633012	
other()	Fetal Bovine Serum; FBS; FCS	HyClone	Cat # 30396.03	
other()	sodium pyruvate 100 mM	Gibco	Cat # 11360070	
other()	N-2-hydroxyethylpiperazine-N-2-ethane sulfonic acid; HEPES 1M	Gibco	Cat # 15630080	
other()	L-Glutamine 200 mM	Gibco	Cat # 25030081	
other()	Penicillin-Streptomycin (10,000 U/mL; Pen-Strep)	Gibco	Cat # 15140122	
other()	Collagenase VIII	Sigma-Aldrich	Cat # C2139-500MG	
commercial assay or kit()	Invitrogen™ CountBright™ Absolute Counting Beads, for flow cytometry; Counting Beads	Invitrogen	Cat # C36950	
antibody()	CD45 Monoclonal Antibody (30-F11), APC-eFluor 780, eBioscience(TM), Thermo Fisher Scientific; CD45-APC/eFluor 780 (30-F11) (Rat monoclonal; 1:200)	eBioscience	RRID:AB_1548781; Cat # 47-0451-82	
antibody()	CD11b Monoclonal Antibody (M1/70), PE-Cyanine7, eBioscience(TM), Thermo Fisher Scientific; CD11b-PE/Cy7 (M1/70) (Rat monoclonal; 1:200)	BD Biosciences	RRID:AB_469588; Cat # 25-0112-82	
antibody()	PE-Cyanine7 Anti-Human/Mouse CD45R (B220) (RA3-6B2) Antibody, Tonbo Biosciences; B220-PE/Cy7 (RA3-6B2) (Rat monoclonal; 1:200)	Tonbo Biosciences	RRID:AB_2621849; Cat # 60-0452	
antibody()	CD11c Monoclonal Antibody (N418), PE-Cyanine7, eBioscience(TM), Thermo Fisher Scientific; CD11c-	eBioscience	RRID:AB_469590; Cat # 25-0114-82	

	PE/Cy7 (N418) (Armenian Hamster monoclonal; 1:200)			
antibody()	CD3e Monoclonal Antibody (145-2C11), FITC, eBioscience(TM), Thermo Fisher Scientific; CD3-FITC (145-2C11) (Armenian Hamster monoclonal; 1:200)	eBioscience	RRID:AB_464882; Cat # 11-0031-82	
antibody()	Brilliant Violet 785™ anti-mouse CD8a antibody, BioLegend; CD8-BV785 (53-6.7) (Rat monoclonal; 1:200)	Biolegend	RRID:AB_1121880; Cat # 100749	
antibody()	Rat Anti-CD4 Monoclonal Antibody, Phycoerythrin Conjugated, Clone GK1.5, BD Biosciences; CD4-PE (GK1.5) (Rat monoclonal; 1:200)	BD Biosciences	RRID:AB_395014; Cat # 553730	
antibody()	Alexa Fluor® 647 anti-mouse TCR γ/δ Antibody; gdTCR-AF647 (GL3) (Armenian Hamster monoclonal; 1:200)	Biolegend	RRID:AB_313826; Cat # 118133	
antibody()	CD117 (c-Kit) Monoclonal Antibody (2B8), Biotin; c-Kit-Biotin (ACK2) (Rat monoclonal; 1:200)	eBioscience	RRID:AB_466569; Cat # 13-1171-82	
antibody()	FceR1 alpha Monoclonal Antibody (MAR-1), PE, eBioscience; FceRI-PE (MAR-1) (Armenian Hamster monoclonal; 1:200)	eBioscience	RRID:AB_466028; Cat # 12-5898-82	
antibody()	CD49b (Integrin alpha 2) Monoclonal Antibody (DX5), PE-Cyanine7, eBioscience; CD49b-PE/Cy7 (DX5) (Rat monoclonal; 1:200)	eBioscience	RRID:AB_469667; Cat # 25-5971-82	
antibody()	Anti-Siglec-F-APC, mouse (clone: REA798); SiglecF-APC; (Rat monoclonal; 1:200)	Miltenyi Biotech	RRID:AB_2653441; Cat # 130-112-333	
other()	Streptavidin FITC; SA-FITC	eBioscience	RRID:AB_11431787 ; Cat # 11-4317-87	
antibody()	Ly-6C Monoclonal Antibody (HK1.4), PerCP-Cyanine5.5, eBioscience; Ly6C-PerCP/Cy5.5 (HK1.4) (Rat monoclonal; 1:200)	eBioscience	RRID:AB_1518762; Cat # 45-5932-82	
antibody()	violetFluor™ 450 Anti-Human/Mouse CD11b (M1/70); CD11b-violet fluor 450 (M1/70) (Rat monoclonal; 1:200)	Tonbo Biosciences	RRID:AB_2621936; Cat # 75-0112	
antibody()	AF700 anti-mouse Ly-6G Antibody (1A8); Ly6G-AF700 (1A8) (Rat monoclonal; 1:200)	BioLegend	RRID:AB_1064045; Cat # 127621	
antibody()	CD45.2 Monoclonal Antibody (104), APC-Cy7, eBioscience; CD45.2-APC/Cy7 (104) (Mouse monoclonal, 1:200)	eBioscience	RRID:AB_1272175; Cat # 47-0454-82	

software, algorithm()	IgorPro version 6.3	WaveMetrics	https://www.wavemetrics.com/order/order_igordownloads6.htm
software, algorithm()	Microsoft Excel 2011	Microsoft	https://www.microsoft.com/en-us/store/d/excel-2016-for-mac/
software, algorithm()	Fiji	NIH	https://imagej.net/Fiji/Downloads
software, algorithm()	Graphpad Prism 7	Graphpad	https://www.graphpad.com/scientific-software/prism/
software, algorithm()	R-3.6.0	The R Project for Statistical Computing	https://cran.r-project.org/bin/macosx/
software, algorithm()	Python 2.7	Anaconda	https://www.anaconda.com/distribution/
software, algorithm()	HTSeq 0.11.1	Python Package Index	https://htseq.readthedocs.io/en/release_0.11.1/install.html
software, algorithm()	Trimmomatic	PMID: 24695404	https://github.com/timflutre/trimmomatic
software, algorithm()	Tophat 2.1.1	PMID: 19289445	https://ccb.jhu.edu/software/tophat/
software, algorithm()	EdgeR	PMID: 19910308; PMID: 22287627	https://bioconductor.org/packages/release/bioc/html/edgeR.html
software, algorithm()	DESeq	PMID: 20979621	https://bioconductor.org/packages/release/bioc/html/DESeq.html
software, algorithm()	FlowJo 10.4.2	FlowJo; Treestar	https://www.flowjo.com/solutions/flowjo/downloads
other()	Bovine serum albumin, cold ethanol fraction, pH 5.2, ≥96%; BSA	Sigma-Aldrich	CAS 9048-46-8; Cat # A4503
other()	NGS; Goat serum; Normal goat serum	Abcam	Cat # ab7481

767

768 *Mouse studies*

769 All mice were housed in standard conditions in accordance with standards approved by the
770 Animal Care and Use Committee of the University of California Berkeley (12 hr light-dark cycle,
771 21°C). Wild-type C57BL/6 mice were obtained from Charles River or Jackson Laboratories and
772 raised in-house. TSLPR KO mice were kindly provided by Dr. Steven Ziegler (*Cr1f2^{tm1Jn59}*) and
773 backcrossed onto C57BL/6. All experiments were performed under the policies and
774 recommendations of the International Association for the Study of Pain and approved by the
775 University of California Berkeley Animal Care and Use Committee. Where appropriate,
776 genotypes were assessed using standard PCR.

777

778 *MC903 model of atopic dermatitis*

779 MC903 (Calcipotriol; R&D Systems) was applied to the shaved mouse cheek (20 μ l of 0.2 mM in
780 ethanol) or rostral back (40 μ l of 0.2 mM in ethanol) once per day for 1-12 days using a pipette.
781 100% ethanol was used. All MC903 studies were performed on 8-12 week old age-matched
782 mice. Behavior, RNA-seq, flow cytometry, and immunohistochemistry were performed on days
783 1, 2, 3, 5, 8 and/or 12. For AMG 487 experiments in the MC903 model, 50 μ L 3.31 mM AMG
784 487 (Tocris) or 20% HPCD-PBS vehicle was injected subcutaneously one hour prior to
785 recording behavior.⁷⁵ Spontaneous scratching was manually scored for the first 30 minutes of
786 observation. Both bout number and length were recorded. Behavioral scoring was performed
787 while blind to experimental condition and mouse genotype.

788

789 *MC903 RNA isolation and sequencing*

790 On days 1 (six hours post-treatment), 2, 5, or 8 post-treatment, mice treated with MC903 and
791 vehicle were euthanized via isoflurane and cervical dislocation. Cheek skin was removed, flash-
792 frozen in liquid nitrogen, and cryo-homogenized with a mortar and pestle. Ipsilateral trigeminal
793 ganglia were dissected and both skin and trigeminal ganglia were homogenized for three
794 minutes (skin) or one minute (TG) in 1 mL RNazol RT (Sigma-Aldrich). Thoracic spinal cord was
795 dissected from mice treated with 40 μ L MC903 or ethanol on the shaved rostral back skin and
796 homogenized for one minute in 1 mL RNazol. Large RNA was extracted using RNazol RT per
797 manufacturer's instructions. RNA pellets were DNase treated (Ambion), resuspended in 50 μ L
798 DEPC-treated water, and subjected to poly(A) selection and RNA-seq library preparation (Apollo
799 324) at the Functional Genomics Laboratory (UC Berkeley). Single-end read sequencing (length
800 = 50 bp) was performed by the QB3 Vincent G. Coates Genomic Sequencing Laboratory (UC
801 Berkeley) on an Illumina HiSeq4000. See **Supplementary File 1** for number of mice per
802 experimental condition and number of mapped reads per sample. Data are available at Gene
803 Expression Omnibus under GSE132173.

804

805 *MC903 RNA sequencing analysis*

806 Reads were mapped to the mm10 mouse genome using Bowtie2 and Tophat, and reads were
807 assigned to transcripts using htseq-count.^{113,114} For a given time point, replicate measurements
808 for each gene from treated and control mice were used as input for DESeq (R) and genes with
809 $p_{\text{adjusted}} < 0.05$ (for skin and spinal cord) or $p_{\text{adjusted}} < 0.1$ (for trigeminal ganglia) for at least one
810 time point were retained for analysis.^{115,116} For the skin dataset, we collated a set of AD-related
811 immune cell markers, cytokines, atopic dermatitis disease genes, neurite outgrowth/axonal
812 guidance genes, and locally expressed neuronal transcripts, and from this list visualized genes
813 that were significantly differentially expressed for at least one time point. For the trigeminal
814 ganglia dataset, we plotted all genes that were significantly differentially expressed for at least
815 one time point. Genes from these lists were plotted with hierarchical clustering using heatmap2
816 (R).¹²³

817

818 *Custom gene groups*

819 Genes were clustered into functional groups and significance was evaluated using a
820 permutation test. Briefly, we first tabulated the absolute value of the \log_2 fold change of gene
821 expression (between MC903 and EtOH) of each gene in a given group of n genes in turn, and
822 then we calculated the median of these fold change values, Z_{true} . We then drew n random genes
823 from the set of all genes detected in the samples and computed the median \log_2 fold change as
824 above using this null set, Z_{null} . Repeating the latter 10,000 times established a null distribution of
825 median \log_2 fold change values; we took the proportion of resampled gene groups that exhibited

826 ($Z_{true} \geq Z_{null}$) as an empirical p -value reporting the significance of changes in gene expression for
 827 a given group of n genes.

828

829 *Flow Cytometry*

830 Skin samples were collected from the cheek of mice at the indicated time points with a 4- or 6-
 831 mm biopsy punch into cold RPMI 1640 medium (RPMI; Gibco) and minced into smaller pieces
 832 with surgical scissors. When ear skin was collected, whole ears were dissected postmortem into
 833 cold RPMI and finely minced with scissors. For isolation of immune cells, skin samples were
 834 digested for 1h at 37°C using 1 U/mL Liberase TM (Roche) and 5 µg/mL DNase I (Sigma). At
 835 the end of the digestion, samples were washed in FACS buffer (PBS with 0.5% FCS and 2 mM
 836 EDTA) and filtered through a 70 or 100 µm strainer (Falcon). Cells were stained with
 837 LIVE/DEAD fixable stain Aqua in PBS (Invitrogen), then blocked with anti-CD16/32 (UCSF
 838 Core) and stained with the following fluorophore-conjugated antibodies (all from eBiosciences
 839 unless stated otherwise) in FACS buffer: cKit-Biotin (clone ACK2; secondary stain with SA-
 840 FITC), CD11b-violet fluor 450 (Tonbo; clone M1/70), Ly6C-PerCP/Cy5.5 (clone HK1.4), CD49b-
 841 PE/Cy7 (clone DX5), CD45.2-APC/Cy7 (clone 104), FcεRI-PE (MAR-1), Ly6G-AF700 (clone
 842 1A8). 10 µL of counting beads (Invitrogen) were added after the last wash to measure absolute
 843 cell counts. For measurement of CD4⁺ T cells, 6-mm skin biopsy punch samples were digested
 844 for 30 minutes at 37°C using Collagenase VIII (Sigma). At the end of the digestion, cells were
 845 washed in RPMI buffer (RPMI with: 5% FCS, 1% penicillin-streptomycin, 2 mM L-glutamine, 10
 846 mM HEPES buffer, 1 mM sodium pyruvate). Cells were blocked with anti-CD16/32 (UCSF Core)
 847 and stained with the following fluorophore-conjugated antibodies in FACS buffer (PBS with 5%
 848 FCS and 2 mM EDTA): CD45-APC-eFluor780 (clone 30-F11; eBiosciences), CD11b-PE/Cy7
 849 (clone M1/70; BD Biosciences), B220-PE/Cy7 (clone RA3-6B2; Tonbo Biosciences), CD11c-
 850 PE/Cy7 (clone N418; eBiosciences), CD3-FITC (clone 145-2C11; eBiosciences), CD8-BV785
 851 (clone 53-6.7; Biolegend), CD4-PE (clone GK1.5; BD Biosciences), gdTCR-AF647 (clone GL3;
 852 Biolegend). 10 µL of counting beads (Invitrogen) were added after the last wash to measure
 853 absolute cell counts, and samples were resuspended in DAPI LIVE/DEAD (Invitrogen). Blood
 854 samples were collected from saphenous vein or from terminal bleed following decapitation. Red
 855 blood cells were lysed using ACK lysis buffer (Gibco), and samples were washed with FACS
 856 buffer (PBS with 0.5% FCS and 2 mM EDTA), and blocked with anti-CD16/32. Cells were
 857 stained with Ly6G-PE (1A8; BD Biosciences), CD11b-violet fluor 450 (M1/70, Tonbo), Ly6C-
 858 PerCP/Cy5.5 (HK1.4, Biolegend), and aGr1-APC/Cy7 (RB6-8C5, eBiosciences). For all
 859 experiments, single cell suspensions were analyzed on an LSR II or LSR Fortessa (BD
 860 Biosciences), and data were analyzed using FlowJo (TreeStar, v.9.9.3) software.

861

862 *Human keratinocyte RNA sequencing*

863 Normal human epidermal keratinocytes from juvenile skin (PromoCell #C-12001) were cultured
 864 in PromoCell Keratinocyte Growth Medium 2 and passaged fewer than 5 times. Cells were
 865 treated for three hours at room temperature with 100 µM SLIGRL or vehicle (Ringer's + 0.1%
 866 DMSO). Total RNA was extracted by column purification (Qiagen RNeasy Mini Kit). RNA was
 867 sent to the Vincent J. Coates Sequencing Laboratory at UC Berkeley for standard library
 868 preparation and sequenced on an Illumina HiSeq2500 or 4000. Sequences were trimmed
 869 (Trimmomatic), mapped (hg19, TopHat) and assigned to transcripts using htseq-count.
 870 Differential gene expression was assessed using R (edgeR).¹²³ Data are available at Gene
 871 Expression Omnibus under GSE132174.

872

873 *IHC of whole-mount skin*

874 Staining was performed as previously described.^{117,118} Briefly, 8-week old mice were euthanized
 875 and the cheek skin was shaved. The removed skin was fixed overnight in 4% PFA, then washed

876 in PBS (3X for 10 min each). Dermal fat was scraped away with a scalpel and skin was washed
877 in PBST (0.3% Triton X-100; 3X for two hours each) then incubated in 1:500 primary antibody
878 (Rabbit anti beta-Tubulin II; Abcam #ab18207 or Rabbit anti-CGRP; Immunostar #24112) in
879 blocking buffer (PBST with 5% goat serum and 20% DMSO) for 6 days at 4°C. Skin was
880 washed as before and incubated in 1:500 secondary antibody (Goat anti-Rabbit Alexa 594;
881 Invitrogen #R37117) in blocking buffer for 3 days at 4°C. Skin was washed in PBST, serially
882 dried in methanol: PBS solutions, incubated overnight in 100% methanol, and finally cleared
883 with a 1:2 solution of benzyl alcohol: benzyl benzoate (BABB; Sigma) before mounting between
884 No. 1.5 coverglass. Whole mount skin samples were imaged on a Zeiss LSM 880 confocal
885 microscope with OPO using a 20x water objective. Image analysis was performed using a
886 custom macro in FIJI. Briefly, maximum intensity z-projections of the beta-tubulin III or CGRP
887 channel were converted to binary files that underwent edge-detection analysis. Regions were
888 defined by circling all stained regions. Region sizes and locations were saved.

889

890 *IHC of sectioned trigeminal ganglia*

891 TG were dissected from 8- to 12-week old adult mice and post-fixed in 4% PFA for one hour.
892 TG were cryo-protected overnight at 4°C in 30% sucrose-PBS, embedded in OCT, and then
893 cryosectioned at 14 µm onto slides for staining. Slides were washed 3x in PBST (0.3% Triton X-
894 100), blocked in 2.5% Normal Goat serum + 2.5% BSA-PBST, washed 3X in PBST, blocked in
895 endogenous IgG block (1:10 F(ab) anti-mouse IgG (Abcam ab6668) + 1:1000 Rat anti-mouse
896 CD16/CD32 (UCSF MAB Core) in 0.3% PBST), washed 3X in PBST and incubated overnight at
897 4°C in 1:1000 primary antibody in PBST + 0.5% Normal Goat Serum + 0.5% BSA. Slides were
898 washed 3x in PBS, incubated 2 hr at RT in 1:1000 secondary antibody, washed 3X in PBS, and
899 then incubated 30 min in 1:2000 DAPI-PBS. Slides were washed 3x in PBS and mounted in
900 Fluoromount-G with No. 1.5 coverglass. Primary antibodies used: Mouse anti-CD45
901 (eBioscience #14-054-82) and Chicken anti-Peripherin (Abcam #39374). Secondary antibodies
902 used: Goat anti-Chicken Alexa 594 (ThermoFisher #A11042) and Goat anti-Mouse Alexa 488
903 (Abcam #150117). DAPI (ThermoFisher #D1306) was also used to mark nuclei. Imaging of TG
904 IHC experiments was performed on an Olympus IX71 microscope with a Lambda LS-xl light
905 source (Sutter Instruments). For TG IHC analysis, images were analyzed using automated
906 scripts in FIJI (ImageJ) software.¹²³ Briefly, images were separated into the DAPI, CD45, and
907 Peripherin channels. The minimum/maximum intensity thresholds were batch-adjusted to pre-
908 determined levels, and adjusted images were converted to binary files. Regions were defined by
909 circling all stained regions with pre-determined size-criteria. Region sizes and locations were
910 saved.

911

912 *Neutrophil depletion*

913 Neutrophils were acutely depleted using intraperitoneal injection with 250 µg aGR1 in PBS
914 (clone RB6-8C5, a gift from D. Portnoy, UC Berkeley, or from Biologend), 16-24 hours before
915 behavioral and flow cytometry experiments. Depletion was verified using flow cytometry on
916 blood collected from terminal bleed following decapitation. For longer depletion experiments
917 using the MC903 model, mice were injected (with 250 µg aGR1 in PBS or PBS vehicle, i.p.)
918 beginning one day prior to MC903 administration and each afternoon thereafter through day 7 of
919 the model, or on days 8-11 for measurement of day 12 itch behaviors, and blood was collected
920 via saphenous venipuncture at days 3, 5, or by decapitation at day 8 to verify depletion.

921

922 *CXCL10 ELISA measurements in skin*

923 Neutrophil-depleted or uninjected mice were treated with MC903 or ethanol for 7 days. On day
924 8, 6-mm biopsy punches of cheek skin were harvested, flash-frozen in liquid nitrogen, cryo-
925 homogenized by mortar and pestle, and homogenized on ice for three minutes at maximum
926 speed in 0.5 mL of the following tissue homogenization buffer (all reagents from Sigma unless

927 stated otherwise): 100 mM Tris, pH 7.4; 150 mM NaCl, 1 mM EGTA, 1 mM EDTA, 1% Triton X-
928 100, and 0.5% Sodium deoxycholate in ddH₂O; on the day of the experiment, 200 mM fresh
929 PMSF in 100% ethanol was added to 1mM, with 1 tablet cOmplete protease inhibitor (Roche)
930 per 50 mL, and 5 tablets PhosSTOP inhibitor (Roche) per 50 mL buffer. Tissues were agitated
931 in buffer for two hours at 4°C, and centrifuged at 13,000 rpm for 20 minutes at 4°C.
932 Supernatants were aliquoted and stored at -80°C for up to one week. After thawing, samples
933 were centrifuged at 10,000 rpm for five minutes at 4°C. Protein content of skin homogenates
934 was quantified by BCA (Thermo Scientific) and homogenates were diluted to 2 mg/mL protein in
935 PBS and were subsequently diluted 1:2 in Reagent Diluent (R&D Systems). CXCL10 protein
936 was quantified using the Mouse CXCL10 Duoset ELISA kit (R&D Systems; #DY466-05)
937 according to manufacturer's instructions. Plate was read at 450 nm and CXCL10 was quantified
938 using a seven-point standard curve (with blank and buffer controls) and fitted with a 4-parameter
939 logistic curve.

940

941 *Acute itch behavior*

942 Itch behavioral measurements were performed as previously described.^{56,119,120} Mice were
943 shaved one week prior to itch behavior and acclimated in behavior chambers once for thirty
944 minutes at the same time of day on the day prior to the experiment. Behavioral experiments
945 were performed during the day. Compounds injected: 1 µg carrier-free CXCL1 (R&D systems) in
946 PBS, 3.31 mM AMG 487 (Tocris, prepared from 100 mM DMSO stock) in 20% HPCD-PBS, 50
947 mM Chloroquine diphosphate (Sigma) in PBS, along with corresponding vehicle controls. Acute
948 pruritogens were injected using the cheek model (20 µL, subcutaneous/s.c.) of itch, as
949 previously described.⁵⁶ AMG 487 (50 µL) or vehicle was injected s.c. into the rostral back skin
950 one hour prior to recording of behavior. Behavioral scoring was performed as described above.

951

952 *Lipidomics*

953 Skin was collected from the cheek of mice post-mortem with a 6-mm biopsy punch and
954 immediately flash-frozen in liquid nitrogen. Lipid mediators and metabolites were quantified via
955 liquid chromatography-tandem mass spectrometry (LC-MS/MS) as described before.¹²¹ In brief,
956 skin was homogenized in cold methanol to stabilize lipid mediators. Deuterated internal
957 standards (PGE₂-d₄, LTB₄-d₄, 15-HETE-d₈, LXA₄-d₅, DHA-d₅, AA-d₈) were added to samples
958 to calculate extraction recovery. LC-MS/MS system consisted of an Agilent 1200 Series HPLC,
959 Luna C18 column (Phenomenex, Torrance, CA, USA), and AB Sciex QTRAP 4500 mass
960 spectrometer. Analysis was carried out in negative ion mode, and lipid 30 mediators quantified
961 using scheduled multiple reaction monitoring (MRM) mode using four to six specific transition
962 ions per analyte.¹²²

963

964 *1-Fluoro-2,4-dinitrobenzene (DNFB) model of atopic dermatitis*

965 The DNFB model was conducted as described previously.⁶³ Briefly, the rostral backs of
966 isofluorane-anesthetized mice were shaved using surgical clippers. Two days after shaving,
967 mice were treated with 25 µL 0.5% DNFB (Sigma) dissolved in 4:1 acetone:olive oil vehicle on
968 the rostral back using a pipette. Five days after the initial DNFB sensitization, mice were
969 challenged with 40 µL 0.2% DNFB or 4:1 acetone:olive oil vehicle applied to the outer surface of
970 the right ear. Twenty-four hours after DNFB or vehicle challenge, mice were euthanized and ear
971 skin was harvested for flow cytometry.

972

973 *Statistical analyses*

974 Different control experimental conditions (e.g. uninjected versus PBS-injected animals) were
975 pooled when the appropriate statistical test showed they were not significantly different
976 (Supplementary File 2). For all experiments except RNA-seq (see above), the following
977 statistical tests were used, where appropriate: Student's t-test, one-way ANOVA with Tukey-

978 Kramer post hoc comparison, and two-way ANOVA with Tukey Kramer or Sidak's post-hoc
 979 comparison. Bar graphs show mean \pm SEM. Statistical analyses were performed using PRISM
 980 7 software (GraphPad). For all p values, $*=0.01<p<0.05$, $**=0.001<p<0.01$,
 981 $***=0.0001<p<0.001$, and $****=p<0.0001$.

982

983 **Acknowledgements**

984 The authors would like to thank members of the Bautista and Barton labs for helpful discussions
 985 on the data. We are grateful to S. Ziegler (Ben Aroya Research Institute) for the gift of the
 986 TSLPR KO mouse. We also thank M. Pellegrino and L. Thé for pilot studies on human
 987 keratinocyte transcriptome, and T. Morita and J. Wong for technical assistance with TSLPR KO
 988 mouse behavioral experiments. D.M.B. is supported by the NIH (AR059385; NS07224 and
 989 NS098097, also to R.B.B) and the Howard Hughes Medical Institute. G.M.B. is supported by the
 990 NIH (AI072429, AI063302, AI104914, AI105184) and the Burroughs Wellcome Fund. J.D. was
 991 supported by a Long-Term Fellowship from the Human Frontier Science Program (LT-
 992 000081/2013-L). K.G. is supported by NIH grant EY026082. Confocal imaging experiments
 993 were conducted at the CRL Molecular Imaging Center, supported by the Helen Wills
 994 Neuroscience Institute (UC Berkeley). We would like to thank H. Aaron and F. Ives for their
 995 microscopy training and assistance. This work used the Functional Genomics Laboratory and
 996 the Vincent J. Coates Genomics Sequencing Laboratory at UC Berkeley, supported by NIH S10
 997 OD018174 Instrumentation Grant.

998

999 **Conflict of interest statement**

1000 The authors declare no conflict of interest.

1001

1002 **References**

- 1003 1. Matteredne, U., Apfelbacher, C., Loerbroks, A., Schwarzer, T., Büttner, M., Ofenloch, R.,
 1004 Diepgen, T. & Weisshaar, E. Prevalence, correlates and characteristics of chronic
 1005 pruritus: a population-based cross-sectional study. *Acta Derm. Venereol.* **91**, 674–679
 1006 (2011).
- 1007 2. Mollanazar, N. K., Smith, P. K. & Yosipovitch, G. Mediators of Chronic Pruritus in Atopic
 1008 Dermatitis: Getting the Itch Out? *Clin Rev Allergy Immunol* **51**, 263–292 (2016).
- 1009 3. Dalgard, F. J., Gieler, U., Tomas-Aragones, L., Lien, L., Poot, F., Jemec, G. B. E., Misery,
 1010 L., Szabo, C., Linder, D., Sampogna, F., Evers, A. W. M., Halvorsen, J. A., Balieva, F.,
 1011 Szepletowski, J., Romanov, D., Marron, S. E., Altunay, I. K., Finlay, A. Y., Salek, S. S. &
 1012 Kupfer, J. The Psychological Burden of Skin Diseases: A Cross-Sectional Multicenter
 1013 Study among Dermatological Out-Patients in 13 European Countries. *J. Invest. Dermatol.*
 1014 **135**, 984–991 (2015).
- 1015 4. Ständer, S. & Steinhoff, M. Pathophysiology of pruritus in atopic dermatitis: an overview.
 1016 *Exp. Dermatol.* **11**, 12–24 (2002).
- 1017 5. Oaklander, A. L. Neuropathic itch. *Semin. Cutan. Med. Surg.* **30**, 87–92 (2011).
- 1018 6. Dhand, A. & Aminoff, M. J. The neurology of itch. *Brain* **137**, 313–322 (2014).
- 1019 7. Yosipovitch, G. & Papoiu, A. D. P. What causes itch in atopic dermatitis? *Curr. Allergy*
 1020 *Asthma Rep.* **8**, 306–311 (2008).
- 1021 8. Ikoma, A., Steinhoff, M., Ständer, S., Yosipovitch, G. & Schmelz, M. The neurobiology of
 1022 itch. *Nat. Rev. Neurosci.* **7**, 535–547 (2006).
- 1023 9. Spergel, J. M. & Paller, A. S. Atopic dermatitis and the atopic march. *J Allergy Clin*
 1024 *Immunol* **112**, S118-27 (2003).
- 1025 10. Zheng, T., Yu, J., Oh, M. H. & Zhu, Z. The atopic march: Progression from atopic
 1026 dermatitis to allergic rhinitis and asthma. *Allergy, Asthma Immunol. Res.* **3**, 67–73 (2011).
- 1027 11. Ewald, D. A., Noda, S., Oliva, M., Litman, T., Nakajima, S., Li, X., Xu, H., Workman, C.
 1028 T., Scheipers, P., Svitacheva, N., Labuda, T., Krueger, J. G., Suárez-Fariñas, M.,

- 1029 Kabashima, K. & Guttman-Yassky, E. Major differences between human atopic dermatitis
1030 and murine models, as determined by using global transcriptomic profiling. *J. Allergy Clin.*
1031 *Immunol.* **139**, 562–571 (2017).
- 1032 12. Choy, D. F., Hsu, D. K., Seshasayee, D., Fung, M. A., Modrusan, Z., Martin, F., Liu, F.-T.
1033 & Arron, J. R. Comparative transcriptomic analyses of atopic dermatitis and psoriasis
1034 reveal shared neutrophilic inflammation. *J. Allergy Clin. Immunol.* **130**, 1335–43.e5
1035 (2012).
- 1036 13. Guttman-Yassky, E., Suárez-Fariñas, M., Chiricozzi, A., Nograles, K. E., Shemer, A.,
1037 Fuentes-Duculan, J., Cardinale, I., Lin, P., Bergman, R., Bowcock, A. M. & Krueger, J. G.
1038 Broad defects in epidermal cornification in atopic dermatitis identified through genomic
1039 analysis. *J. Allergy Clin. Immunol.* **124**, (2009).
- 1040 14. Suárez-Fariñas, M., Dhingra, N., Gittler, J., Shemer, A., Cardinale, I., De Guzman Strong,
1041 C., Krueger, J. G. & Guttman-Yassky, E. Intrinsic atopic dermatitis shows similar TH2 and
1042 higher T H17 immune activation compared with extrinsic atopic dermatitis. *J. Allergy Clin.*
1043 *Immunol.* **132**, 361–370 (2013).
- 1044 15. Jabbari, A., Suárez-Fariñas, M., Dewell, S. & Krueger, J. G. Transcriptional profiling of
1045 psoriasis using RNA-seq reveals previously unidentified differentially expressed genes. *J.*
1046 *Invest. Dermatol.* **132**, 246–9 (2012).
- 1047 16. Nattkemper, L. A., Tey, H. L., Valdes-Rodriguez, R., Lee, H., Mollanazar, N. K., Albornoz,
1048 C., Sanders, K. M. & Yosipovitch, G. The Genetics of Chronic Itch: Gene Expression in
1049 the Skin of Patients with Atopic Dermatitis and Psoriasis with Severe Itch. *J. Invest.*
1050 *Dermatol.* **138**, 1311–1317 (2018).
- 1051 17. Dai, J., Choo, M. K., Park, J. M. & Fisher, D. E. Topical ROR Inverse Agonists Suppress
1052 Inflammation in Mouse Models of Atopic Dermatitis and Acute Irritant Dermatitis. *J.*
1053 *Invest. Dermatol.* **137**, 2523–2531 (2017).
- 1054 18. Li, M., Hener, P., Zhang, Z., Ganti, K. P., Metzger, D. & Chambon, P. Induction of thymic
1055 stromal lymphopoietin expression in keratinocytes is necessary for generating an atopic
1056 dermatitis upon application of the active vitamin D3 analogue MC903 on mouse skin. *J.*
1057 *Invest. Dermatol.* **129**, 498–502 (2009).
- 1058 19. Li, M., Hener, P., Zhang, Z., Kato, S., Metzger, D. & Chambon, P. Topical vitamin D3 and
1059 low-calcemic analogs induce thymic stromal lymphopoietin in mouse keratinocytes and
1060 trigger an atopic dermatitis. *Proc. Natl. Acad. Sci.* **103**, 11736–11741 (2006).
- 1061 20. Zhang, Z., Hener, P., Frossard, N., Kato, S., Metzger, D., Li, M. & Chambon, P. Thymic
1062 stromal lymphopoietin overproduced by keratinocytes in mouse skin aggravates
1063 experimental asthma. *Proc. Natl. Acad. Sci.* **106**, 1536–1541 (2009).
- 1064 21. Moosbrugger-Martinz, V., Schmuth, M. & Dubrac, S. A Mouse Model for Atopic Dermatitis
1065 Using Topical Application of Vitamin D3 or of Its Analog MC903. *Methods Mol. Biol.* **1559**,
1066 91–106 (2017).
- 1067 22. Oetjen, L. K., Mack, M. R., Feng, J., Whelan, T. M., Niu, H., Guo, C. J., Chen, S., Trier, A.
1068 M., Xu, A. Z., Tripathi, S. V., Luo, J., Gao, X., Yang, L., Hamilton, S. L., Wang, P. L.,
1069 Brestoff, J. R., Council, M. L., Brasington, R., Schaffer, A., Brombacher, F., Hsieh, C.-S.,
1070 Gereau, R. W., Miller, M. J., Chen, Z.-F., Hu, H., Davidson, S., Liu, Q. & Kim, B. S.
1071 Sensory Neurons Co-opt Classical Immune Signaling Pathways to Mediate Chronic Itch.
1072 *Cell* **171**, 217–228.e13 (2017).
- 1073 23. Morita, T., McClain, S. P., Batia, L. M., Pellegrino, M., Wilson, S. R., Kienzler, M. A.,
1074 Lyman, K., Olsen, A. S. B., Wong, J. F., Stucky, C. L., Brem, R. B. & Bautista, D. M.
1075 HTR7 Mediates Serotonergic Acute and Chronic Itch. *Neuron* 1–15 (2015).
1076 doi:10.1016/j.neuron.2015.05.044
- 1077 24. Kim, D., Kobayashi, T. & Nagao, K. Research Techniques Made Simple: Mouse Models
1078 of Atopic Dermatitis. *J. Invest. Dermatol.* **139**, 984–990.e1 (2019).
- 1079 25. Cevikbas, F., Wang, X., Akiyama, T., Kempkes, C., Savinko, T., Antal, A., Kukova, G.,

- 1080 Buhl, T., Ikoma, A., Buddenkotte, J., Soumelis, V., Feld, M., Alenius, H., Dillon, S. R.,
 1081 Carstens, E. E., Homey, B., Basbaum, A. I. & Steinhoff, M. A sensory neuron-expressed
 1082 IL-31 receptor mediates T helper cell-dependent itch: Involvement of TRPV1 and TRPA1.
 1083 *J. Allergy Clin. Immunol.* **133**, 448–460 (2014).
- 1084 26. Meng, J., Moriyama, M., Feld, M., Buddenkotte, J., Buhl, T., Szöllösi, A., Zhang, J., Miller,
 1085 P., Ghetti, A., Fischer, M., Reeh, P. W., Shan, C., Wang, J. & Steinhoff, M. New
 1086 mechanism underlying IL-31-induced atopic dermatitis. *J. Allergy Clin. Immunol.* (2017).
 1087 doi:10.1016/j.jaci.2017.12.1002
- 1088 27. Martel, B. C., Lovato, P., Bäumer, W. & Olivry, T. Translational animal models of atopic
 1089 dermatitis for preclinical studies. *Yale J. Biol. Med.* **90**, 389–402 (2017).
- 1090 28. Rattenholl, A. & Steinhoff, M. Role of proteinase-activated receptors in cutaneous biology
 1091 and disease. *Drug Dev. Res.* **59**, 408–416 (2003).
- 1092 29. Yosipovitch, G. Dry skin and impairment of barrier function associated with itch - new
 1093 insights. *Int J Cosmet Sci* **26**, 1–7 (2004).
- 1094 30. Briot, A., Lacroix, M., Robin, A., Steinhoff, M., Deraison, C. & Hovnanian, A. Par2
 1095 inactivation inhibits early production of TSLP, but not cutaneous inflammation, in
 1096 netherton syndrome adult mouse model. *J. Invest. Dermatol.* **130**, 2736–2742 (2010).
- 1097 31. Demehri, S., Morimoto, M., Holtzman, M. J. & Kopan, R. Skin-derived TSLP triggers
 1098 progression from epidermal-barrier defects to asthma. *PLoS Biol.* **7**, e1000067 (2009).
- 1099 32. Gao, P. S., Rafaels, N. M., Mu, D., Hand, T., Murray, T., Boguniewicz, M., Hata, T.,
 1100 Schneider, L., Hanifin, J. M., Gallo, R. L., Gao, L., Beaty, T. H., Beck, L. A., Leung, D. Y.
 1101 M. & Barnes, K. C. Genetic variants in thymic stromal lymphopoietin are associated with
 1102 atopic dermatitis and eczema herpeticum. *J. Allergy Clin. Immunol.* **125**, 1403–1407
 1103 (2010).
- 1104 33. Kim, B. S., Siracusa, M. C., Saenz, S. A., Noti, M., Monticelli, L. A., Sonnenberg, G. F.,
 1105 Hepworth, M. R., Van Voorhees, A. S., Comeau, M. R. & Artis, D. TSLP elicits IL-33-
 1106 independent innate lymphoid cell responses to promote skin inflammation. *Sci Transl*
 1107 *Med* **5**, 170ra16-170ra16 (2013).
- 1108 34. Hidaka, T., Ogawa, E., Kobayashi, E. H., Suzuki, T., Funayama, R., Nagashima, T.,
 1109 Fujimura, T., Aiba, S., Nakayama, K., Okuyama, R. & Yamamoto, M. The aryl
 1110 hydrocarbon receptor AhR links atopic dermatitis and air pollution via induction of the
 1111 neurotrophic factor artemin. *Nat. Immunol.* **18**, 64–73 (2017).
- 1112 35. Kou, K., Nakamura, F., Aihara, M., Chen, H., Seto, K., Komuri-Yamaguchi, J., Kambara,
 1113 T., Nagashima, Y., Goshima, Y. & Ikezawa, Z. Decreased expression of semaphorin-3A,
 1114 a neurite-collapsing factor, is associated with itch in psoriatic skin. *Acta Derm. Venereol.*
 1115 **92**, 521–528 (2012).
- 1116 36. Tominaga, M. & Takamori, K. Recent Advances in the Study of Itching An Update on
 1117 Peripheral Mechanisms and Treatments of Itch. **36**, 1241–1247 (2013).
- 1118 37. Tominaga, M., Ozawa, S., Ogawa, H. & Takamori, K. A hypothetical mechanism of
 1119 intraepidermal neurite formation in NC/Nga mice with atopic dermatitis. *J. Dermatol. Sci.*
 1120 **46**, 199–210 (2007).
- 1121 38. Tominaga, M. & Takamori, K. Itch and nerve fibers with special reference to atopic
 1122 dermatitis: therapeutic implications. *J. Dermatol.* **41**, 205–212 (2014).
- 1123 39. Haas, S., Capellino, S., Phan, N. Q., Böhm, M., Luger, T. A., Straub, R. H. & Ständer, S.
 1124 Low density of sympathetic nerve fibers relative to substance P-positive nerve fibers in
 1125 lesional skin of chronic pruritus and prurigo nodularis. *J. Dermatol. Sci.* **58**, 193–197
 1126 (2010).
- 1127 40. Kamo, A., Tominaga, M., Taneda, K., Ogawa, H. & Takamori, K. Neurotrophin inhibits the
 1128 increase in intraepidermal nerve density in the acetone-treated dry-skin mouse model.
 1129 *Clin. Exp. Dermatol.* **38**, 665–668 (2013).
- 1130 41. Oaklander, A. L. & Siegel, S. M. Cutaneous innervation: Form and function. *J. Am. Acad.*

- 1131 *Dermatol.* **53**, 1027–1037 (2005).
- 1132 42. Schüttenhelm, B. N., Duraku, L. S., Dijkstra, J. F., Walbeehm, E. T. & Holstege, J. C.
1133 Differential Changes in the Peptidergic and the Non-Peptidergic Skin Innervation in Rat
1134 Models for Inflammation, Dry Skin Itch, and Dermatitis. *J. Invest. Dermatol.* **135**, 2049–
1135 2057 (2015).
- 1136 43. Pereira, M. P., Mühl, S., Pogatzki-Zahn, E. M., Agelopoulos, K. & Ständer, S.
1137 Intraepidermal Nerve Fiber Density: Diagnostic and Therapeutic Relevance in the
1138 Management of Chronic Pruritus: a Review. *Dermatol. Ther. (Heidelb)*. **6**, 509–517
1139 (2016).
- 1140 44. Tominaga, M., Tenggara, S., Kamo, A., Ogawa, H. & Takamori, K. Psoralen-ultraviolet A
1141 therapy alters epidermal Sema3A and NGF levels and modulates epidermal innervation
1142 in atopic dermatitis. *J. Dermatol. Sci.* **55**, 40–46 (2009).
- 1143 45. Palmer, C. N. a, Irvine, A. D., Terron-Kwiatkowski, A., Zhao, Y., Liao, H., Lee, S. P.,
1144 Goudie, D. R., Sandilands, A., Campbell, L. E., Smith, F. J. D., O'Regan, G. M., Watson,
1145 R. M., Cecil, J. E., Bale, S. J., Compton, J. G., DiGiovanna, J. J., Fleckman, P., Lewis-
1146 Jones, S., Arseculeratne, G., Sergeant, A., Munro, C. S., El Houate, B., McElreavey, K.,
1147 Halkjaer, L. B., Bisgaard, H., Mukhopadhyay, S. & McLean, W. H. I. Common loss-of-
1148 function variants of the epidermal barrier protein filaggrin are a major predisposing factor
1149 for atopic dermatitis. *Nat. Genet.* **38**, 441–446 (2006).
- 1150 46. Sandilands, A., Terron-Kwiatkowski, A., Hull, P. R., O'Regan, G. M., Clayton, T. H.,
1151 Watson, R. M., Carrick, T., Evans, A. T., Liao, H., Zhao, Y., Campbell, L. E., Schmutz,
1152 M., Gruber, R., Janecke, A. R., Elias, P. M., van Steensel, M. A. M., Nagtzaam, I., van
1153 Geel, M., Steijlen, P. M., Munro, C. S., Bradley, D. G., Palmer, C. N. A., Smith, F. J. D.,
1154 McLean, W. H. I. & Irvine, A. D. Comprehensive analysis of the gene encoding filaggrin
1155 uncovers prevalent and rare mutations in ichthyosis vulgaris and atopic eczema. *Nat.*
1156 *Genet.* **39**, 650–654 (2007).
- 1157 47. Gittler, J. K., Shemer, A., Suárez-Fariñas, M., Fuentes-Duculan, J., Gulewicz, K. J.,
1158 Wang, C. Q. F., Mitsui, H., Cardinale, I., De Guzman Strong, C., Krueger, J. G. &
1159 Guttman-Yassky, E. Progressive activation of TH2/TH22 cytokines and selective
1160 epidermal proteins characterizes acute and chronic atopic dermatitis. *J. Allergy Clin.*
1161 *Immunol.* **130**, 1344–1354 (2012).
- 1162 48. Oetjen, L. K. & Kim, B. S. Interactions of the immune and sensory nervous systems in
1163 atopy. *FEBS J.* **285**, 3138–3151 (2018).
- 1164 49. Mansouri, Y. & Guttman-Yassky, E. Immune Pathways in Atopic Dermatitis, and
1165 Definition of Biomarkers through Broad and Targeted Therapeutics. *J Clin Med* **4**, 858–
1166 873 (2015).
- 1167 50. Guttman-Yassky, E. & Krueger, J. G. Atopic dermatitis and psoriasis: two different
1168 immune diseases or one spectrum? *Curr. Opin. Immunol.* **48**, 68–73 (2017).
- 1169 51. Dong, X. X. & Dong, X. X. Peripheral and Central Mechanisms of Itch. *Neuron* **98**, 482–
1170 494 (2018).
- 1171 52. Hashimoto, T., Rosen, J. D., Sanders, K. M. & Yosipovitch, G. Possible role of
1172 neutrophils in itch. *Itch 1* (2018). doi:10.1097/itx.0000000000000017
- 1173 53. Fogh, K., Herlin, T. & Kragballe, K. Eicosanoids in skin of patients with atopic dermatitis:
1174 prostaglandin E2 and leukotriene B4 are present in biologically active concentrations. *J.*
1175 *Allergy Clin. Immunol.* **83**, 450–455 (1989).
- 1176 54. Ghasemlou, N., Chiu, I. M., Julien, J.-P. & Woolf, C. J. CD11b⁺Ly6G[−]myeloid cells
1177 mediate mechanical inflammatory pain hypersensitivity. *Proc. Natl. Acad. Sci.* 201501372
1178 (2015). doi:10.1073/pnas.1501372112
- 1179 55. Sivick, K. E., Arpaia, N., Reiner, G. L., Lee, B. L., Russell, B. R. & Barton, G. M. Toll-like
1180 receptor-deficient mice reveal how innate immune signaling influences Salmonella
1181 virulence strategies. *Cell Host Microbe* **15**, 203–213 (2014).

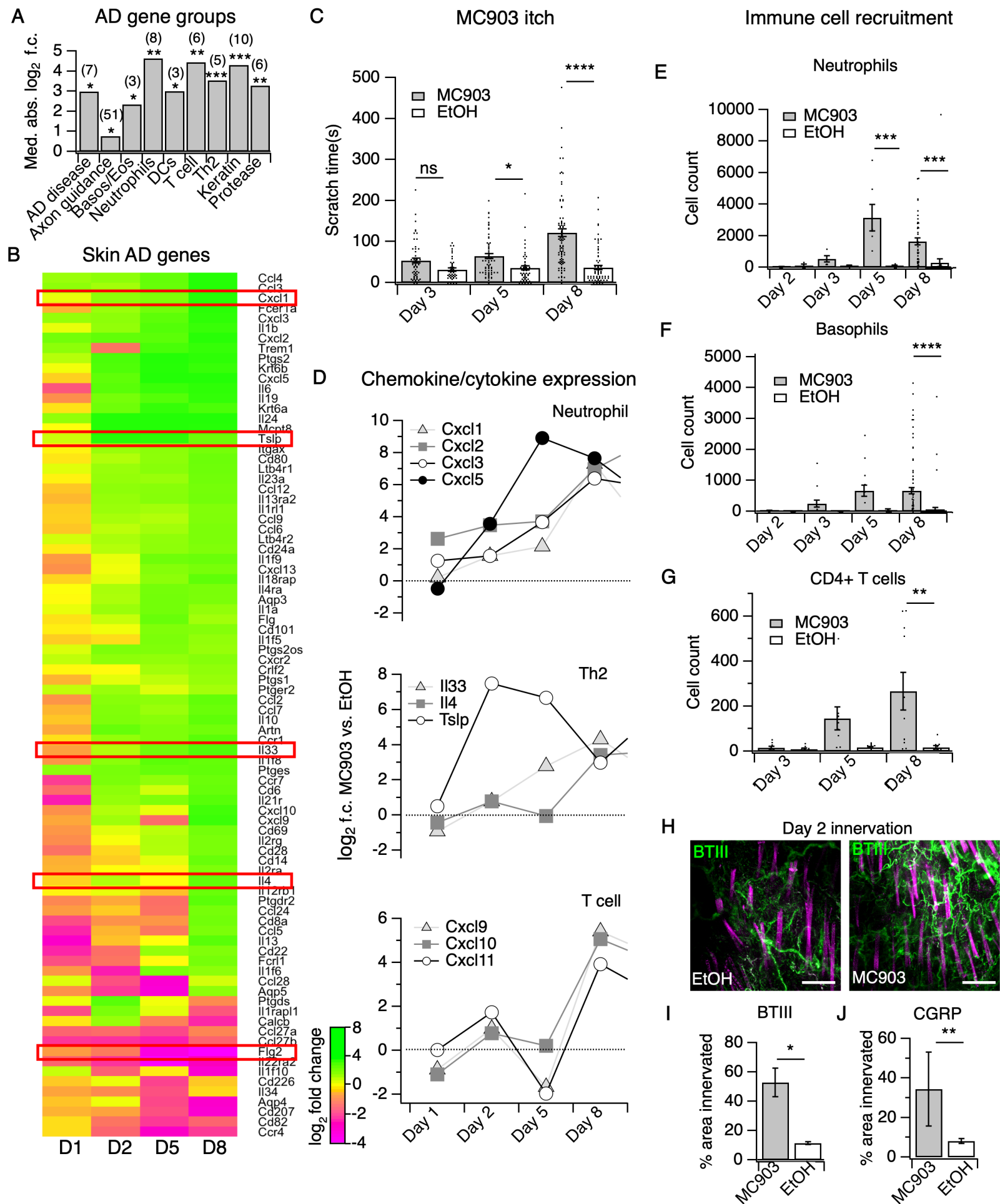
- 1182 56. Shimada, S. G. & LaMotte, R. H. Behavioral differentiation between itch and pain in
1183 mouse. *Pain* **139**, 681–687 (2008).
- 1184 57. Deftu, A. F., Filippi, A., Shibasaki, K., Gheorghe, R. O., Chiritoiu, M. & Ristoiu, V.
1185 Chemokine (C-X-C motif) ligand 1 (CXCL1) and chemokine (C-X-C motif) ligand 2
1186 (CXCL2) modulate the activity of TRPV1+/IB4+ cultured rat dorsal root ganglia neurons
1187 upon short-term and acute application. *J. Physiol. Pharmacol.* **68**, 385–395 (2017).
- 1188 58. Deftu, A. F., Filippi, A., Gheorghe, R. O. & Ristoiu, V. CXCL1 activates TRPV1 via Gi/o
1189 protein and actin filaments. *Life Sci.* **193**, 282–291 (2018).
- 1190 59. Carpino, N., Thierfelder, W. E., Chang, M., Saris, C., Turner, S. J., Ziegler, S. F. & Ihle, J.
1191 N. Absence of an essential role for thymic stromal lymphopoietin receptor in murine B-cell
1192 development. *Mol. Cell. Biol.* **24**, 2584–2592 (2004).
- 1193 60. Briot, A., Deraison, C., Lacroix, M., Bonnart, C., Robin, A., Besson, C., Dubus, P. &
1194 Hovnanian, A. Kallikrein 5 induces atopic dermatitis-like lesions through PAR2-mediated
1195 thymic stromal lymphopoietin expression in Netherton syndrome. *J. Exp. Med.* **206**,
1196 1135–1147 (2009).
- 1197 61. Zhang, Y., Yan, J., Hu, R., Sun, Y., Ma, Y., Chen, Z. & Jiang, H. Microglia are involved in
1198 pruritus induced by DNFB via the CX3CR1/p38 MAPK pathway. *Cell. Physiol. Biochem.*
1199 **35**, 1023–1033 (2015).
- 1200 62. Kitamura, A., Takata, R., Aizawa, S., Watanabe, H. & Wada, T. A murine model of atopic
1201 dermatitis can be generated by painting the dorsal skin with hapten twice 14 days apart.
1202 *Sci. Rep.* **8**, 1–9 (2018).
- 1203 63. Solinski, H. J., Dranchak, P., Oliphant, E., Gu, X., Earnest, T. W., Braisted, J., Inglese, J.
1204 & Hoon, M. A. Inhibition of natriuretic peptide receptor 1 reduces itch in mice. *Sci. Transl.*
1205 *Med.* **11**, eaav5464 (2019).
- 1206 64. Usoskin, D., Furlan, A., Islam, S., Abdo, H., Lönnerberg, P., Lou, D., Hjerling-Leffler, J.,
1207 Haeggström, J., Kharchenko, O., Kharchenko, P. V, Linnarsson, S. & Ernfors, P.
1208 Unbiased classification of sensory neuron types by large-scale single-cell RNA
1209 sequencing. *Nat. Neurosci.* **18**, 145–153 (2015).
- 1210 65. Takeda, M., Takahashi, M. & Matsumoto, S. Contribution of the activation of satellite glia
1211 in sensory ganglia to pathological pain. *Neurosci. Biobehav. Rev.* **33**, 784–792 (2009).
- 1212 66. Huang, J., Polgár, E., Solinski, H. J., Mishra, S. K., Tseng, P.-Y., Iwagaki, N., Boyle, K.
1213 A., Dickie, A. C., Kriegbaum, M. C., Wildner, H., Zeilhofer, H. U., Watanabe, M., Riddell,
1214 J. S., Todd, A. J. & Hoon, M. A. Circuit dissection of the role of somatostatin in itch and
1215 pain. *Nat. Neurosci.* **2018** 1 (2018). doi:10.1038/s41593-018-0119-z
- 1216 67. Solinski, H. J., Kriegbaum, M. C., Tseng, P. Y., Earnest, T. W., Gu, X., Barik, A., Chesler,
1217 A. T. & Hoon, M. A. Nppb Neurons Are Sensors of Mast Cell-Induced Itch. *Cell Rep.* **26**,
1218 3561-3573.e4 (2019).
- 1219 68. Shiratori-Hayashi, M., Koga, K., Tozaki-Saitoh, H., Kohro, Y., Toyonaga, H., Yamaguchi,
1220 C., Hasegawa, A., Nakahara, T., Hachisuka, J., Akira, S., Okano, H., Furue, M., Inoue, K.
1221 & Tsuda, M. STAT3-dependent reactive astrogliosis in the spinal dorsal horn underlies
1222 chronic itch. *Nat. Med.* **21**, 1–8 (2015).
- 1223 69. Ioannidis, L. J., Nie, C. Q., Ly, A., Ryg-Cornejo, V., Chiu, C. Y. & Hansen, D. S.
1224 Monocyte- and Neutrophil-Derived CXCL10 Impairs Efficient Control of Blood-Stage
1225 Malaria Infection and Promotes Severe Disease. *J. Immunol.* **196**, 1227–1238 (2016).
- 1226 70. Kanda, N., Shimizu, T., Tada, Y. & Watanabe, S. IL-18 enhances IFN- γ -induced
1227 production of CXCL9, CXCL10, and CXCL11 in human keratinocytes. *Eur. J. Immunol.*
1228 **37**, 338–350 (2007).
- 1229 71. Koga, C., Kabashima, K., Shiraishi, N., Kobayashi, M. & Tokura, Y. Possible pathogenic
1230 role of Th17 cells for atopic dermatitis. *J. Invest. Dermatol.* **128**, 2625–2630 (2008).
- 1231 72. Michalec, L., Choudhury, B. K., Postlethwait, E., Wild, J. S., Alam, R., Lett-Brown, M. &
1232 Sur, S. CCL7 and CXCL10 Orchestrate Oxidative Stress-Induced Neutrophilic Lung

- 1233 Inflammation. *J. Immunol.* **168**, 846–852 (2002).
- 1234 73. Padovan, E., Spagnoli, G. C., Ferrantini, M. & Heberer, M. IFN- α 2a induces IP-
1235 10/CXCL10 and MIG/CXCL9 production in monocyte-derived dendritic cells and
1236 enhances their capacity to attract and stimulate CD8⁺ effector T cells. *J. Leukoc. Biol.* **71**,
1237 669–676 (2002).
- 1238 74. Tamassia, N., Calzetti, F., Ear, T., Cloutier, A., Gasperini, S., Bazzoni, F., McDonald, P.
1239 P. & Cassatella, M. A. Molecular mechanisms underlying the synergistic induction of
1240 CXCL10 by LPS and IFN- γ in human neutrophils. *Eur. J. Immunol.* **37**, 2627–2634
1241 (2007).
- 1242 75. Qu, L., Fu, K., Yang, J., Shimada, S. G. & LaMotte, R. H. *CXCR3 chemokine receptor*
1243 *signaling mediates itch in experimental allergic contact dermatitis.* *Pain* **156**, (2015).
- 1244 76. Koro, O., Furutani, K., Hide, M., Yamada, S. & Yamamoto, S. Chemical mediators in
1245 atopic dermatitis: Involvement of leukotriene B4 released by a type I allergic reaction in
1246 the pathogenesis of atopic dermatitis. *J. Allergy Clin. Immunol.* **103**, 663–670 (1999).
- 1247 77. Mihm, M. C., Soter, N. A., Dvorak, H. F. & Austen, K. F. The structure of normal skin and
1248 the morphology of atopic eczema. *J. Invest. Dermatol.* **67**, 305–312 (1976).
- 1249 78. Shalit, M., Campbell, D. E., von Allmen, C., Atkins, P. C., Douglas, S. D. & Zweiman, B.
1250 Neutrophil activation in human inflammatory skin reactions. *J. Allergy Clin. Immunol.* **80**,
1251 87–93 (1987).
- 1252 79. Sumida, H., Yanagida, K., Kita, Y., Abe, J., Matsushima, K., Nakamura, M., Ishii, S.,
1253 Sato, S. & Shimizu, T. Interplay between CXCR2 and BLT1 facilitates neutrophil
1254 infiltration and resultant keratinocyte activation in a murine model of imiquimod-induced
1255 psoriasis. *J. Immunol.* **192**, 4361–4369 (2014).
- 1256 80. Perkins, N. M. & Tracey, D. J. Hyperalgesia due to nerve injury: role of neutrophils.
1257 *Neuroscience* **101**, 745–757 (2000).
- 1258 81. Guerrero, A. T. G., Verri, W. A., Cunha, T. M., Silva, T. A., Schivo, I. R. S., Dal-Secco, D.,
1259 Canetti, C., Rocha, F. A. C., Parada, C. A., Cunha, F. Q. & Ferreira, S. H. Involvement of
1260 LTB4 in zymosan-induced joint nociception in mice: participation of neutrophils and
1261 PGE2. *J. Leukoc. Biol.* **83**, 122–130 (2008).
- 1262 82. Cunha, J. M., Sachs, D., Canetti, C. A., Poole, S., Ferreira, S. H. & Cunha, F. Q. The
1263 critical role of leukotriene B 4 in antigen-induced mechanical hyperalgesia in immunised
1264 rats. *Br. J. Pharmacol.* **139**, 1135–1145 (2003).
- 1265 83. Finley, a, Chen, Z., Esposito, E., Cuzzocrea, S., Sabbadini, R. & Salvemini, D.
1266 Sphingosine 1-phosphate mediates hyperalgesia via a neutrophil-dependent mechanism.
1267 *PLoS One* **8**, e55255 (2013).
- 1268 84. Carreira, E. U., Carregaro, V., Teixeira, M. M., Moriconi, A., Aramini, A., Verri, W. A.,
1269 Ferreira, S. H., Cunha, F. Q. & Cunha, T. M. Neutrophils recruited by CXCR1/2 signalling
1270 mediate post-incisional pain. *Eur J Pain* **17**, 654–663 (2013).
- 1271 85. Levine, J. D., Khasar, S. G. & Green, P. G. Neurogenic inflammation and arthritis. *Ann.*
1272 *N. Y. Acad. Sci.* **1069**, 155–167 (2006).
- 1273 86. Schön, M., Kubitzka, R. C., Ruzicka, T., Schön, M. P. & Denzer, D. Critical Role of
1274 Neutrophils for the Generation of Psoriasiform Skin Lesions in Flaky Skin Mice. *J. Invest.*
1275 *Dermatol.* **114**, 976–983 (2003).
- 1276 87. Oyoshi, M. K., He, R., Li, Y., Mondal, S., Yoon, J., Afshar, R., Chen, M., Lee, D. M., Luo,
1277 H. R., Luster, A. D., Cho, J. S., Miller, L. S., Larson, A., Murphy, G. F. & Geha, R. S.
1278 Leukotriene B4-driven neutrophil recruitment to the skin is essential for allergic skin
1279 inflammation. *Immunity* **37**, 747–758 (2012).
- 1280 88. Meixiong, J., Anderson, M., Limjunyawong, N., Sabbagh, M. F., Hu, E., Mack, M. R.,
1281 Oetjen, L. K., Wang, F., Kim, B. S. & Dong, X. Activation of Mast-Cell-Expressed Mas-
1282 Related G-Protein-Coupled Receptors Drives Non-histaminergic Itch. *Immunity* **50**, 1163-
1283 1171.e5 (2019).

- 1284 89. Chatterjea, D. & Martinov, T. Mast cells: versatile gatekeepers of pain. *Mol. Immunol.* **63**,
1285 38–44 (2015).
- 1286 90. Pinho-Ribeiro, F. A., Haarsma, R., Yang, N. J., Blake, K. J., Portley, M., Chiu, I. M.,
1287 Baddal, B., O’Seaghdha, M., Wessels, M. R., Verri, W. A. & Dale, J. B. Blocking Neuronal
1288 Signaling to Immune Cells Treats Streptococcal Invasive Infection. *Cell* **173**, 1083-
1289 1097.e22 (2018).
- 1290 91. Salvemini, D., Little, J. W., Doyle, T. & Neumann, W. L. Roles of reactive oxygen and
1291 nitrogen species in pain. *Free Radic. Biol. Med.* **51**, 951–966 (2011).
- 1292 92. Bautista, D. M., Jordt, S. E., Nikai, T., Tsuruda, P. R., Read, A. J., Poblete, J., Yamoah,
1293 E. N., Basbaum, A. I. & Julius, D. TRPA1 Mediates the Inflammatory Actions of
1294 Environmental Irritants and Proalgesic Agents. *Cell* **124**, 1269–1282 (2006).
- 1295 93. Liu, T. & Ji, R.-R. Oxidative stress induces itch via activation of transient receptor
1296 potential subtype ankyrin 1 in mice. *Neurosci Bull* **28**, 145–154 (2012).
- 1297 94. Caceres, A. I., Brackmann, M., Elia, M. D., Bessac, B. F., del Camino, D.,
1298 D’Amours, M., Witek, J. S., Fanger, C. M., Chong, J. A., Hayward, N. J., Homer, R.
1299 J., Cohn, L., Huang, X., Moran, M. M. & Jordt, S.-E. A sensory neuronal ion channel
1300 essential for airway inflammation and hyperreactivity in asthma. *Proc. Natl. Acad. Sci.*
1301 *U.S.A.* **106**, 9099–9104 (2009).
- 1302 95. Wang, J. Neutrophils in tissue injury and repair. *Cell Tissue Res.* **371**, 531–539 (2018).
- 1303 96. Hammond, T. R., Robinton, D. & Stevens, B. Microglia and the Brain: Complementary
1304 Partners in Development and Disease. *Annu. Rev. Cell Dev. Biol.* **34**, 523–544 (2018).
- 1305 97. Brunner, P. M., Guttman-Yassky, E. & Leung, D. Y. M. The immunology of atopic
1306 dermatitis and its reversibility with broad-spectrum and targeted therapies. *J. Allergy Clin.*
1307 *Immunol.* **139**, S65–S76 (2017).
- 1308 98. Li, C., Maillet, I., Mackowiak, C., Viala, C., Padova, F. Di, Li, M., Togbe, D., Quesniaux,
1309 V., Lai, Y. & Ryffel, B. Experimental atopic dermatitis depends on IL-33R signaling via
1310 MyD88 in dendritic cells. *Cell Death Dis.* **8**, (2017).
- 1311 99. Saunders, S. P., Moran, T., Floudas, A., Wurlod, F., Kaszlikowska, A., Salimi, M., Quinn,
1312 E. M., Oliphant, C. J., Núñez, G., McManus, R., Hams, E., Irvine, A. D., McKenzie, A. N.
1313 J., Ogg, G. S. & Fallon, P. G. Spontaneous atopic dermatitis is mediated by innate
1314 immunity, with the secondary lung inflammation of the atopic March requiring adaptive
1315 immunity. *J. Allergy Clin. Immunol.* **137**, 482–491 (2016).
- 1316 100. Andersson, S. The role of mast cells and mast cell mediators in the development of
1317 atopic dermatitis in a mouse model. *52* (2014).
- 1318 101. Liu, B., Tai, Y., Liu, B., Caceres, A. I., Yin, C. & Jordt, S.-E. Transcriptome profiling
1319 reveals Th2 bias and identifies endogenous itch mediators in poison ivy contact
1320 dermatitis. *JCI Insight* (2019). doi:10.1172/jci.insight.124497
- 1321 102. Malik, K., Ungar, B., Garcet, S., Dutt, R., Dickstein, D., Zheng, X., Xu, H., Estrada, Y. D.,
1322 Suárez-Fariñas, M., Shemer, A., Krueger, J. G. & Guttman-Yassky, E. Dust mite induces
1323 multiple polar T cell axes in human skin. *Clin. Exp. Allergy* **47**, 1648–1660 (2017).
- 1324 103. Qu, L., Fu, K., Shimada, S. G. & LaMotte, R. H. Cl⁻ channel is required for CXCL10-
1325 induced neuronal activation and itch response in a murine model of allergic contact
1326 dermatitis. *J. Neurophysiol.* **118**, 619–624 (2017).
- 1327 104. Jing, P. B., Cao, D. L., Li, S. S., Zhu, M., Bai, X. Q., Wu, X. B. & Gao, Y. J. Chemokine
1328 Receptor CXCR3 in the Spinal Cord Contributes to Chronic Itch in Mice. *Neurosci. Bull.*
1329 **34**, 54–63 (2018).
- 1330 105. Hamilton, J. D., Suárez-Fariñas, M., Dhingra, N., Cardinale, I., Li, X., Kostic, A., Ming,
1331 J. E., Radin, A. R., Krueger, J. G., Graham, N., Yancopoulos, G. D., Pirozzi, G. &
1332 Guttman-Yassky, E. Dupilumab improves the molecular signature in skin of patients with
1333 moderate-to-severe atopic dermatitis. *J. Allergy Clin. Immunol.* **134**, 1293–1300 (2014).
- 1334 106. Simpson, E. L., Bieber, T., Guttman-Yassky, E., Beck, L. A., Blauvelt, A., Cork, M. J.,

- 1335 Silverberg, J. I., Deleuran, M., Kataoka, Y., Lacour, J.-P., Kingo, K., Worm, M., Poulin, Y.,
 1336 Wollenberg, A., Soo, Y., Graham, N. M. H., Pirozzi, G., Akinlade, B., Staudinger, H.,
 1337 Mastey, V., Eckert, L., Gadkari, A., Stahl, N., Yancopoulos, G. D., Ardeleanu, M. &
 1338 Investigators, S. 1 and S. 2. Two Phase 3 Trials of Dupilumab versus Placebo in Atopic
 1339 Dermatitis. *N. Engl. J. Med.* **375**, 2335–2348 (2016).
- 1340 107. Yellin, M., Paliienko, I., Balanescu, A., Ter-Vartanian, S., Tseluyko, V., Xu, L. A., Tao, X.,
 1341 Cardarelli, P. M., Leblanc, H., Nichol, G., Ancuta, C., Chirieac, R. & Luo, A. A phase II,
 1342 randomized, double-blind, placebo-controlled study evaluating the efficacy and safety of
 1343 MDX-1100, a fully human anti-CXCL10 monoclonal antibody, in combination with
 1344 methotrexate in patients with rheumatoid arthritis. *Arthritis Rheum.* **64**, 1730–1739
 1345 (2012).
- 1346 108. Scott, D., Wolfe, F. & Huizinga, T. Rheumatoid arthritis. *Lancet* **376**, 53–79 (2010).
- 1347 109. Liu, B., Tai, Y., Achanta, S., Kaelberer, M. M., Caceres, A. I., Shao, X. & Fang, J. IL-33 /
 1348 ST2 signaling excites sensory neurons and mediates itch response in a mouse model of
 1349 poison ivy contact allergy. **1**, (2016).
- 1350 110. Baral, P., Umans, B. D., Li, L., Wallrapp, A., Bist, M., Kirschbaum, T., Wei, Y., Zhou, Y.,
 1351 Kuchroo, V. K., Burkett, P. R., Yipp, B. G., Liberles, S. D. & Chiu, I. M. Nociceptor
 1352 sensory neurons suppress neutrophil and $\gamma\delta$ T cell responses in bacterial lung infections
 1353 and lethal pneumonia. *Nat. Med.* **24**, 417–426 (2018).
- 1354 111. Pinho-Ribeiro, F. A., Verri, W. A. & Chiu, I. M. Nociceptor Sensory Neuron–Immune
 1355 Interactions in Pain and Inflammation. *Trends Immunol.* **38**, 5–19 (2017).
- 1356 112. Blake, K. J., Baral, P., Voisin, T., Lubkin, A., Pinho-Ribeiro, F. A., Adams, K. L.,
 1357 Roberson, D. P., Ma, Y. C., Otto, M., Woolf, C. J., Torres, V. J. & Chiu, I. M.
 1358 *Staphylococcus aureus* produces pain through pore-forming toxins and neuronal TRPV1
 1359 that is silenced by QX-314. *Nat. Commun.* **9**, (2018).
- 1360 113. Langmead, B., Trapnell, C., Pop, M. & Salzberg, S. L. Ultrafast and memory-efficient
 1361 alignment of short DNA sequences to the human genome. *Genome Biol.* **10**, R25 (2009).
- 1362 114. Langmead, B. & Salzberg, S. L. Fast gapped-read alignment with Bowtie 2. *Nat. Methods*
 1363 **9**, 357–359 (2012).
- 1364 115. Anders, S. & Huber, W. Differential expression of RNA-Seq data at the gene level—the
 1365 DESeq package. *Heidelberg* (2012). at
 1366 <http://watson.nci.nih.gov/bioc_mirror/packages/2.11/bioc/vignettes/DESeq/inst/doc/DESeq.pdf>
 1367
- 1368 116. Anders, S., McCarthy, D. J., Chen, Y., Okoniewski, M., Smyth, G. K., Huber, W. &
 1369 Robinson, M. D. Count-based differential expression analysis of RNA sequencing data
 1370 using R and Bioconductor. *Nat Protoc* **8**, 1765–1786 (2013).
- 1371 117. Hill, R. Z., Hoffman, B. U., Morita, T., Campos, S. M., Lumpkin, E. A., Brem, R. B. &
 1372 Bautista, D. M. The signaling lipid sphingosine 1-phosphate regulates mechanical pain.
 1373 *Elife* **7**, e33285 (2018).
- 1374 118. Marshall, K. L., Clary, R. C., Baba, Y., Orlowsky, R. L., Gerling, G. J. & Lumpkin, E. A.
 1375 Touch Receptors Undergo Rapid Remodeling in Healthy Skin. *Cell Rep.* **17**, 1719–1727
 1376 (2016).
- 1377 119. Wilson, S. R., Gerhold, K. A., Bifolck-Fisher, A., Liu, Q., Patel, K. N., Dong, X. & Bautista,
 1378 D. M. TRPA1 is required for histamine-independent, Mas-related G protein-coupled
 1379 receptor-mediated itch. *Nat. Neurosci.* **14**, 595–602 (2011).
- 1380 120. Morita, T., McClain, S. P. P., Batia, L. M. M., Pellegrino, M., Wilson, S. R. R., Kienzler, M.
 1381 A. A., Lyman, K., Olsen, A. S. B. S. B., Wong, J. F. F., Stucky, C. L. L., Brem, R. B. B. &
 1382 Bautista, D. M. M. HTR7 Mediates Serotonergic Acute and Chronic Itch. *Neuron* **87**, 124–
 1383 138 (2015).
- 1384 121. von Moltke, J., Trinidad, N. J., Moayeri, M., Kintzer, A. F., Wang, S. B., Van Rooijen, N.,
 1385 Brown, C. R., Krantz, B. A., Leppla, S. H., Gronert, K. & Vance, R. E. Rapid induction of

- 1386 inflammatory lipid mediators by the inflammasome in vivo. *Nat. Publ. Gr.* **490**, 107–111
1387 (2012).
- 1388 122. Sapieha, P., Stahl, A., Chen, J., Seaward, M. R., Willett, K. L., Krah, N. M., Dennison, R.
1389 J., Connor, K. M., Aderman, C. M., Licican, E., Carughi, A., Perelman, D., Kanaoka, Y.,
1390 Sangiovanni, J. P., Gronert, K. & Smith, L. E. H. 5-Lipoxygenase metabolite 4-HDHA is a
1391 mediator of the antiangiogenic effect of ω -3 polyunsaturated fatty acids. *Sci Transl Med*
1392 **3**, 69ra12-69ra12 (2011).
- 1393 123. Hill RZ. 2019. 10.1101-653873. Github. <https://github.com/rzhill/10.1101-653873>. bcbb047.
1394
1395



A Mouse and human itch genes

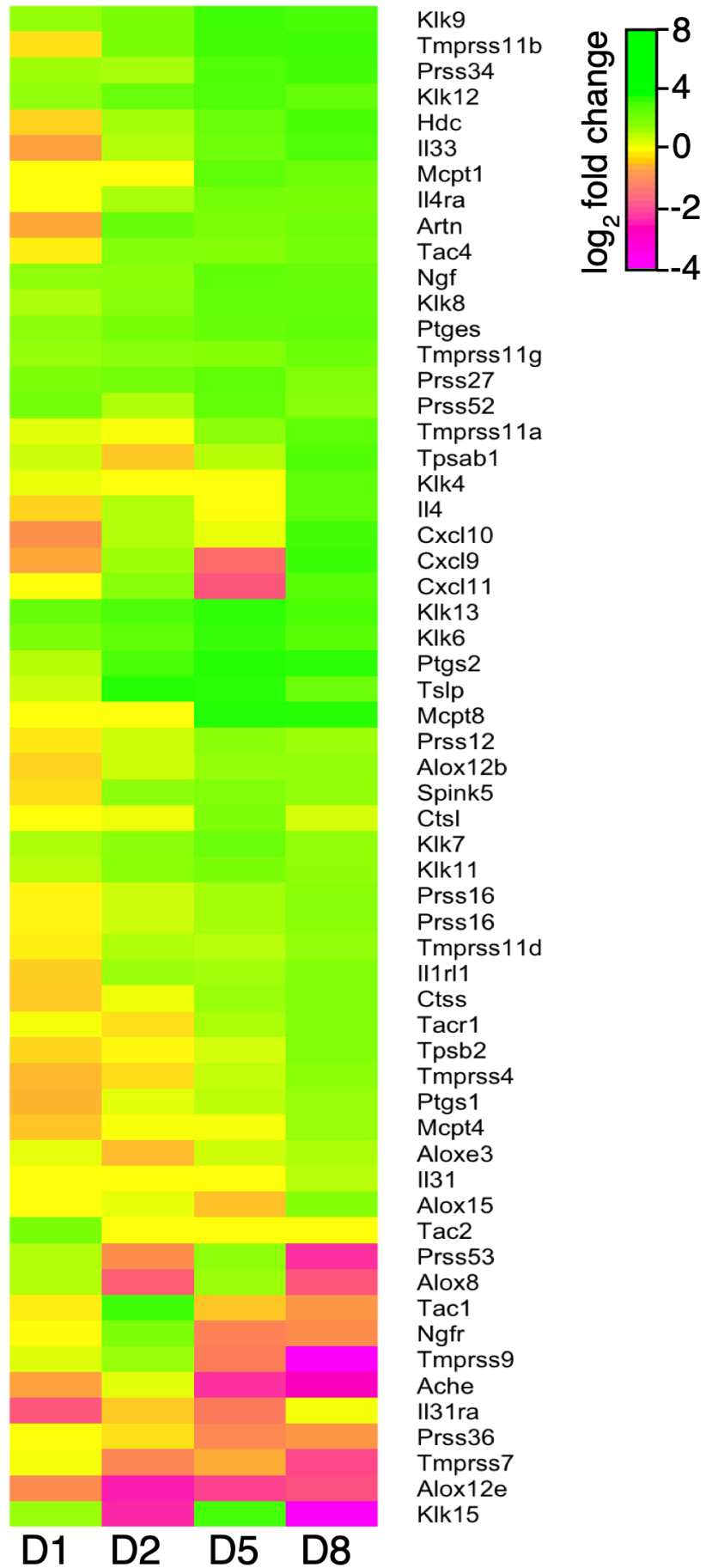


Figure 1-Figure Supplement 1

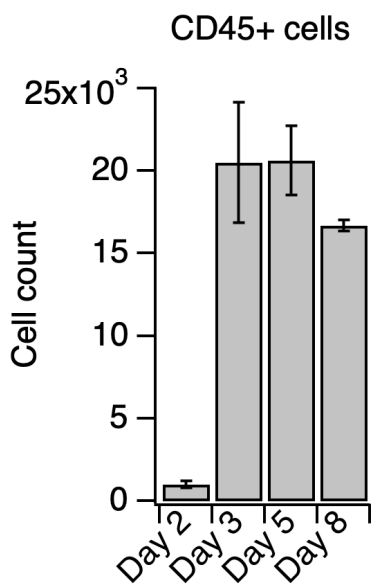
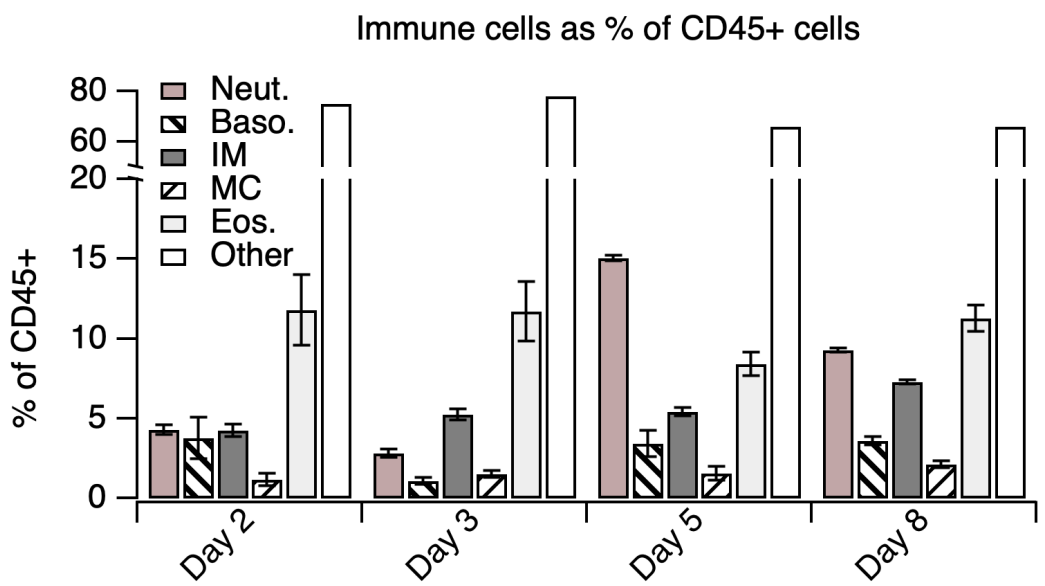
A**B**

Figure 1-Figure Supplement 2

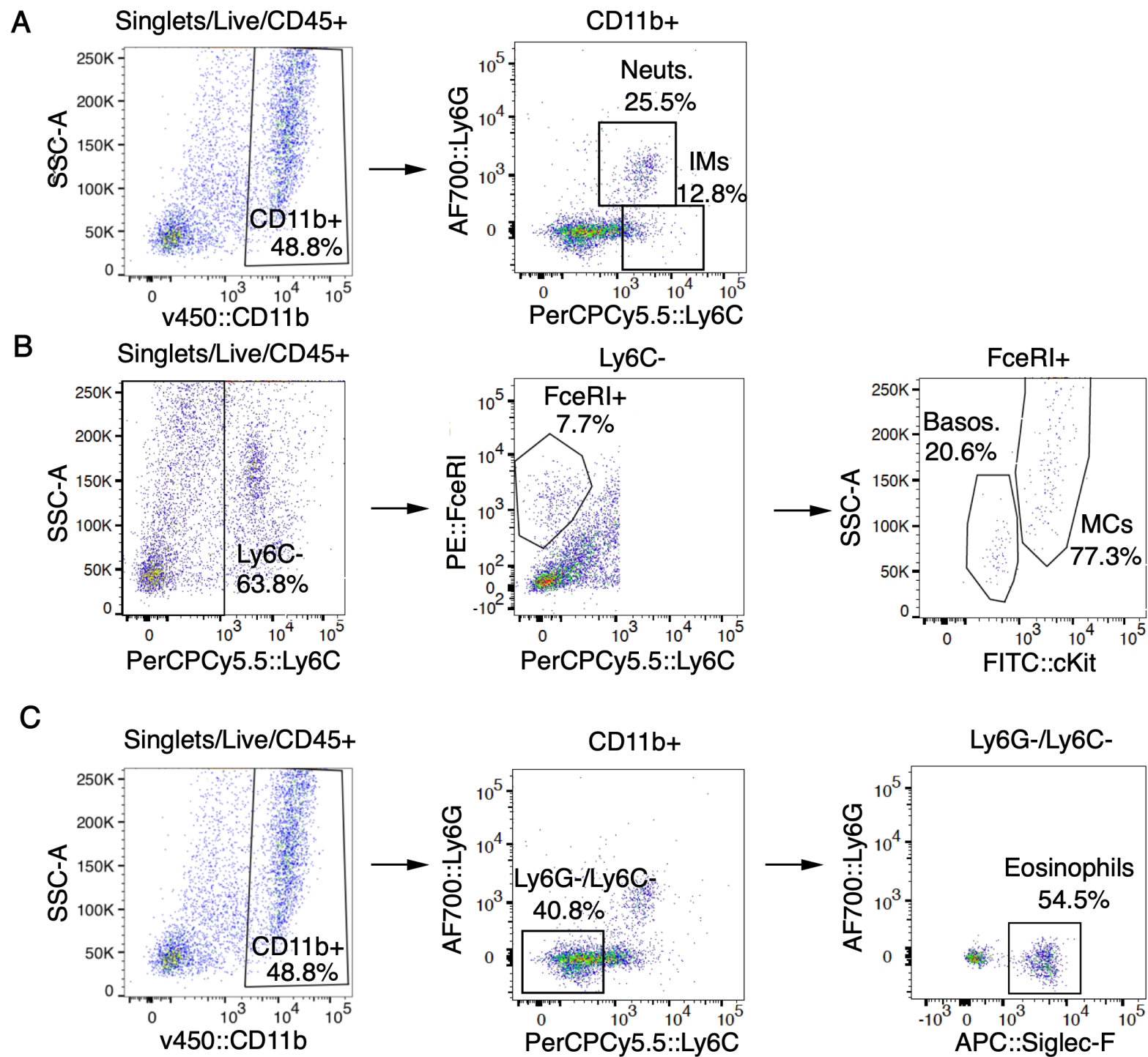


Figure 1-Figure Supplement 3

A

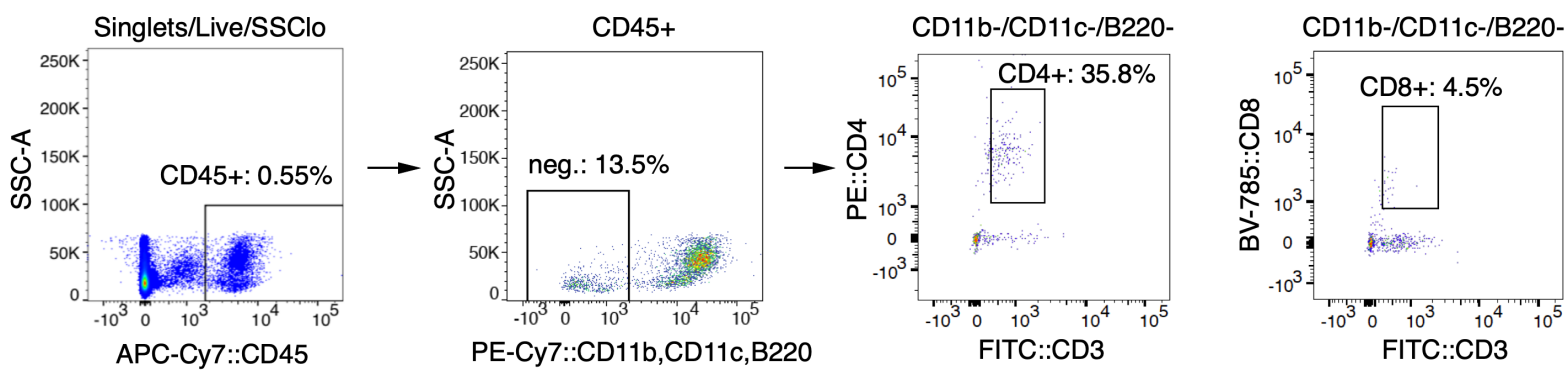
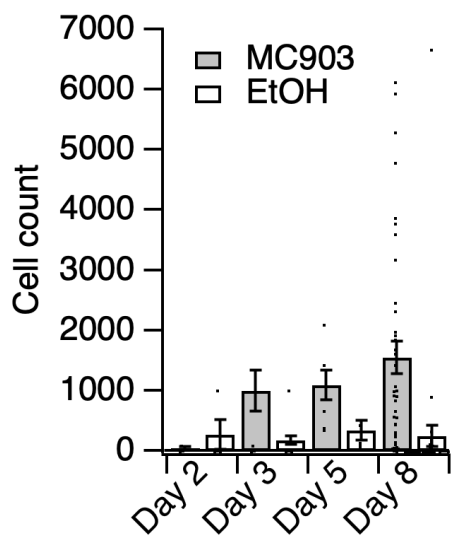
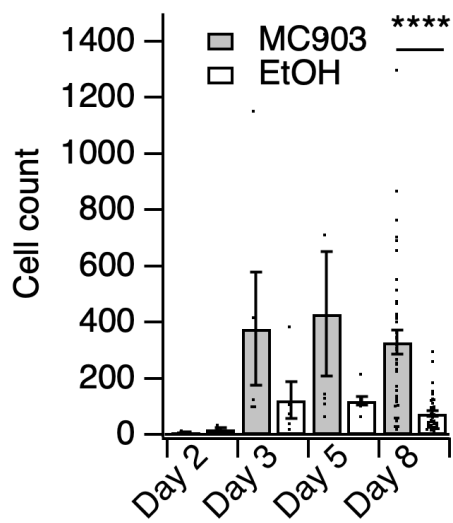


Figure 1-Figure Supplement 4

A Inflammatory monocytes



B Mast cells



C Eosinophils

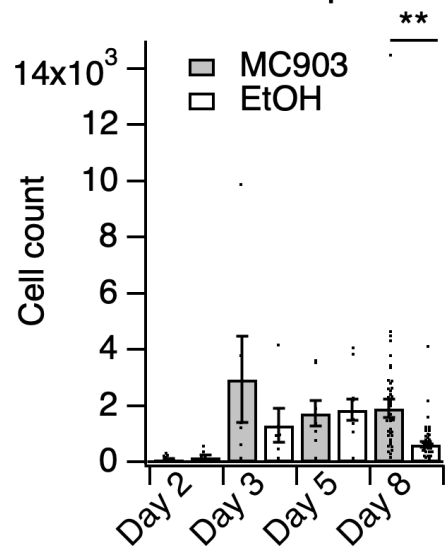


Figure 1-Figure Supplement 5

A SLIGRL-treated human keratinocytes

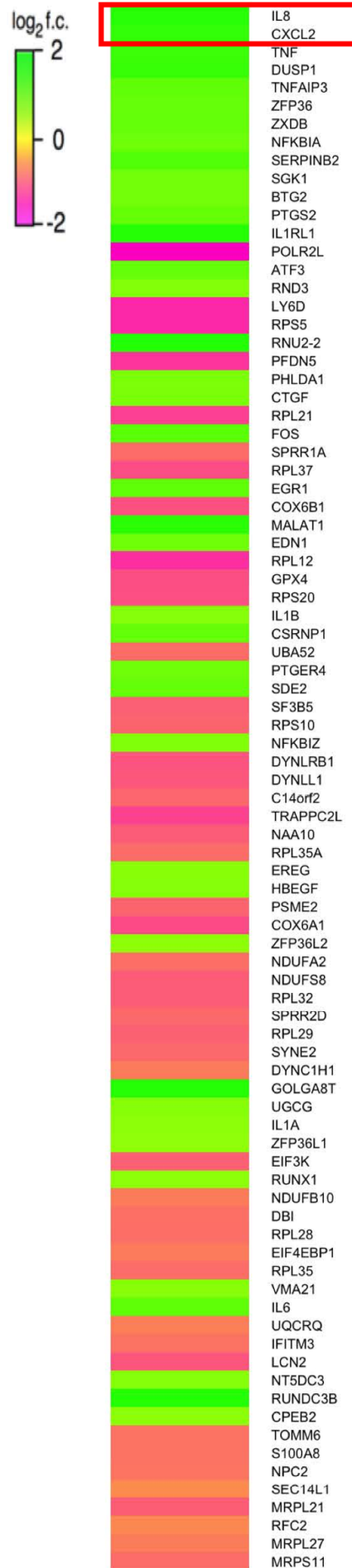


Figure 1-Figure Supplement 6

A Neuronal genes in skin

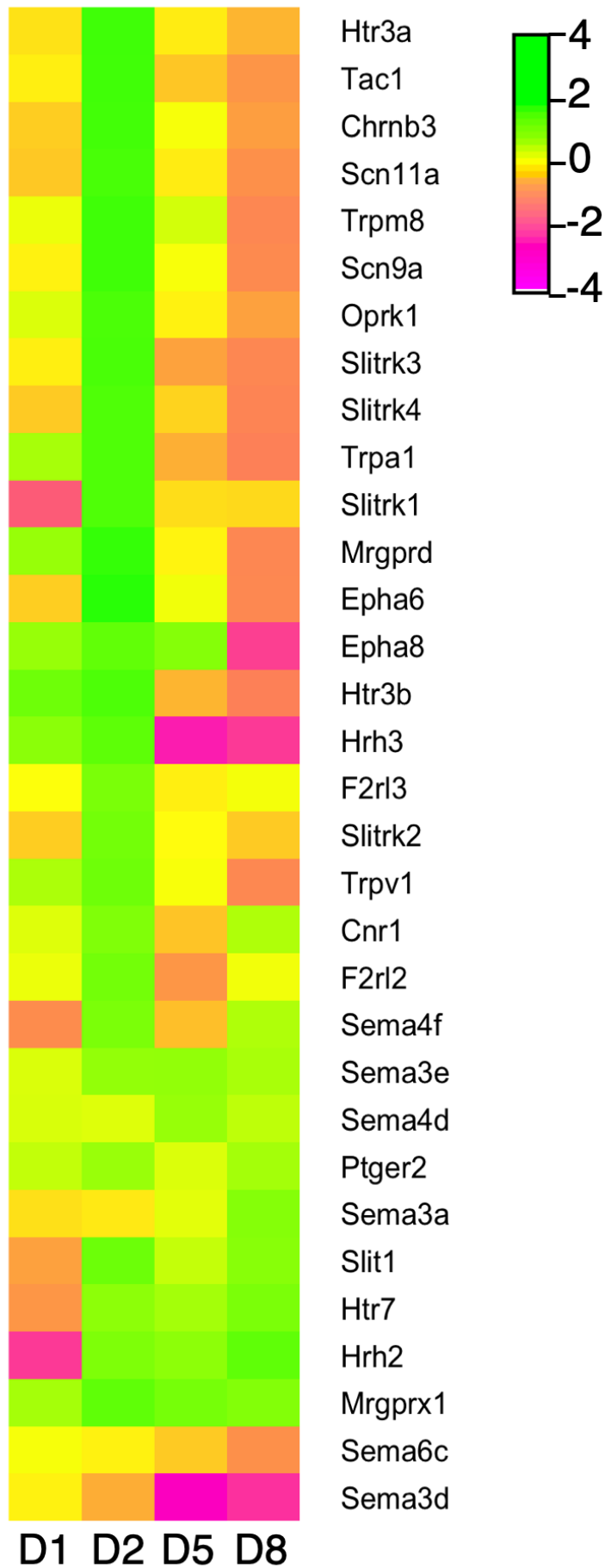
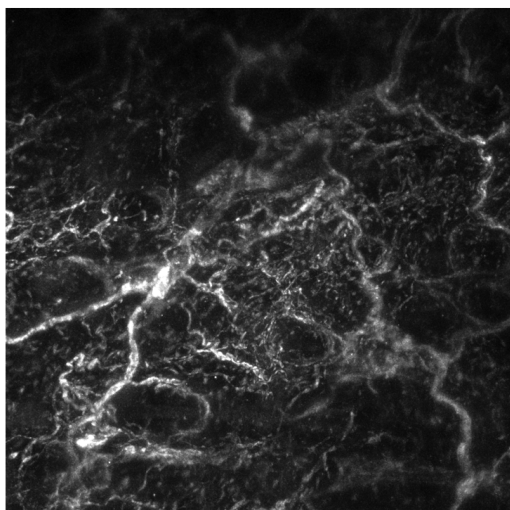
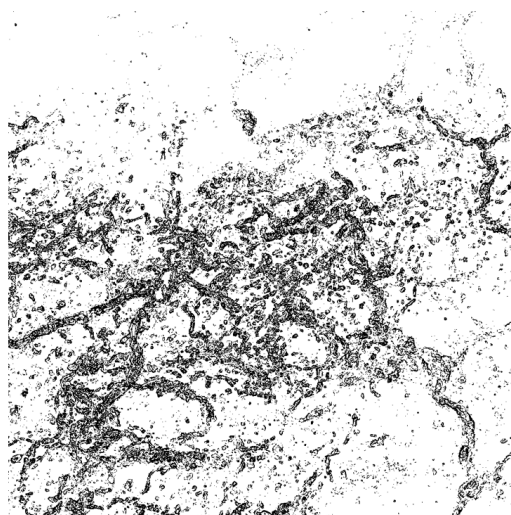


Figure 1-Figure Supplement 7

A



B



C

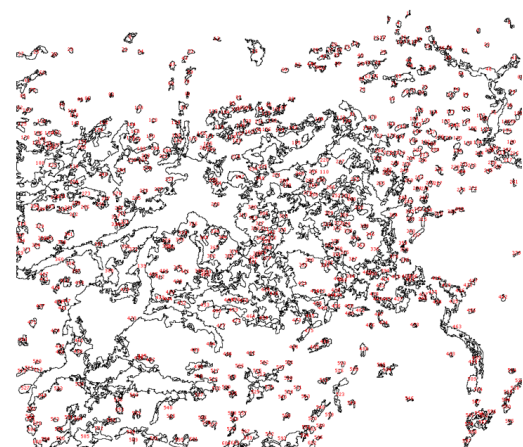


Figure 1-Figure Supplement 8

A

Day 2 CGRP innervation

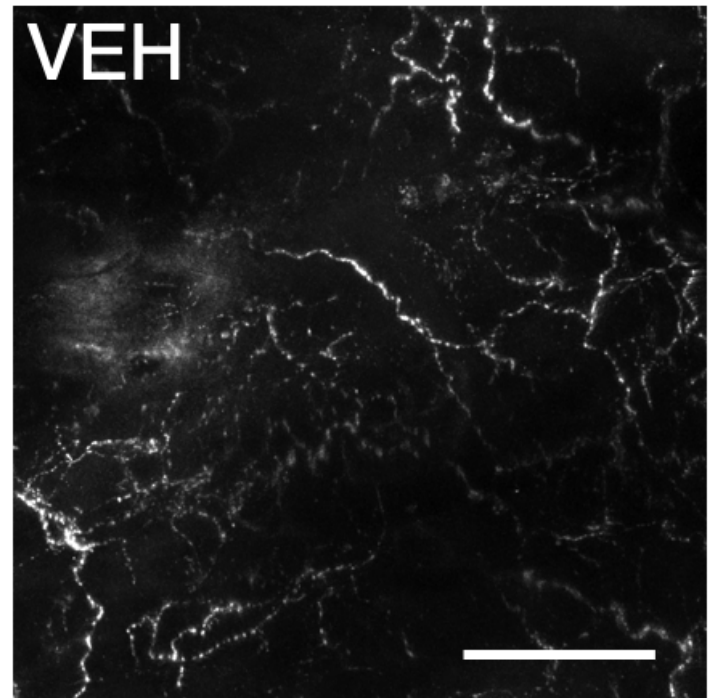
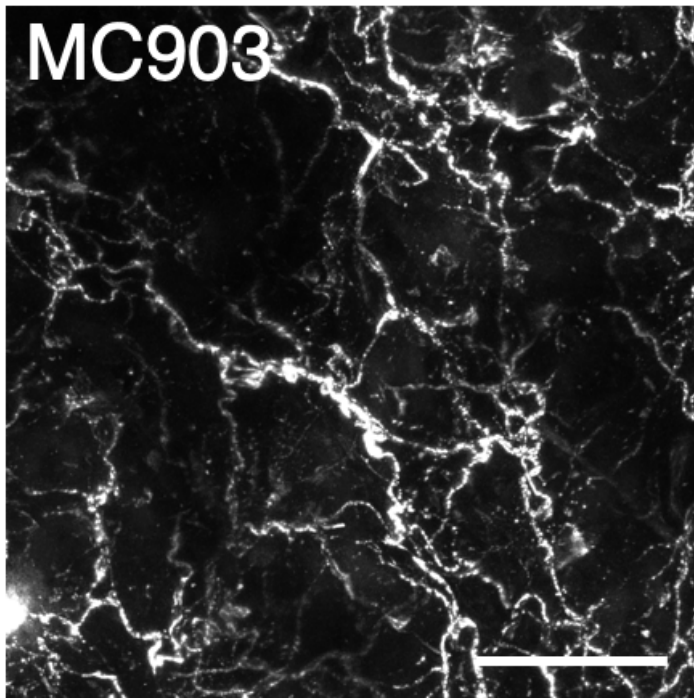


Figure 1-Figure Supplement 9

A

Lipid MS of skin

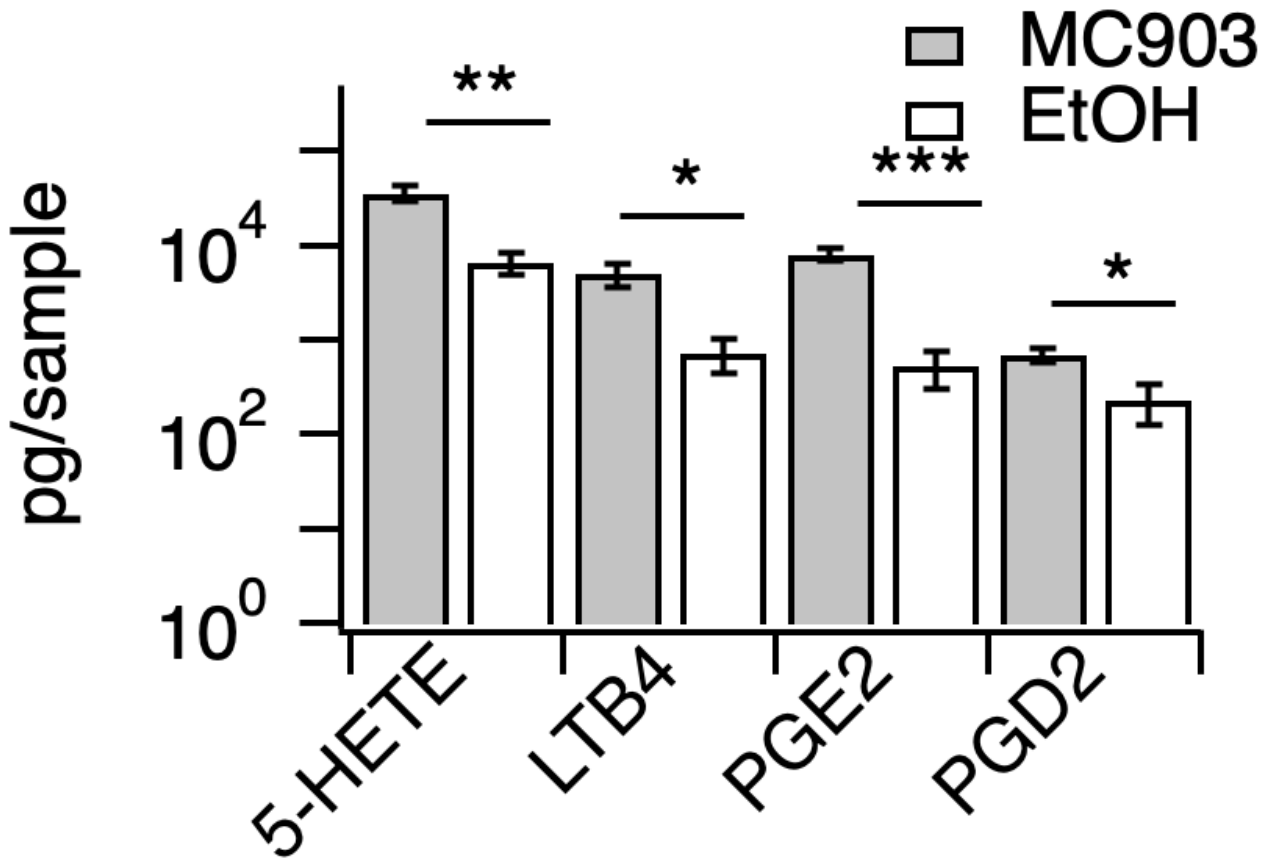


Figure 1-Figure Supplement 10

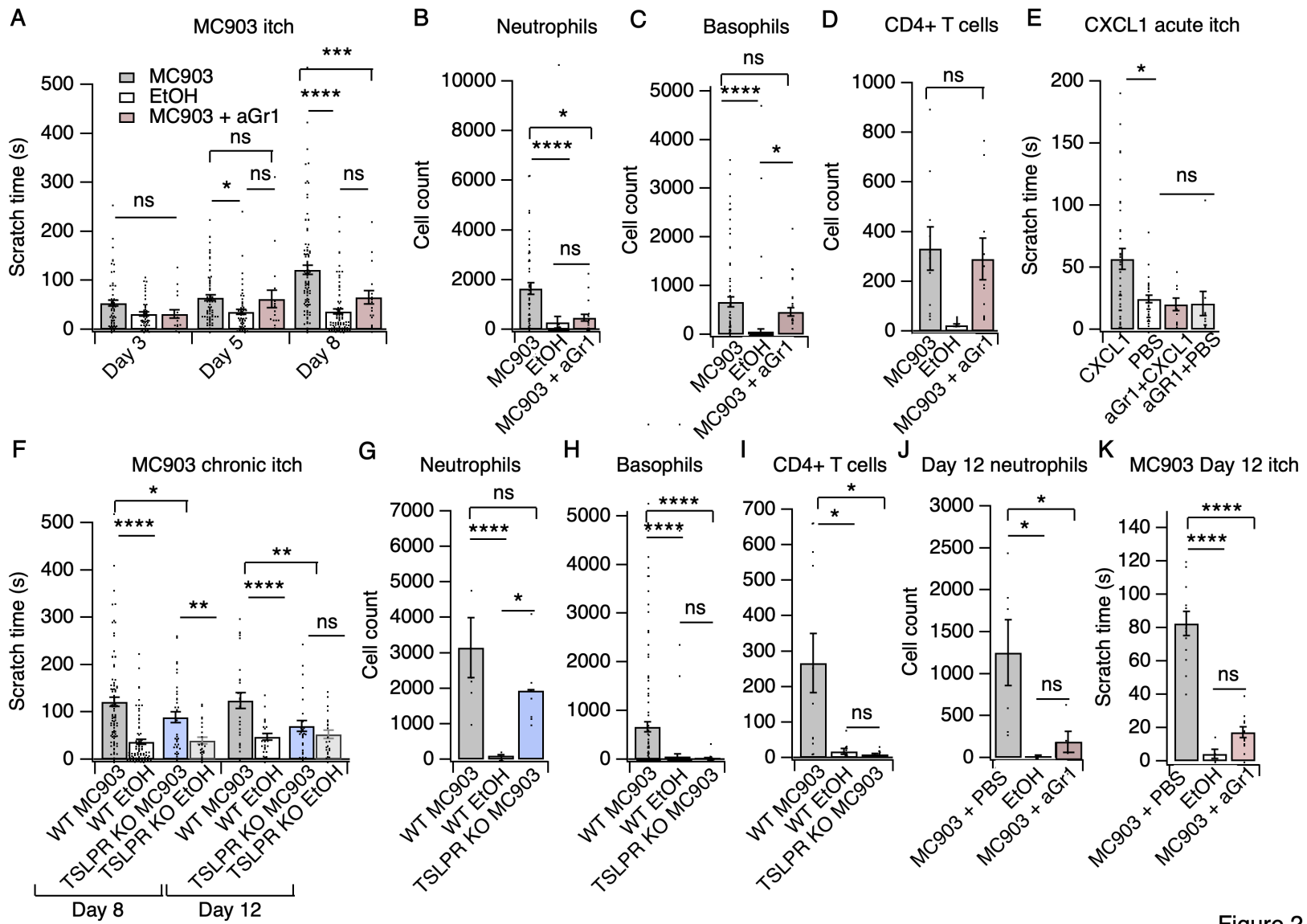
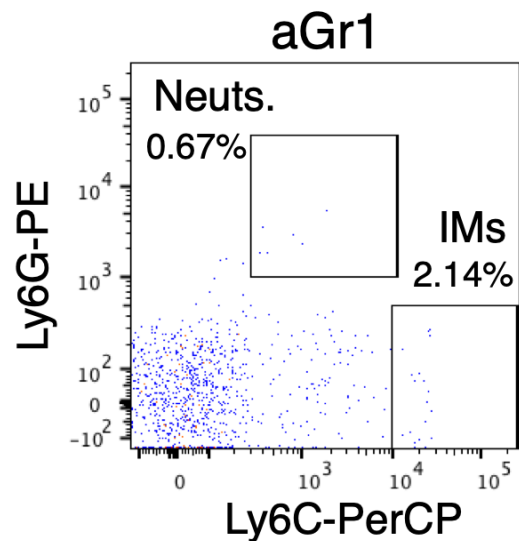
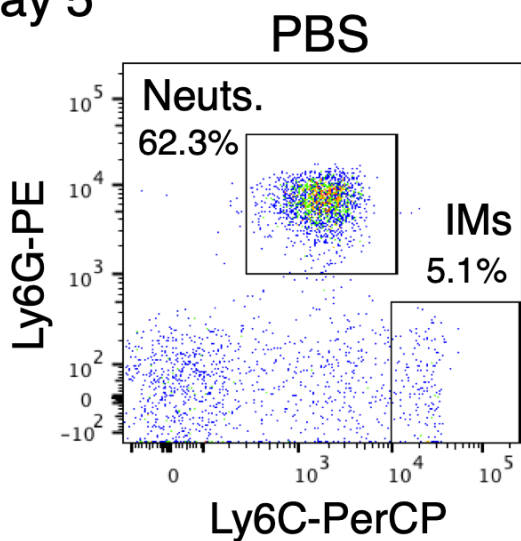
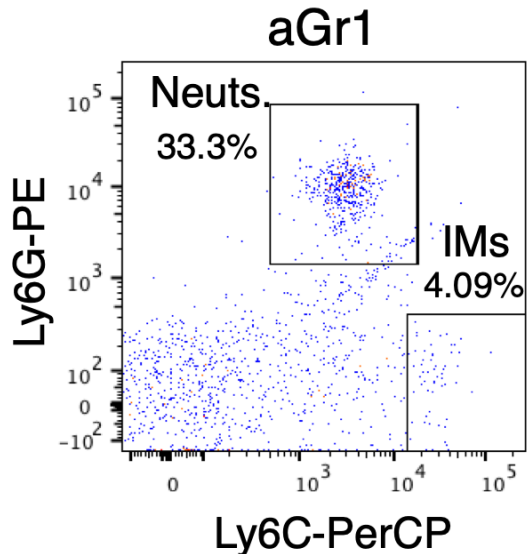
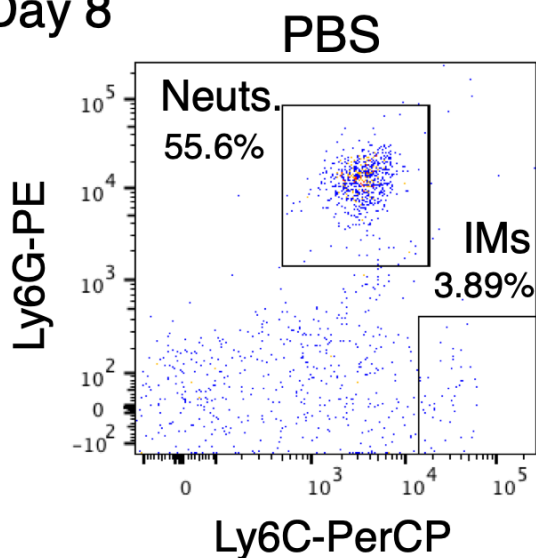


Figure 2

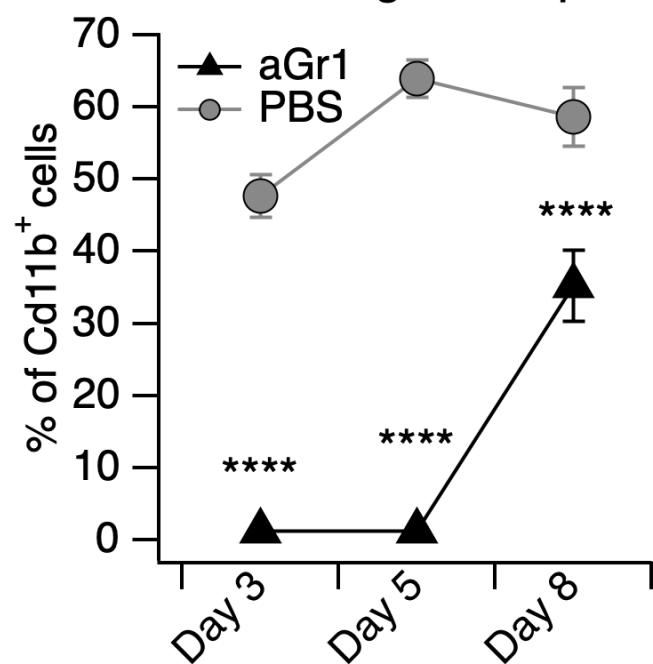
A Day 5



B Day 8



C Circulating neutrophils



Circulating IMs

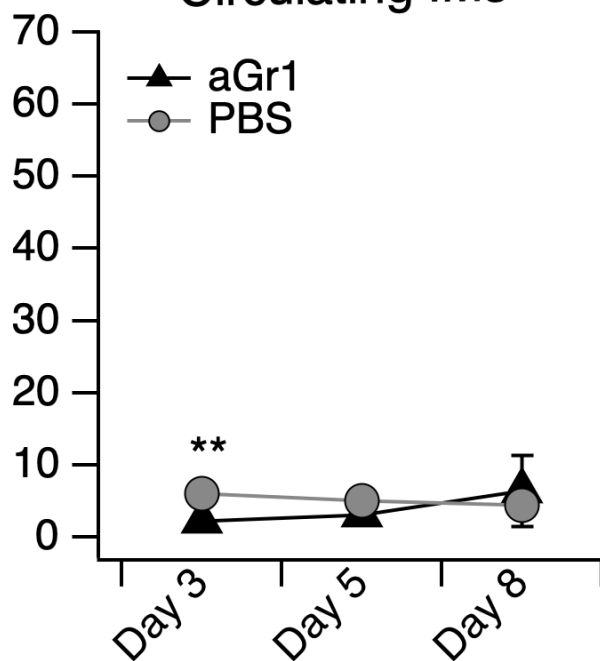


Figure 2-Figure Supplement 1

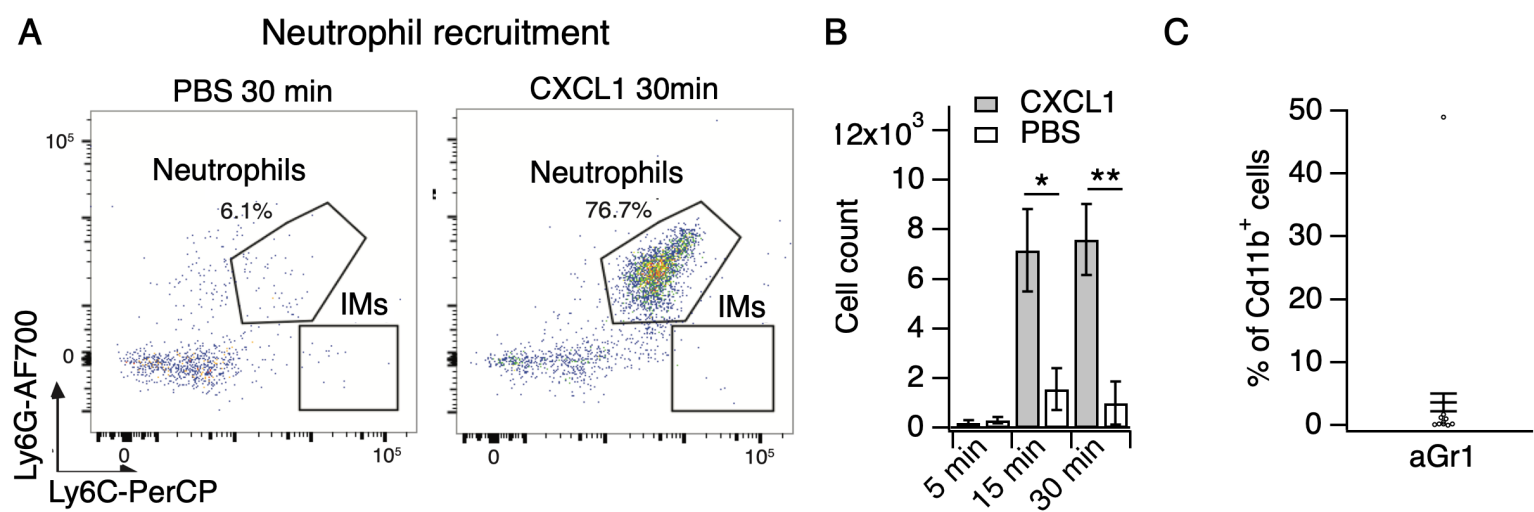


Figure 2-Figure Supplement 2

A

Chloroquine-evoked itch

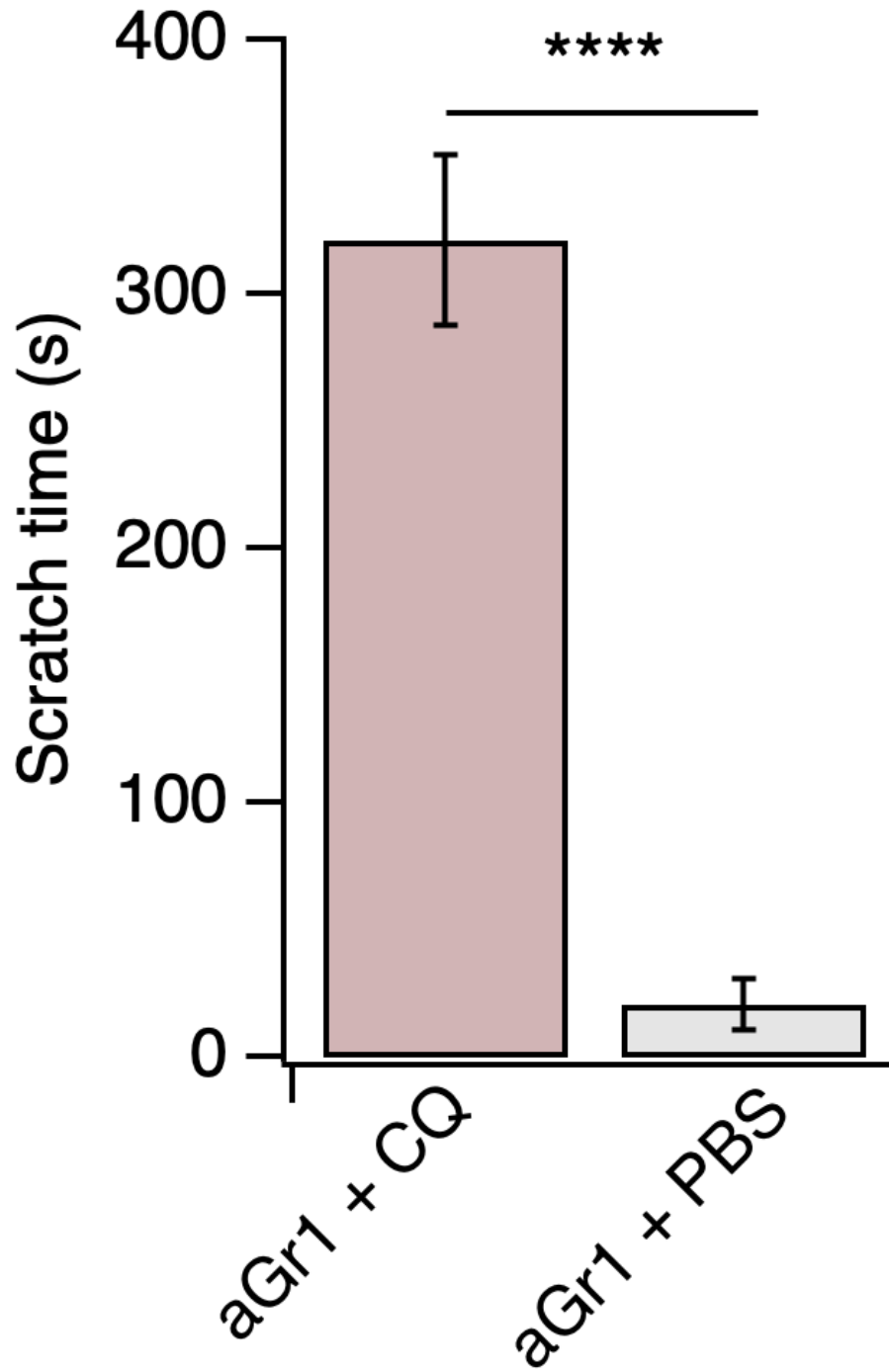


Figure 2-Figure Supplement 3

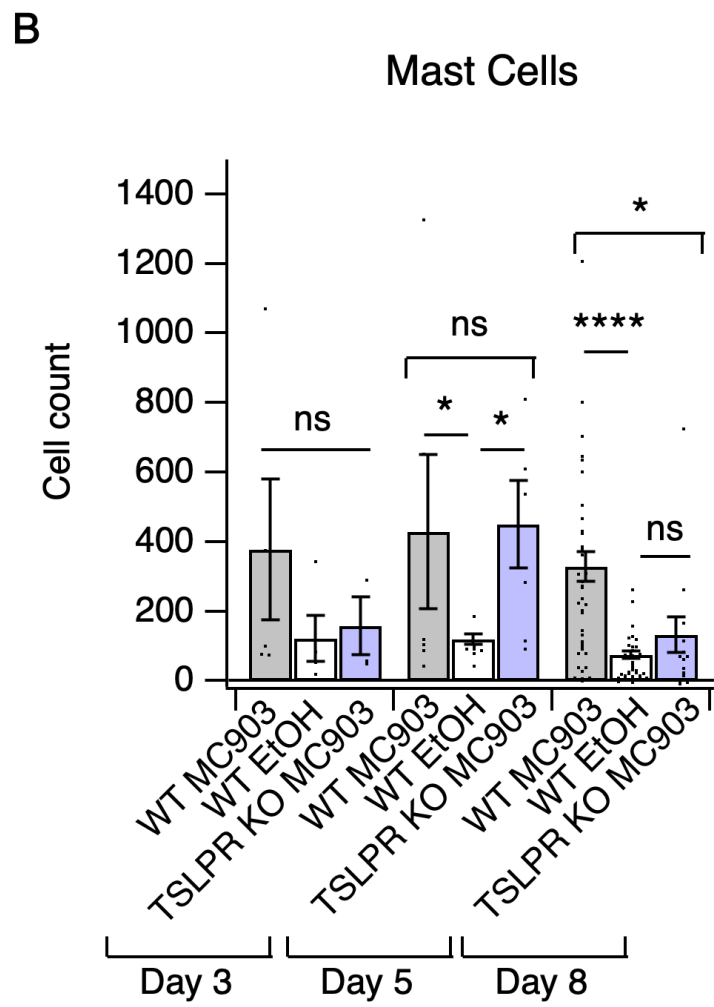
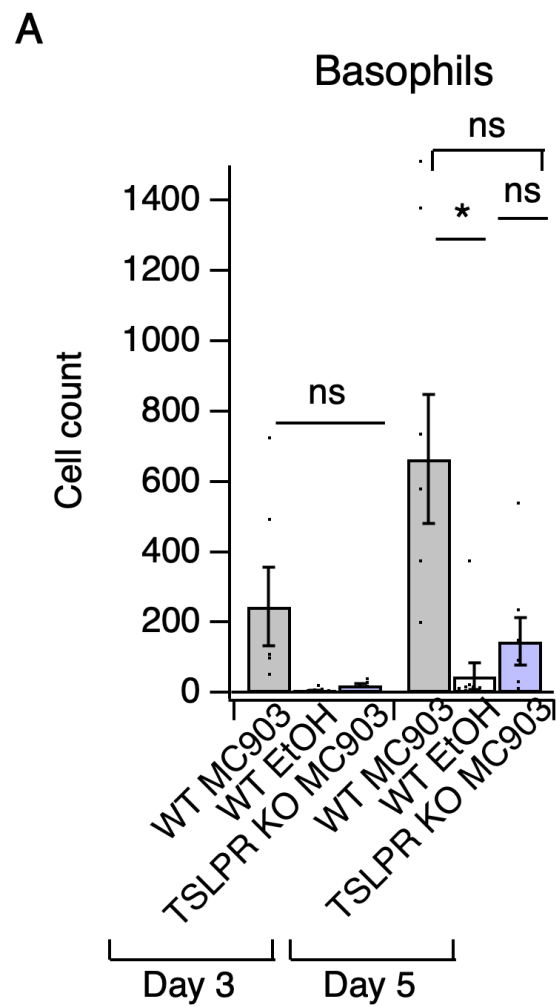


Figure 2-Figure Supplement 4

A Neutrophil counts in ear skin

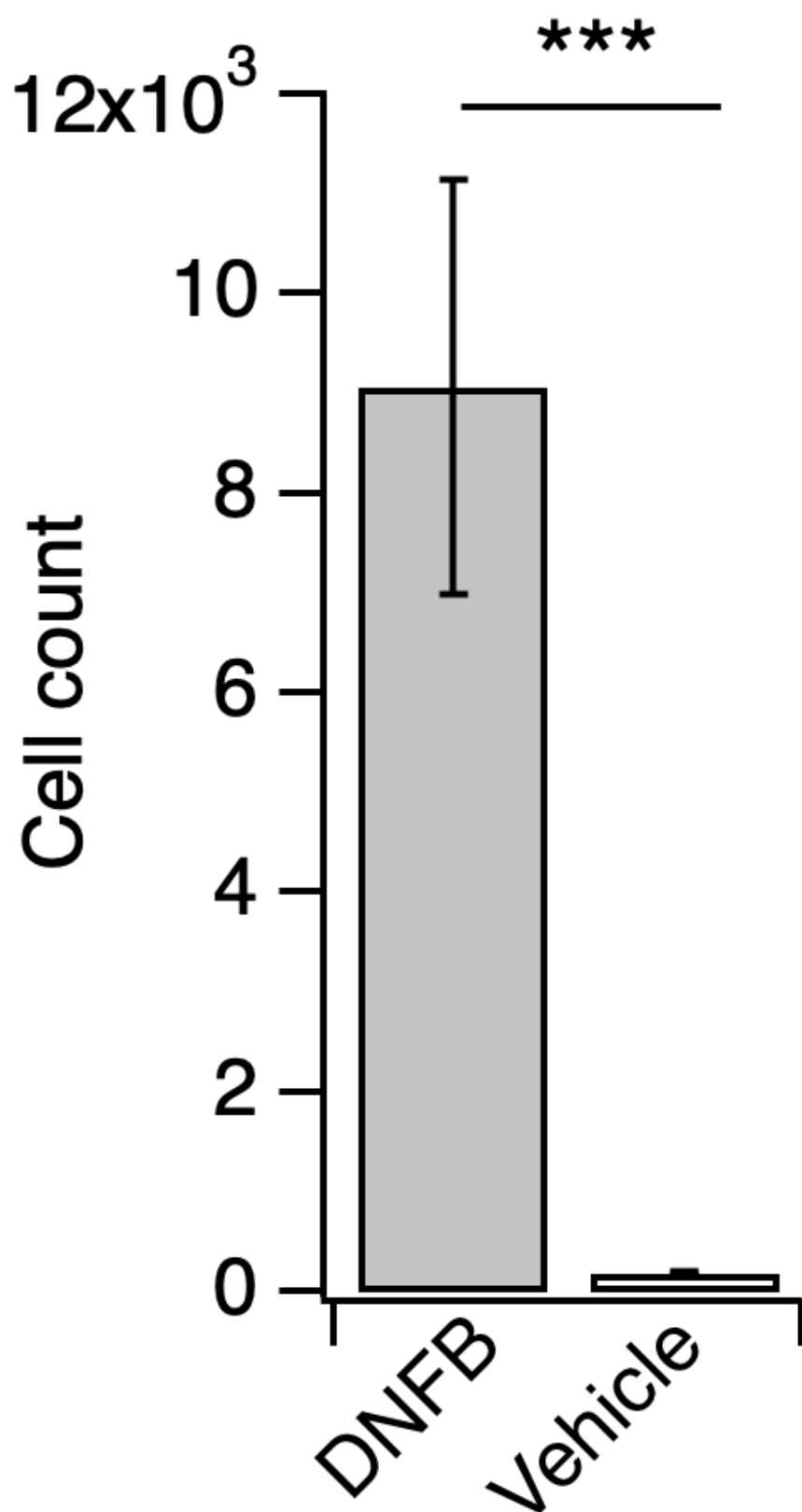


Figure 2-Figure Supplement 5

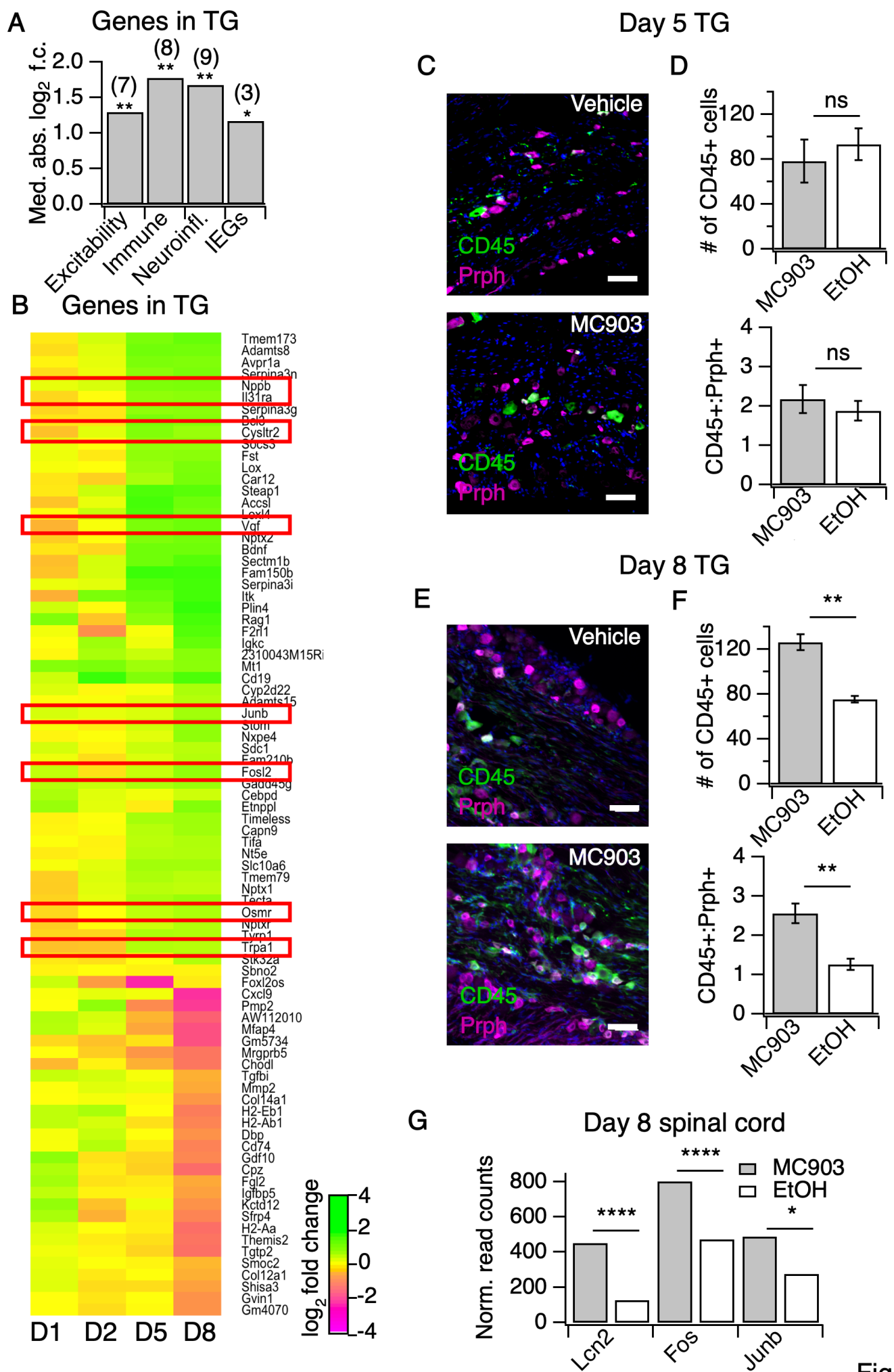
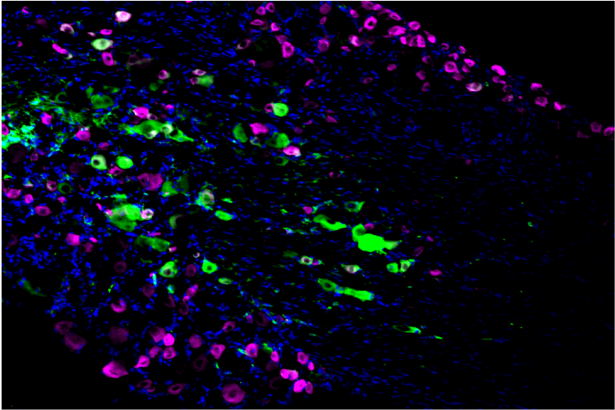
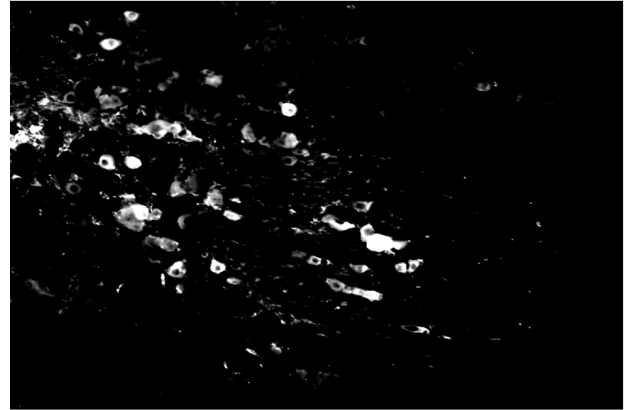


Figure 3

A



B



C



D



Figure 3-Figure Supplement 1

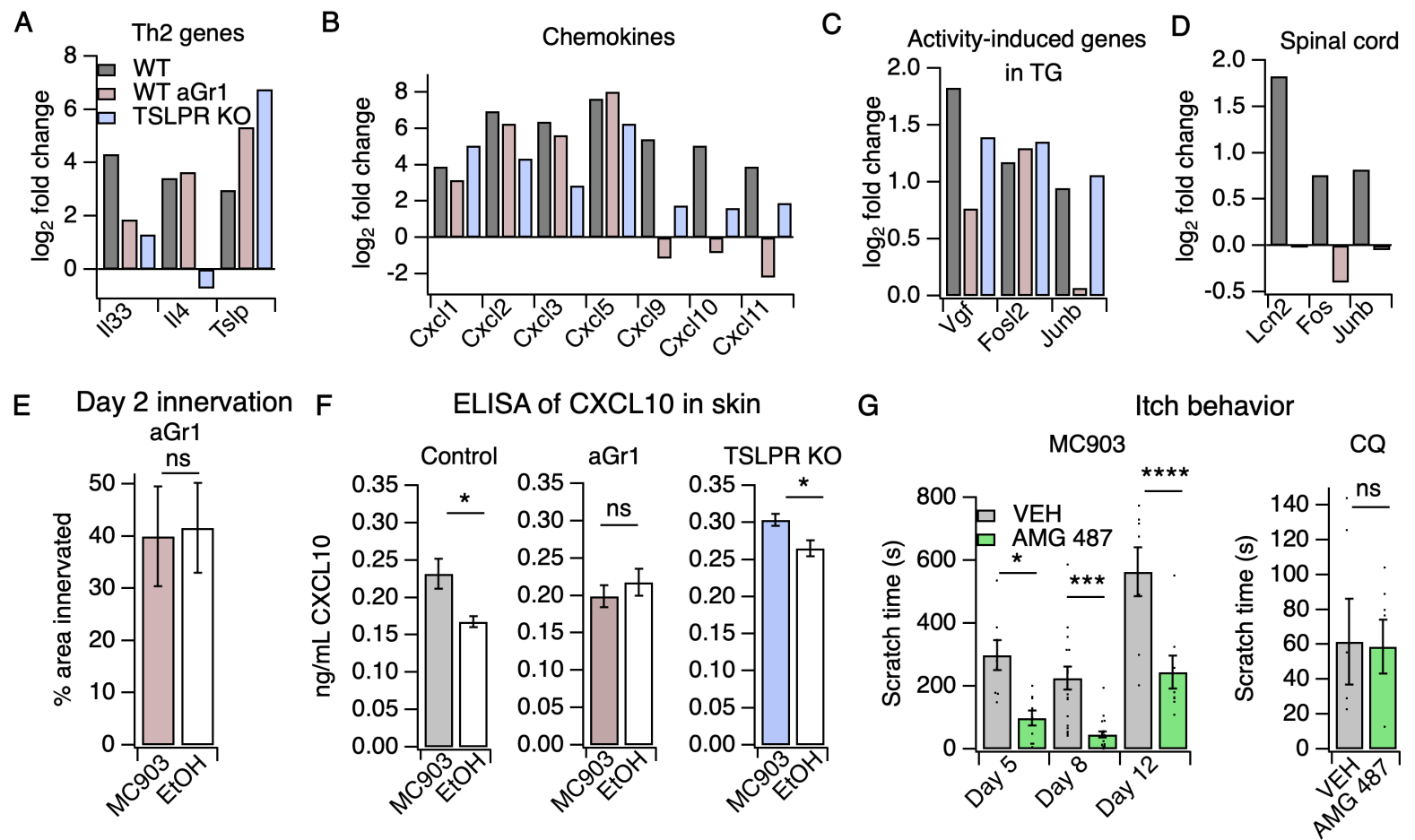
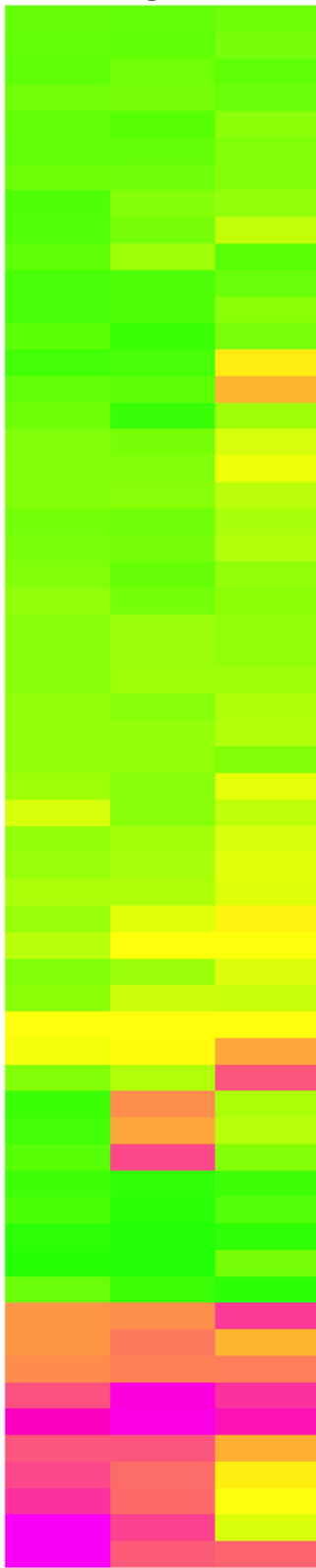


Figure 4

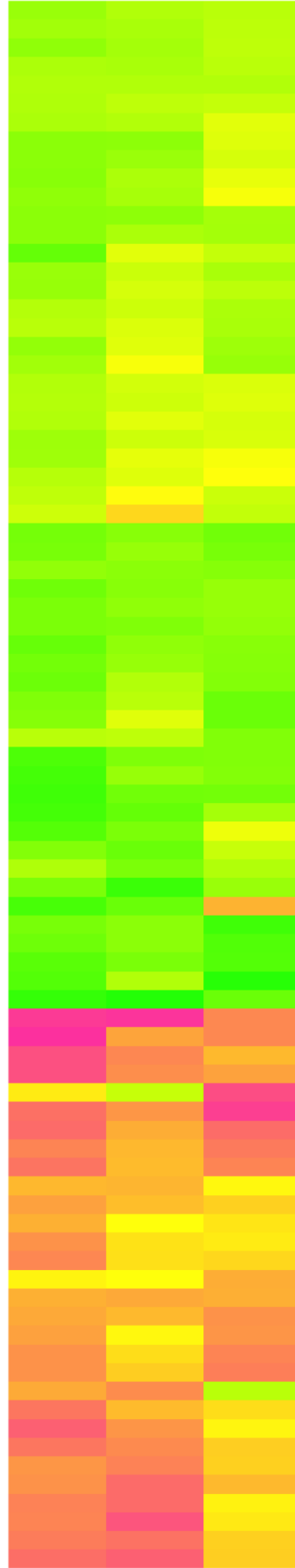
A Itch genes



WT
anti-Gr1
Tslpr KO

Ngf
Klk8
Tmprss11a
Artn
Klk12
Ptges
Tmprss11g
Il33
Tpsab1
Klk4
Klk9
Hdc
Klk6
Prss34
Il4
Mcpt1
Il1rl1
Tpsb2
Tacr1
Tac4
Il4ra
Prss27
Klk7
Prss16
Prss16
Prss52
Spink5
Klk11
Tmprss11d
Prss12
Ctsl
Alox12b
Mcpt4
Aloxe3
Ptgs1
Il31
Ctss
Tmprss4
Tac2
Il31ra
Alox15
Cxcl9
Cxcl10
Cxcl11
Tmprss11b
Klk13
Ptgs2
Mcpt8
Tslp
Tac1
Prss36
Ngfr
Alox12e
Ache
Alox8
Tmprss7
Prss53
Tmprss9
Klk15

B Genes in TG



WT
anti-Gr1
Tslpr KO

Cysltr2
Slc10a6
Stom
Osmr
Nt5e
Tifa
Cyp2d22
Fst
Mt1
2310043M15Ri
Nxpe4
Il31ra
Serpina3g
Igkc
Gadd45g
Tecta
Fam210b
Tmem79
Socs3
Junb
Nptxr
Adamts15
Stk32a
Timeless
Capn9
Trpa1
Nptx1
Cebpd
Nptx2
Loxl4
Fosl2
Bdnf
Serpina3n
Nppb
Tmem173
Adamts8
Vgf
Avpr1a
Bcl3
Sdc1
Cd19
Itk
Fam150b
Serpina3i
Sectm1b
Etnppl
Typr1
Lox
Rag1
Car12
Accs1
Steap1
F2r1
Plin4
Pmp2
Cxcl9
Gm5734
Mfap4
Foxl2os
Tgtp2
Cpz
Sfrp4
Themis2
Smoc2
Igfbp5
Col12a1
Kctd12
Gdf10
Sbno2
Tgfb1
Fgl2
Shisa3
Gvin1
Gm4070
Mmp2
Chodl
AW112010
Mrgprb5
Col14a1
Dbp
Cd74
H2-Ab1
H2-Eb1
H2-Aa

log₂ fold change
4
2
0
-2
-4

Figure 4-Figure Supplement 1

A

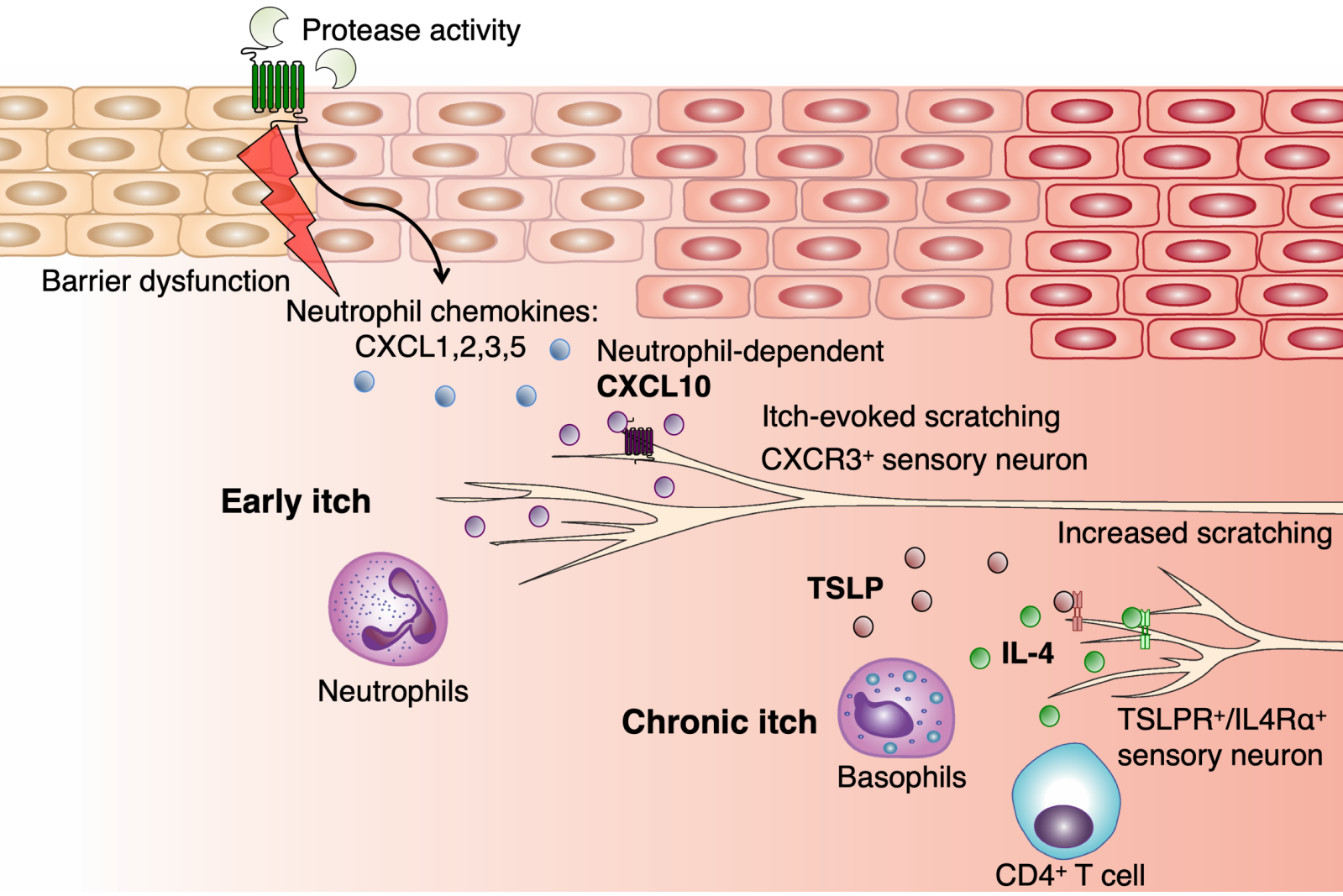


Figure 5